FROM THE DEPARTMENT OF MICROBIOLOGY, TUMOR AND CELL BIOLOGY (MTC)
KAROLINSKA INSTITUTET, STOCKHOLM, SWEDEN

VIRUS HOST INTERACTIONS IN SARS CORONAVIRUS INFECTION

Vithiagaran GUNALAN

Karolinska Institutet

Stockholm 2011

Published by Karolinska University Press. Printed by US-AB.
Box 200, SE-171 77 Stockholm, Sweden

ISBN 978-91-7457-510-1

ABSTRACT

The global outbreak of Severe Acute Respiratory Syndrome which began in 2002 and ended in 2003 resulted in over 8000 cases in 29 countries, causing an atypical pneumonia which resulted in a case fatality rate of ~10%. The etiological agent of this disease was found to be a novel coronavirus dubbed SARS Coronavirus (SARS-CoV). One of the distinguishing features of this virus is the presence of several accessory genes in its positive-stranded RNA genome which have no known homologs in the coronavirus family. In this thesis we examine virus host interactions in the context of SARS coronavirus in order that some insight may be gained into the biology of this virus, which is still the subject of investigation.

A lot of work has been done to study the function of SARS-CoV accessory proteins. One of these is the ORF6 accessory protein, which has been shown to accelerate infection, interfere with interferon production and signaling by impeding nuclear translocation, induce membrane rearrangements in the host cell and induce ER stress and subsequent caspase-mediated apoptosis. Examination of the ability of ORF6 to interact with other virus proteins by a yeast-two-hybrid assay showed an interaction with the nsp8 replicase protein. A direct interaction was shown using a cell-free system, and subsequently, transient transfection and immunoprecipitation experiments in Vero E6 cells showed that these proteins interacted in mammalian cells, which was confirmed in SARS-CoV infected cells. Examination of the co-localisation of these proteins in infected Vero E6 cells also showed a subcellular localization of the ORF6 protein to a intracellular vesicular population which was Lamp1- and CD63-positive.

The impedance of nuclear translocation by the ORF6 protein is linked to its ability to function as an interferon antagonist. A plasmid-based system comprising a CMV-derived promoter was used to replicate this impedance, and it was found that the impedance is dose-dependent. Additionally, plasmid-expressed ORF6 was shown by immunofluorescence to colocalise with an intracellular vesicular population positive for Lamp1 and CD63. Alanine substitution of a putative diacidic motif in the ORF6 protein showed a reduction in the impedance of nuclear translocation and when examined by immunofluorescence also showed clustering of ORF6-stained vesicles, suggesting that the impedance of nuclear import by ORF6 and its localisation to this specific vesicular population are linked.

In order to characterize the differential expression of genes in host cells which might lead to ORF6-mediated apoptosis, a defective recombinant vaccinia virus expressing ORF6 was generated. Analyses were performed using a QPCR array specific to human apoptotic signaling as well as microarray analysis for examination of genome-wide differential expression. Subsequent analysis of these results suggested that the extrinsic pathway of apoptosis was upregulated in cells expressing ORF6, and that intracellular calcium flux might have a role to play in ORF6-mediated apoptosis.

The introduction of an exogenous nitric oxide donor into Vero E6 cells infected with SARS-CoV has been shown to exert a negative effect on viral replication. Here an attempt was made to explore the mechanism of this inhibition. Nitric oxide can exert an effect on viruses either directly or through several redox intermediates, one of which is peroxynitrite, which is formed through the reaction of nitric oxide and superoxide. It was shown that the effect of the exogenous nitric oxide donor SNAP on SARS-CoV replication was not due to the effect of peroxynitrite, but probably through direct action of nitric oxide or another derivative. Examination of the palmitoylation of the S protein in SNAP-treated cells showed that SNAP treatment was able to reduce S palmitoylation and consequently its binding to the ACE-2 receptor in an *in vitro* cell-cell fusion assay. Also, QPCR analysis of viral RNA production showed a significant reduction in SNAP-treated cells. Examination of the cleavage of viral replicase polyproteins in these cells showed an alteration in the cleavage pattern of the replicase polyproteins.

LIST OF PUBLICATIONS

I. Kumar, P*., Gunalan, V*., Liu, B., Chow, V. T. K., Druce, J., Birch, C., Catton, M., et al. (2007). The nonstructural protein 8 (nsp8) of the SARS coronavirus interacts with its ORF6 accessory protein. *Virology*, *366*(2), 293-303.

II. Akerström, S*., Gunalan, V*., Keng, C. T., Tan, Y.-J., & Mirazimi, A. (2009). Dual effect of nitric oxide on SARS-CoV replication: viral RNA production and palmitoylation of the S protein are affected. *Virology*, *395*(1), 1-9.

III. Gunalan, V., Mirazimi, A., & Tan, Y.-J. (2011). A putative diacidic motif in the SARS-CoV ORF6 protein influences its subcellular localization and suppression of expression of co-transfected expression constructs. *BMC Research Notes (in press)*.

IV. Gunalan, V., Mirazimi, A., & Tan, Y.-J. (2011). Characterisation of apoptotic induction by the SARS-CoV ORF6 protein expressed via a defective recombinant vaccinia virus system *(manuscript)*.

* *Co-authored*

TABLE OF CONTENTS

LIST OF ABBREVIATIONS

ACE-2	Angiotensin-Converting Enzyme 2
DNA	Deoxyribonucleic Acid
cDNA	copy Deoxyribonucleic Acid
ER	Endoplasmic Reticulum
ERGIC	ER-Golgi Intermediate Complex
IFN	Interferon
IgG	Immunoglobulin G
MOI	Measure of Infection
NAP	Nitric oxide enhanced ADP-ribosylated protein
ORF	Open Reading Frame
PAGE	Polyacrylamide Gel Electrophoresis
QPCR	Quantitative Realtime Polymerase Chain Reaction
RNA	Ribonucleic Acid
mRNA	Messenger Ribonucleic Acid
SARS-CoV	Severe Acute Respiratory Syndrome Coronavirus
SIN-1	5-amino-3-(4-morpholinyl)-1,2,3-oxadiazolium chloride
SNAP	S-nitroso-N-acetylpenicillamine

1 INTRODUCTION

Coronaviruses are a family of enveloped, positive-stranded RNA viruses. These viruses are classified under the order Nidovirales, within the family Coronaviridae. The other family of viruses under this order are the Arteriviridae, which comprise viruses of veterinary importance, such as equine arteritis virus (EAV). Other members of the coronavirus family include the porcine virus transmissible gastroenteritis virus, (TGEV), the avian virus infectious bronchitis virus (IBV), feline infectious peritonitis virus (FIPV), mouse hepatitis virus (MHV) and the human coronaviruses 229E and OC43 which are well documented in the literature. The name Coronavirus is derived from the characteristic appearance of these viruses in electron micrographs, which resemble a solar corona. These viruses have among the largest genomes of any virus family, and encode a variety of proteins. Up till recently, the only coronaviruses known to be pathogenic to humans were 229E and OC43, and these were only responsible for mild flu-like symptoms in patients.

With the onset of the Severe Acute Respiratory Syndrome (SARS) epidemic in 2003, coronaviruses attained an unprecedented notoriety in the eyes of the public, and coronavirologists accordingly attained an unprecedented popularity. By most accounts, the outbreak of SARS began in Guangdong Province in Southern China in late 2002. By the time the World Health Organisation (WHO) office in Beijing had been notified of a strange respiratory disease spreading through the province in the same year, there were rumoured to be over 100 fatalities in Guangdong alone. Official statements released in February of 2003 described approximately 300 cases of this respiratory disease. By the time the WHO had called an end to this epidemic in July 2003, there had been 8096 documented cases with 774 deaths, indicating a case fatality rate of about 9.6% (http://www.who.int/csr/don/2003_07_04/en/index.html). But these numbers did not just arise from Guangdong - during the course of the epidemic, 29 different countries were affected by SARS. While most of the documented cases were in China, there were significant numbers of SARS cases in Hong Kong, Singapore, Taiwan and Canada, mostly related to the Chinese diaspora. Travellers to China and emigrants who had returned home for the Lunar New Year in early 2003 had brought this disease back with them, resulting in the global spread of a disease that brought death, widespread panic and an economic toll of approximately US$ 20bn over the course of just a few months. Hong Kong was considered to be the epicenter of the global spread of SARS, and it was from here that the first clinical reports of the outbreak emerged, describing an 'atypical pneumonia' that attending physicians were confronted with. Reports from the WHO document the role of one hotel where travellers from Singapore, Vietnam and Canada all came into contact with infected individuals from Guangdong province and became index patients in their respective countries. In April that year, just a month after the initial reports of the outbreak in Hong Kong, a novel coronavirus was described as being the etiological agent of this disease (Peiris et al 2003b, Ksiazek et al 2003, Drosten et al 2003).

Clinically, SARS resembled the symptoms of influenza - indeed, when SARS emerged, infectious disease physicians thought that this was the emergence of a human strain of highly pathogenic avian influenza (HPAI, personal communication). Along these lines, the WHO published a case definition of SARS in order to differentiate potential SARS cases from other illnesses resulting in respiratory syndromes. However, in the interest of prudence, the case definition was itself vague:

"A suspected case of SARS is an individual with fever (temperature 38°C [100.4°F]), cough or dyspnea, and contact with an individual believed to have SARS or to have traveled to a region where there has been documented transmission of the disease. A probable case is an individual meeting criteria for a suspected case along with radiographic features of pneumonia, respiratory distress syndrome, or an unexplained respiratory illness resulting in death with autopsy results demonstrating pathology of respiratory distress syndrome without an identifiable cause."

- WHO Global Alert and Response, May 2003

The progression of the disease itself was triphasic. Infected individuals underwent an incubation period of about 1-11 days, before the presentation of the first phase of symptoms which included fever, myalgia and lung radiographs which showed air spaces. Within the first week, most patients showed incremental improvement which was widely attributed to the administration of a combination of ribavirin and corticosteroids by attending physicians (Peiris et al 2003a, Tsang 2003, Tsui et al 2003). However, into the second week, symptoms usually began to worsen, with the recurrence of fever and the onset of diarrhea. Lung radiographs also show increasing consolidation of air spaces during this phase of the disease. By the 10th day after initial presentation, most patients were observed to undergo IgG seroconversion (Peiris et al 2003a). The onset of the third and severe phase of SARS in marked by acute respiratory distress syndrome (ARDS), oxygen desaturation, severe lymphopenia and thrombocytopenia, which was suspected to have resulted in nosocomial sepsis in several patients, and eventually death (Peiris et al 2003a, Lew et al 2003). This phase was seen as a turning point in the disease as far as patient prognosis was concerned, and many patients were observed to not progress to this stage, eventually going into recovery. Complicating this was also reports of toxicity in patients due to the administration of ribavirin (Booth et al 2003). Because of the unknown nature of the disease, several combinations of therapies were used in diverse settings, with some reporting limited success. An example of this was interferon Alfacon-1, which showed promise in combination with corticosteroids in the Toronto SARS cohort (Loutfy et al 2003), with a later study also showing potential with the use of interferon treatment on SARS isolates in in vitro experiments (Cinatl et al 2003).

2 THE SARS CORONAVIRUS

2.1 IDENTIFICATION OF A NOVEL CORONAVIRUS

During the initial phases of the outbreak both in Asia and globally, the medical community was racing against time to treat SARS patients, but the cause of the disease itself was unknown. But there were clues to the infectious nature of the disease, in particular the fact that several cases of the disease came from unrelated individuals who were staying at the same hotel in Hong Kong. In order to identify the etiological agent of a disease, Robert Koch devised a series of postulates in the 1880s, which in modern-day science came to be known as Koch's postulates. These postulates, while initially developed with bacterial diseases in mind, were subsequently modified by Thomas Rivers for viral diseases in 1936. In order for a virus to be proven as the etiological agent of a given disease, the burden of proof rests on:

1) Isolation of virus from a diseased host
2) Cultivation of virus in host cells
3) Proof of filterability
4) Production of comparable disease in the original host species or a related one
5) Re-isolation of the virus
6) Detection of a specific immune response

It was eventually in June 2003 that several groups identified a novel coronavirus as having fulfilled these requirements to be deemed responsible for the SARS epidemic (Drosten et al 2003, Fouchier et al 2003, Ksiazek et al 2003, Peiris et al 2003b, Poutanen et al 2003). The coronavirus responsible for the outbreak of SARS was first imaged when it was isolated from patient samples in Vero E6 cells in Hong Kong, and carried this characteristic corona appearance:

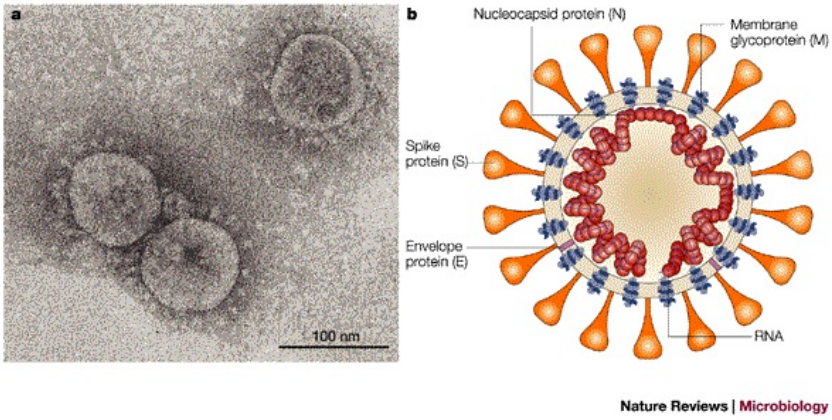

Figure 1. Structure of the SARS Coronavirus as seen by (a) electron microscopy, (b) stylized diagram of virus structure showing structural proteins and viral RNA genome. Reprinted by permission from Macmillan Publishers Ltd: Nature Reviews Microbiology (Stadler, K., et al. SARS - Beginning to Understand a New Virus. Nature Reviews Microbiology 2003, 1(3): 209-

218), copyright (2003).

The identification and subsequent isolation of the virus, changed the face of the outbreak and heralded a surge in antiviral research targeted at gathering information on disrupting the virus' natural cycle and slowing down or inhibiting its transmission altogether. However, to date, no efficient therapeutic or prophylactic vaccine has been found for the SARS Coronavirus.

The outbreaks at the Metropole Hotel and Amoy Gardens apartment complex in Hong Kong, when considered in the light of the discovery of this novel coronavirus shed more light on the transmissibility of the virus. At the sites of both community-based outbreaks, contact-tracing determined that infected individuals did not come into contact with each other in most instances. Because of the respiratory pathology of the virus, it was suspected to be a respiratory virus, but it is well-documented that coronavirus tropism extends beyond the respiratory system - the gastroenterological nature of many coronaviruses suggests that the community-based outbreaks in Hong Kong may have been due to fecal-oral transmission of the virus, thanks to faulty sewage systems (Peiris et al 2003a, Drosten et al 2003). The respiratory nature of the virus meant that it was easily transmitted through the kind of aerosolization caused by coughing and sneezing. Along these lines, nosocomial infections in the sterile environment of a hospital where one could expect that the fecal-oral route of transmission would be minimal, were responsible for most of the infections observed in many of the countries affected, particularly where infections among the healthcare community were concerned. Respiratory equipment used in hospitals were deemed to have aided the aerosolization of the virus, which could have been a significant factor in the nosocomial transmission of the virus (Lee and Sung 2003). Given this information, a huge effort was put into the containment of the spread of SARS - the efforts of governments to screen and quarantine the symptomatic was crucial in halting the spread of the virus in its tracks, far before any significant progress had been made towards understanding the virus and designing therapeutic interventions.

2.2 THE SARS-COV GENOME

One of the first steps towards our understanding of the SARS coronavirus was attained with the sequencing of its genome in May of 2003, barely 3 months into the global outbreak. The initial characterization of the SARS-CoV genome was carried out through sequencing of 14 different virus isolates - from the Singapore index case, 3 primary strains in the Singapore outbreak, as well as other strains from Hong Kong and China, in an effort to examine the mutational dynamics of the virus as well as to carry out a more detailed study of the virus genome (Ruan et al 2003). This was followed soon after by almost simultaneously published sequencing reports of the Urbani strain (Rota et al 2003), the Tor2 strain (Marra et al 2003) and the Frankfurt-1 strain (Thiel et al 2003). The genome of the prototypical coronavirus is, as in the case of SARS-CoV, a positive-stranded, polyadenylated RNA genome. The layout of the SARS-CoV genome is shown below:

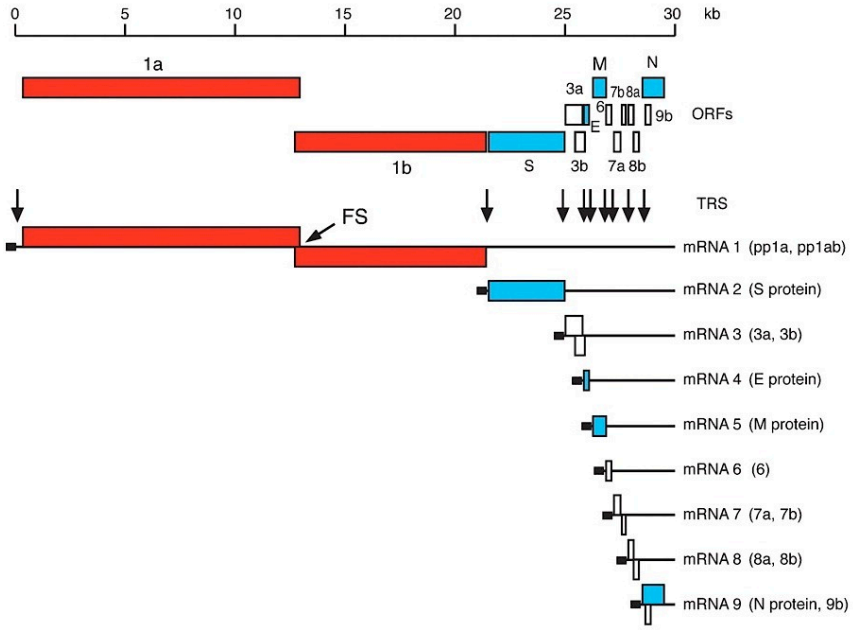

Figure 2. Diagram of the SARS-CoV genome showing virus genes (above) and subgenomic RNA (sgRNA) species (below). Red denotes Replicase genes and sgRNAs. Blue for structural genes and sgRNAs and white denotes accessory genes and sgRNAs. Adapted from Thiel et al (2003).

The SARS-CoV genome is an approximately 29.7kb long polyadenylated RNA genome. It can be seen that the virus genome contains 2 large replicase genes at the 5' end of the genome; *Orf1a* and *Orf1b* encode for the replicase polyproteins pp1a and pp1b. The replicase gene *Orf1b* is located -1 to the reading frame of *Orf1a*. Downstream of these genes are prototypical coronavirus structural genes - spike (*S*), envelope (*E*), membrane (*M*) and nucleocapsid (*N*). It was also noticed that encoded amongst these structural genes were other open reading frames which were assumed to encode for nonstructural genes. These were eventually labeled 'accessory genes', and their nomenclature, which differed between reports on the sequences, was eventually resolved. Also observed on the SARS-CoV genome were a 72nt leader sequence at the 5' end of the genome and a terminal sequence at its 3' end. The examination of the SARS-CoV genome led to a great deal of discussion over the classification of SARS-CoV within the three existing phylogenetic groups of the Coronavirus family. It was initially postulated that SARS was phylogenetically dissimilar to other coronaviruses and therefore ought to be classified in a group unto itself (Rota et al 2003, Marra et al 2003). This initial determination was carried out by either antigenic cross-reactivity or the examination of viral proteases as well as structural proteins. Based on these analyses, the

SARS_CoV genome did not fall into any of the three existing groups of coronaviruses. Based on analysis of the proteolytic cleavage and domain organization of the replicase polyproteins of SARS-CoV, a third proposal was posited - that SARS-CoV was an early split-off from the Group 2 coronaviruses, which included mouse hepatitis virus (MHV) and bovine coronavirus (BCoV). While this sparked considerable debate in the coronavirus community, the classification of SARS-CoV was eventually settled and the virus denoted part of the Group 2 coronaviruses, albeit as a subgroup - Group IIb. The prolonged (and contentious) classification exercise of the SARS-CoV genome was later noted as being beneficial to the entire coronavirus family, as it resolved many of the discrepancies and inconsistencies in the classification of these viruses (Gorbalenya et al 2004).

The accessory genes encoded within the SARS-CoV genome were of particular interest to many coronavirologists as well as other virologists who took an interest in this novel coronavirus. The existence of accessory genes in coronaviruses is not novel in itself; other coronaviruses such as MHV encode for accessory genes within their genomes. However, the fact that SARS-CoV is a human coronavirus of moderate pathogenicity lends credence to the study of these accessory genes in particular. There are a total of 8 putative accessory genes encoded with the genome of SARS-CoV, *3a*, *3b*, *6*, *7a*, *7b*, *8a*, *8b* and *9b*, which is a hidden reading frame within the nucleocapsid gene. Antibodies against the protein products of all of these accessory genes were detected in human patient sera, indicating that these genes code for actual proteins and that these are actively expressed during infection (Guan et al 2004a,b, Guo et al 2004, Tan et al 2004b, Chow et al 2006). The interest taken in these genes by coronavirologists has led to a large number of varied observations of the characteristics of their protein products, and these are summarized in Table 1.

Gene	Characteristics of Protein Product	References
3a	• Pro-apoptotic, Induction of mitochondrial death pathway	Law et al 2005, Chan et al 2009, Padhan et al 2008
	• Immunogenic, elicits humoral and cellular responses	Lu et al 2009, Åkerström et al 2006, Zhong et al 2006,
	• Promotes membrane rearrangement	Freundt et al 2010
	• Downregulation of Type I IFN receptor	Minakshi et al 2009
	• Induces G1 cell cycle arrest	Yuan et al 2007
	• Interacts with 5' UTR of SARS-CoV genome	Sharma et al 2007
	• Interacts with caveolin	Padhan et al 2007
	• Potassium-permeable ion channel activity	Lu et al 2006
	• Structural contribution to virion	Ito et al 2005, Shen et al 2005
	• Localizes to cell surface, undergoes endocytosis	Tan et al 2004
	• Upregulates fribrinogen in lung epithelia	Tan et al 2005
3b	• Activation of JNK/ERK pathways	Varshney et al 2011
	• Induction of cell death	Khan et al 2006
	• Localizes to nucleolus	Yuan et al 2005
	• G0/G1 cell cyle arrest	Yuan et al 2005
	• Interferon antagonism	Kopecky-Bromberg et al 2007
ORF6	• Acceleration of infection in a recombinant murine coronavirus	Pewe et al 2005, Tangudu et al 2007, Netland et al 2007
	• Required for optimal SARS-CoV replication	Zhao et al 2007
	• Interacts with nsp8 replicase protein	Kumar et al 2007
	• Antagonism of STAT1 nuclear import	Frieman et al 2007, Hussain et al 2010
	• Promotes membrane rearrangment	Zhou et al 2010
	• Localises to lysosomal compartment	Kumar et al 2007, Gunalan et al 2011
	• Interferon antagonism	Kopecky-Bromberg et al 2007
	• Induction of JNK-dependent apoptosis	Ye et al 2008
7a	• Induction of apoptosis	Tan et al 2004, Schaecher et al 2007
	• RNA silencing suppression	Karjee et al 2010
	• Interaction with human Ap4A-hydrolase	Vasilenko et al 2010
	• Interaction with Bcl-XL	Tan et al 2007
	• Contribution to virus structure	Huang et al 2006
	• Interaction with hSGT	Fielding et al 2006
	• Inhibition of cellular protein synthesis	Kopecky-Bromberg et al 2006
7b	• Attenuates viral replication	Pfefferle et al 2009
	• Induction of apoptosis	Schaecher et al 2007
8a	• Induction of apoptosis	Chen et al 2007
8b	• Proteasome-dependent downregulation of E protein	Keng et al 2006, Keng et al 2011
9b	• Shuttling across nuclear membrane	Moshynkyy et al 2007, Sharma et al 2011
	• Association with virion	Xu et al 2009
	• Lipid binding	Meier et al 2006

Table 1. Observed characteristics of SARS-CoV accessory proteins

One of these accessory genes, *ORF6*, encodes for a ~7kDa protein with a hydrophobic N–terminal and that has been suggested to have a N-endo-C-endo conformation (Netland et al 2007). Several

groups have undertaken to characterize the protein product of the *ORF6* gene and found that it interacts with the nsp8 protein from the SARS replicase complex (Kumar et al 2007), is able to increase infection titer during early infection at low MOI (Zhao et al 2009), increase the rate of cellular gene synthesis (Geng et al 2005), inhibit interferon production (Kopecky-Bromberg et al 2006), and inhibit the nuclear translocation of STAT1 by interacting with karyopherin α2 (Frieman et al 2007). Most recently, the ORF6 protein has been suggested to induce intracellular membrane rearrangements resulting in a vesicular population in the infected cell which could possibly serve some role in increasing replication (Zhou et al 2010). Such virus-induced or virus associated vesicles have previously been shown in other viral infections, such as protein trafficking in Herpes simplex virus (Miranda-Saksena et al 2009) and Sendai virus (Chambers & Takimoto 2010). Members of the coronavirus family have been shown by several groups to also utilize vesicular structures within the infected cell; most of these studies suggest that vesicles play a role in viral replication (Sims et al 2000, Snijder et al 2006, Knoops et al 2008).

2.3 VIRUS LIFE CYCLE

The infection process for any given virus begins with the binding of the virus to its cognate cellular receptor. In the case of SARS-CoV, this receptor was identified as the angiotensin-converting enzyme 2 (ACE-2) receptor. Mass spectrometry analysis of proteins bound to a pulldown complex using the spike protein of the virus identified this receptor as also being the receptor for virus entry (Li et al 2003), and this finding was subsequently confirmed by other groups (Wang et al 2004). It was also shown shortly afterwards that L-SIGN could function as a SARS-CoV receptor as well (Jeffers et al 2004), although subsequent work showed that L-SIGN promiscuously binds to many viruses outside the coronavirus family such as Human Immunodeficiency virus (da Silva et al 2011), Hepatitis C virus (Gardner et al 2003) and Ebolavirus (Alvarez et al 2002), and that L-SIGN could have a protective effect against SARS-CoV infection by mopping up virus particles for internalization and subsequent degradation by proteasomes (Chan et al 2006).

Upon binding of the S protein to the ACE-2 receptor, the virus is internalized by endocytosis and presumably undergoes pH-dependent uncoating within endosomes in order to release the viral genome as well as viral proteins. From here, viral RNA undergoes replication and the expression of viral genes commences. It has been suggested on the basis of experiments showing the incorporation of accessory protein ORF6 into the virion that the surface of the virus contains several proteins other than the main structural proteins such as S, E and M and these other proteins, including accessory proteins, might be able to exert an immediate host effect instead of undergoing the usual lag time between uncoating, mRNA synthesis and translation of viral proteins (Huang et al 2007), which taking into account the expression of late viral genes, takes up to 12 hours from the point of infection (unpublished observations). As the SARS-CoV genome was positive-stranded, it was assumed that a negative strand template was transcribed from this positive-stranded genome to serve in the replication of the genome, although none of the initial sequencing work looked for the existence of a negative-polarity template for the virus genome. The transcription of the open reading frames in the virus genome, however, were much more complex than its replication. According to the existing model of coronavirus transcription, genes are transcribed as a set of nested subgenomic mRNAs, each encoding for a different gene or set of genes(Sawicki and Sawicki 2007). Through the use of Northern hybridization using probes

targeted at the terminal sequence of the coronavirus genome, a series of RNA fragments of varying lengths were discovered, confirming that this mode of transcription also applied to SARS-CoV (Marra et al 2003, Rota et al 2003, Thiel et al 2003). The mechanism behind the creation of these subgenomic mRNAs is predicted to be a discontinuous synthesis model, which leads to the generation of a subgenomic mRNA containing a leader sequence known as a transcriptional regulatory sequence (TRS) at the 5' end, a terminal sequence at the 3' end just upstream of the polyadenylated tail, and the body of which contains the gene to be expressed at the 5' region downstream of the leader sequence, followed by the genes downstream of it (see Fig 2). A total of 7 subgenomic mRNAs were detected in the case of SARS-CoV, and eventual sequencing identified the genes expressed from each of these mRNA species, with the exception of the replicase genes, which were presumed to be expressed from the genome itself (Thiel et al 2003), which differs from its subgenomic mRNAs only by inclusion of the replicase genes. This determination was consistent with the prevailing idea that the replicase genes carried the highest priority of expression, as the virus genome encoded for these genes at its 5' end, downstream of the primary TRS sequence in the genome. Translation of the replicase genes from the SARS-CoV genome produces 2 replicase polyproteins, pp1a which contains nsps 1-10 and and pp1ab which contains nsps 1-16. Autoproteolytic cleavage of the replicase polyproteins yields the nonstructural proteins nsp1 to nsp16, which contains proteases, two RNA-dependent RNA polymerases, and a host of other enzymes crucial to viral replication (Snijder 2003). It is assumed that the heteromeric nature of the expressed polyproteins is indicative of a dependency relationship between the various nonstructural proteins which dictates that they be expressed simultaneously. To this end, replicase polyproteins have been found to localize at the same subcellular compartments (Prentice et al 2004) and structural studies have elucidated a torus-like structure for the nsp7-nsp8 complex (Zhai et al 2005). This putative complex of nonstructural proteins, referred to as the replication complex, is thought to localise in the infected cell to particular vesicular compartments. The strategy of employing vesicular compartments to facilitate viral replication is a well-known strategy used by several viruses, among these other coronaviruses such as MHV and EAV, which have been suggested to utilise the autophagic pathway for the generation of these vesicles (Prentice et al 2004). Recent evidence has shown that SARS-CoV utilizes a modified reticulovesicular network derived from the ER to encapsulate and protect these replication complexes (Knoops et al 2008), and no evidence of autophagy has been found in SARS-CoV infection (Snijder et al 2006), although it can be argued that this simply reflects the diverse strategies by which different viruses generate vesicular compartments for use in replication, even within the same virus family.

The assembly and egress of progeny virions was first shown using electron microscopy of SARS-CoV infected cells (Ng et al 2003), showing nascent virus particles budding from swollen Golgi sacs. Other efforts soon followed and were consistent with initial findings (Goldsmith et al 2004). However, electron microscopy is of limited value in deciphering the actual mechanism as well as the sites of assembly, as well as the viral and host determinants of this process. One useful strategy to address this issue is to use VLPs, or virus-like particles, as a least common denominator of a virus particle. Given that SARS has 4 canonical structural proteins, S, M, E, and N, VLPs were constructed by adding different combinations of viral structural proteins in order to determine the exact mechanism of virus assembly. VLPs have been constructed using a combination of M and N or M, E and N (Siu et al 2008) or using all 4 structural proteins (Nakauchi et al 2008). It is clear from these studies that the M protein seems to be the common denominator of viral assembly, a point which was reinforced by the finding that the M protein is able to homoploymerize (Tseng et al 2010), suggesting that the M protein forms the backbone for virus assembly. Clues as to the

sites of SARS assembly have come from the detection of a Golgi targeting signal in the E protein (Cohen et al 2011) and the observation of a dibasic COPI-binding ER retrieval signal in the spike protein which also promotes the interaction of the M and S proteins (McBride et al 2007). The COPI retrieval signal carries the canonical KKxxx motif and aids in the retrieval of ER-resident proteins from the Golgi complex to their proper locations in either the ERGIC or ER (Lee et al 2004). This suggests that the site of SARS assembly could be the ERGIC, and this is supported by immunogold EM and immunofluorescence studies which have placed the structural proteins in the vicinity of cellular markers corresponding to the Golgi and the ERGIC (Stertz et al 2006). As the sites of SARS replication are thought to have been ER-derived, it makes sense to postulate that the assembly compartments in the ERGIC and Golgi are closely connected to these replication sites. However, it is unclear if the assembly of progeny virions depends only on the 4 canonical structural proteins - accessory proteins of the virus have been suggested to make structural contributions to progeny virions. By studies of incorporation in VLPs and purification and immunoanalysis of SARS-CoV particles, the 3a, ORF6, 7a and 9b proteins have been found to be associated with virions (Ito et al 2005, Shen et al 2005, Huang et al 2006, Xu et al 2009). In the case of 3a, it has also been suggested to affect virus release by forming putative postassium-permeable ion channels at the plasma membrane of the host cell (Lu et al 2006). The use of siRNA against the 3a protein also exhibited a dose-dependent reduction in virus release, suggesting that the 3a protein modulates virus release, although it is unclear if the ion channel activity of the protein is directly responsible for virus release.

3 RESPONSE TO INFECTION

The characteristic clinical presentation in SARS patients was an atypical pneumonia with symptoms including fever, myalgia, and the progressive consolidation of lung space with later symptoms including lymphopenia, thrombocytopenia, diarrhea and eventually acute respiratory distress. While these are easily observed pathological changes which can be attributed to infection, there are several processes in infected cell of the host which underly these pathological outcomes. A lot of work done towards our understanding of SARS has been accordingly focused on the pathogenicity of the virus in an attempt to elucidate the pathogenic determinants of SARS-CoV infection. While there have been pathological features observed in the course of characterisation of several viral proteins, the response of the host to infection can also be an important determinant of pathogenicity.

3.1 THE INNATE IMMUNE RESPONSE IN SARS

A study performed in the early days of the outbreak looked at viral load and IgG seroconversion in 14 SARS patients over the course of infection. The study showed a peak in viral load in almost all of these patients at day 10 after the onset of symptoms, with viral load subsequently dropping off at 15 days. Coincidentally, IgG seroconversion also began to increase greatly around the 15th day, when viral load was observed to undergo a reduction. While the reduction in viral load is easily attributable to the increasing IgG seroconversion and thereby the activation of the adaptive immune response in these patients, it was also noted that the patients exhibited clinical worsening (Peiris et al 2003a). At the same time, a study done on a lung biopsy from a SARS patient who had succumbed to the disease showed predominantly macrophage-based infiltration in the lung which was deemed responsible for the diffuse alveolar damage which was observed (Nicholls et al 2003), a finding that was echoed in other pathological studies performed on lung tissue from SARS patients (He et al 2006, Lang et al 2003). These studies lent credence to the possibility that the immune response might have been partially responsible for the pathology of SARS. Concomitant with this, the overproduction of pro-inflammatory cytokines such as TGF-β1, TNF-a, IL1β and IL-6 was also observed (He et al 2006) as well as inflammatory chemokines such as MIP-1a, RANTES, IP-10 and MCP-1 from infected DCs (Law et al 2005), and also from *in vitro* infected macrophages (Cheung et al 2005). However, the magnitude of the alveolar damage seen in the lungs of SARS patients cannot easily be explained by the secretions of a few proteins. One model proposed for this immune-mediated lung pathology involves 2 steps: firstly, lung epithelial cells infected with SARS-CoV were found to secrete chemoattractant proteins such as MCP-1 and IL-8, which could recruit monocytes and macrophages to the site of infection. The same study then found that a THP-1 monocyte line could secrete more chemoattractants which were observed to attract monocytes and macrophages, along with neutrophils and activated T cells in a chemotactic assay. This would form the second step of immune infiltration into the lungs, exacerbating the damage already done by the first wave of immune cell infiltration (Yen et al 2006). This line of thinking was strengthened by the finding that PBMCs infected with SARS-CoV exhibited the upregulation of similar sets of proinflammatory cytokines and chemoattractants as observed in previous studies. It was proposed that these served as attractant factors for the infiltration of immune cells such as monocytes and macrophages to the lungs, acting in a similar fashion to

infected lung epithelial cells to initiate a 'second wave' of infiltration (Ng et al 2004).

The same studies examining the secretion and differential expression of various cytokines and chemokines in infected tissues from patients as well as in vitro studies noticed a very interesting feature of the immune response to infection - a lack of IFNα/β. This difference has been cited as the reason for the longer time taken for virus load in SARS-CoV infection to peak (at 10 days) as opposed to other respiratory infections such as influenza A, which has been known to achieve peak viral load within a day of infection. By comparison, the magnitude of IFNβ downregulation by influenza A was not as great as it is in SARS-CoV infection, and the peak virus load coincides with the secretion of interferon as opposed to the peak of SARS-CoV coinciding with IgG seroconversion (Cheung et al 2005, Kaiser et al 2001). Subsequent studies have shown that SARS-CoV does indeed inhibit the interferon response actively, and several proteins encoded within the SARS-CoV genome have been shown to downregulate the expression of interferons at different steps of the induction pathway. Using a plasmid construct utilizing an interferon-β promoter tagged to a *GFP* reporter gene, it was shown that the accessory proteins ORFs 3b and 6, and the nucleocapsid protein were able to block the expression of IFNβ (Kopecky-Bromberg et al 2007). The ORF6 protein has been shown to prevent the nuclear localization of STAT1 in order to inhibit the downstream effects of interferon signaling via the JAK/STAT pathway (Frieman et al 2006). The papain-like protease domain of the SARS-CoV replicase complex as well as the accessory proteins ORF3a and ORF6 have been shown to inhibit the phosphorylation and subsequent nuclear translocation of IRF-3, thereby inhibiting its ability to induce the expression of interferons (Devaraj et al 2007, Kopecky-Bromberg et al 2007). In addition to the induction of interferon expression by phosphorylated, nuclear translocated IRF-3, a second method of induction exists via the nuclear translocation of NFkB. Using an NFkB-responsive promoter, it was shown the the SARS-CoV nucleocapsid protein was able to block NFkB-dependent activation of interferon expression (Kopecky-Bromberg 2007). Thus it is clear that SARS-CoV possesses several mechanisms to inhibit the interferon response. However, it is possible to overturn this multi-faceted inhibition of the IFN response. Priming of non-lymphatic cells with small amounts of IFNa was shown to induce a sufficient IFN response during SARS-CoV infection (Kuri et al 2009).

3.2 ADAPTIVE IMMUNE RESPONSE

The adaptive immune response to infection comprises of the humoral immune response, mediated by B lymphocytes, and the cellular response, mediated by T lymphocytes. Both of these responses were observed in SARS patients. The humoral response to SARS-CoV infection was observed in the IgG seroconversion of patients at an average of 2 weeks after the first signs of symptoms (Peiris et al 2003a). Studies examining the antibody response in SARS patients in China showed that this antibody response was able to neutralize pseudotypes viruses containing spike proteins from different strains of SARS-CoV (Nie et al 2004). However, it was also found that a correlation existed between IgG levels in patients and the severity of disease (Lee et al 2006), suggesting that the humoral response to the virus might be part of the immunopathogenesis of SARS, and not necessarily protective. In order to determine the relative immunogenicity of proteins encoded by the SARS-CoV genome, various recombinant viral proteins were tested for reactivity against patient sera from both acute and convalescent phases of infection. Reactivity of all the sera to the nucleocapsid proteins suggested that it was the most immunogenic of viral

proteins. Interestingly though, acute phase sera did not show reactivity to the S proteins where convalescent phase sera did (Tan et al 2003). Based on these results, an ELISA-based diagnostic kit was designed to detect anti-N IgG in patients, using a recombinant N protein (Guan et al 2004).

One of the hallmarks of SARS-CoV infection is observed lymphopenia in patients. A study looking at T lymphocyte subsets in a cohort of 271 patients in China found decreases in several lymphocyte subsets, particularly in CD4+ and CD8+ T lymphocytes. The researchers also found a correlation between the severity of disease in this patient cohort and and levels of CD4+ and CD8+ lymphocytes, with patients who recovered showing a restoration of lymphocyte levels (He et al 2005). However, an earlier study of a cohort of 50 patients in Hong Kong did not observe a similar correlation between lymphocyte count and progression to ARDS (Peiris et al 2003a). In parallel to these results, it was found that BALB/C mice infected with a mouse-adapted strain of the virus developed a poor T-cell response (Zhao et al 2009). An adoptive transfer of SARS-CoV immune splenocytes from infected BALB/C mice or *in vitro* generated T-cells from these mice to severe combined immunodeficiency (SCID) or naïve BALB/C mice resulted in enhanced survival and reduced virus titers in the lungs of these mice, suggesting that T lymphocytes might be important for viral clearance *in vivo* (Zhao et al 2010).

Several studies on the cell-mediated immune response also examined immunological memory against SARS-CoV in recovered patients. Using a peptide library comprising fragments of different viral structural proteins to stimulate peripheral blood mononuclear cells (PBMCs) from recovered patients, it was found that central memory CD4+ and effector memory CD8+ were elicited in these individuals against the S, M, E and N proteins, suggesting that these responses were part of the response against initial infection (Peng et al 2006a, Peng et al 2006b, Yang et al 2006, Yang et al 2007). However, no comparison was made between these responses to determine the magnitude of the response to different structural proteins . It is also not known if these long-term memory responses would be sufficient in the event of re-infection.

3.3 APOPTOSIS IN SARS-COV INFECTION

Apoptosis is a genetically controlled form of eukaryotic cell death which is evolutionarily conserved, having been observed in an array of cell types from budding yeast to mammalian cells. The genetic coordination of apoptosis is seen in 3 different cellular pathways towards this end: 1) the intrinsic or mitochondrial pathway, 2) the extrinsic or death-receptor mediated pathway, and 3) the caspase – independent pathway which is mediated by the action of granzymes where the intrinsic and extrinsic pathways are dependent on the action of cellular proteases known as caspases. The hallmarks of apoptosis are a series of morphological events: nuclear condensation, DNA fragmentation, ‘blebbing’ of the plasma membrane and eventual phagocytosis. Apoptosis, as morbid as the implications of this term are, also has a role to play during the course of morphogenesis and development. However, apoptosis is also a valuable tool in countering microbial infection. Elimination of the infected cell and eventual phagocytosis is a known element of the immune response to infection.

Viral apoptosis is an intriguing aspect of the infection process, as viruses can induce apoptosis towards different, and opposing ends. Viruses may inhibit apoptosis in order to prevent the use of the apoptotic program by infected cells or immune cells to halt the spread of infection, and at

the same time, apoptosis may be a useful tool used by viruses either to neutralize cells of the immune system or to aid viral spread by the breakdown of infected cells (Best et al 2008, Galluzzi et al 2008). In SARS-CoV infection, viral apoptosis has been postulated to form part of the pathogenic mechanism of infection. One of the hallmarks of SARS-CoV infection was observed to be lymphopenia, as observed in studies of different patient cohorts (Wong et al 2003, Cui et al 2003, He et al 2005). It was subsequently suggested, by analogy to lymphopenia observed in measles infections, that apoptosis might be the underlying cause for this observed lymphopenia (O'Donnell et al 2003), although this was countered by the argument that the lymphopenia might have arisen out of adrenal insufficiency and glucocorticoid treatment (Panesar 2003). Evidence of apoptosis related to SARS-CoV infection was found though, in hepatocytes (Chau et al 2004) as well as in thyroid tissue (Wei et al 2007). The induction of apoptosis was also detected in Vero E6 mammalian cell cultures infected with SARS-CoV (Ren et al 2005, Yan et al 2004), and it was suggested that the phosphorylation of p38MAPK might be involved in this apoptotic induction (Mizutani et al 2004). However, the role that apoptosis might play in SARS -CoV infection was not clear. Inhibition of apoptosis in Vero E6 cells either by blocking p38MAPK phosphorylation or *Bcl-2* overexpression did not seem to have an effect on the replication of the virus but it was observed to reduce the cytopathic effect of infection (Bordi et al 2004, Mizutani et al 2004).

Despite this, the idea that apoptosis was a crucial part of SARS pathogenesis remained popular, and several laboratories published work that pointed to the pro-apoptotic nature of several SARS proteins, and in some cases there were indications that apoptosis had a distinct role to play in the function of a given pro-apoptotic SARS-CoV protein. The 3a protein of this virus was shown to induce apoptosis in Vero E6 cells (Law et al 2005) and this induction was linked to the mitochondrial death pathway though p38MAPK activation (Padhan et al 2008). In addition, blocking of the ion channel activity of the 3a protein abolished caspase-dependent apoptosis (Chan et al 2009). It was also shown that ER stress induced by the 3a protein resulted in PERK activation which in turn caused a downregulation of the interferon alpha 1 receptor (Minakshi et al 2009), suggesting that the pro-apoptotic nature of the 3a protein had a discrete function in terms of immune evasion. The 7a protein of SARS-CoV was also the subject of several studies on the induction of viral apoptosis. In addition to a demonstration of the pro-apoptotic activity of overexpressed 7a protein in Vero E6 cells (Tan et al 2004), it was also shown by the same group that this apoptotic activity is linked to its interaction with prosurvival proteins such as Bcl-XL, MCL-1, Bcl-2, Bcl-2w and A1 (Tan et al 2007). In addition, the 7a protein was also shown to inhibit cellular protein translation and initiate apoptosis via p38MAPK activation but not through JNK activation (Kopecky-Bromberg 2006). Construction of viruses with disruptions in the *ORF7* reading frames encoding for the 7a and 7b proteins showed a reduction in apoptotic induction by the virus as compared to the wildtytpe virus, indicating that these genes have a role to play in virus-induced apoptosis (Schaecher et al 2007). However, the same study also showed that deletion of ORF7 from the virus did not have an effect on viral replication or on the observations of early markers for apoptosis, but rather markers for the terminal stages of apoptosis such as DNA fragmentation, indicating that other proteins encoded within the SARS-CoV genome are responsible for induction of apoptosis by the virus. In this respect, 2 other accessory proteins have been observed to induce apoptosis. A GFP-tagged ORF6 fusion protein has been shown to induce apoptosis in Vero E6 cells via the induction of ER stress and the activation of the JNK pathway (Ye et al 2008) and a YFP-tagged ORF9b fusion protein was observed to induce caspase-dependent apoptosis when its active nuclear export was inhibited using Leptomycin-B (Sharma et al 2011). In the case of 9b, a causal relationship between protein function and apoptotic induction

was shown, albeit not in the classical sense as the inhibition of function led to the induction of apoptosis in this instance. Another such unorthodox observation of a causal relationship between the induction of apoptosis and protein function was observed for the nucleocapsid protein of SARS-CoV. Using caspase inhibitors specific to effector caspases, it was found that the N protein of SARS-CoV induced the intrinsic pathway of apoptosis and the resulting activated effector caspases cleaved the N protein. However, this phenomenon did not occur in all cell lines, only being observed in Vero E6 and A549 cells but not in CaCo2 or N2a cells (Diemer et al 2008).

3.4 NITRIC OXIDE

Nitric oxide in an important intracellular messenger involved in several cellular processes such as the modulation of blood flow, thrombosis, and neural activity. It also forms part of the host defense against pathogens, with documented antimicrobial activity against bacteria and some viruses. There exists a fine line between the physiological and pathological activity of nitric oxide. Nitric oxide by itself is relatively unreactive, which may go some way towards explaining its suitability as an intracellular messenger in diverse physiological processes. However, the reaction of nitric oxide (NO) with the superoxide ($O2^-$) anion produces peroxynitrite ($ONOO^-$), which is a potent reactive nitrogen species (RNS). The formation of peroxynitrite is thought to a spontaneous, constitutive reaction in steady-state physiology. However, the redox potential of peroxynitrite is governed by biological minimization of the compounds which form this reactive species. NO itself rapidly diffuses through tissues (another reason for its suitability as an intracellular messenger) into red blood cells where it forms nitrates by reacting with oxyhaemoglobin, effectively scrubbing available nitric oxide and limiting the half-life of this molecule. The superoxide anion is physiologically limited through the action of superoxide dismutase (SOD), an enzyme which catalyzes the breakdown of superoxide to yield oxygen and hydrogen peroxide. This also aids in protecting cells from the oxidative damage potential of superoxide radicals. The balance, then, between the physiological concentrations of both NO and $O2^-$ are rate-limiting for the spontaneous formation of peroxynitrite, and this limitation forms that fine line between physiology and pathology where reactive nitrogen species are concerned. One of the ways in which this fine line can be crossed is through the overproduction of nitric oxide by nitric oxide synthases (NOS).

There are 3 kinds of NOS enzymes, originally dubbed eNOS (epithelial NOS), iNOS (inducible NOS), and nNOS (neuronal NOS) - in light of their detection in tissues other than those they were named, for, these are now known as NOS-1, NOS-2, and NOS-3 respectively. These enzymes catalyze the oxidation of L-arginine to yield nitric oxide and L-citrulline. NOS-1 and NOS-3 are calcium sensitive, constitutively expressed nitric oxide synthases. NOS-2, however, is inducible and has a very low constitutive level of expression, and is triggered during periods of cellular stress, for example during the immune response to infection by bacterial, fungal and viral pathogens. The TLR signaling pathway activates NOS-2 expression by way of activated MAPKs and NFκB, and cytokines such as TNFα and IL-1β are also able to activate such expression as part of this response to infection. IFNγ is also able to activate NOS-2 expression via the JAK-STAT signaling pathway (Lowenstein & Padalko 2004). The expression of NOS-2 by these pathways then results in the overproduction of nitric oxide in order to tip the equilibrium in favor of peroxynitrite production, which is thought to mediate the effects of nitric

oxide (Pacher et al 2007). And in this regard, nitric oxide has been shown to exert antiviral effects on a number of viruses. Nitric oxide has been shown to exert antiviral effects on Japanese encephalitis virus (Saxena et al 2001), hantaviruses (Klingström et al 2006), Crimean-Congo haemorrhagic fever virus (Simon et al 2006), and even against SARS-CoV (Åkerström et al 2005). An interesting aspect of the antiviral activity of nitric oxide was shown in coxsackieviruses. Two different groups showed that nitric oxide was able to inhibit the 3C and 2A proteases of coxsackievirus by S-nitrosylation of a cysteine residue at the active site of each of these proteases (Saura et al 1999, Badorff et al 2000). It has been quite a while since the S-nitrosylation of proteins was described (Stamler et al 1992), but since then, it has been observed in a variety of intracellular processes, including the regulation of gene transcription by directly modifying transcription factors such as NFκB (Sha et al 2011).

In addition to the induction of NOS-2 expression by the immune system, such expression has also been shown to be induced directly by viruses themselves. The gp41 glycoprotein of HIV-1 and infection of A549 cells with respiratory syncitial virus have been shown to directly induce NOS-2 expression. It is believed that this sort of induction has a role to play in virus-induced cytotoxicity (Akaike et al 2000). Where pathogenicity did not involve the generation of nitric oxide by the virus to a cytotoxic end, the interactions of virus and host often induced sufficient levels of NOS-2, and thereby nitric oxide and reactive nitrogen species to induce cytotoxicity. It was shown that nitric oxide had a role to play in the pathogencity of influenza-induced pneumonia (Akaike et al 1996). Nitric oxide also has also been shown to be a pro-apoptotic factor, possibly in viral infections. Activated macrophages are thought to release large amounts of nitric oxide and superoxide, and this is believed to induce apoptosis in both the producing macrophages as well as in neighboring cells (Hortelano 1999). Even without the contribution of macrophages or viral infection, nitric oxide might be able to induce cytotoxic effects such as apoptosis and necrosis. S-nitrosylation of cysteine-450 on the RING domain of X-linked inhibitor of apoptosis (XIAP) was shown to inhibit its E3 ligase activity and thereby stabilize caspase-3, allowing for pro-apoptotic signaling in neurons (Nakamura 2010). Nitric oxide signaling has also been consistently observed to upregulate pro-apoptotic factors in the intrinsic pathway of apoptosis such as *TP53*, *Bax* and other pro-apoptotic members of the Bcl-2 family (Bosca et al 1999).

3.5 ANIMAL MODELS

In the course of the study of a microbe, the use of animal models is crucial. Animal models allow for for the study of systemic, pathologic characteristics of infection, as well as giving researchers insight into viral replication kinetics and the dynamics of viral spread within an organismal host. There is also valuable information to be gleaned about the host response at the systemic level, for example in the nature and magnitude of the immune and inflammatory response to such infection. Such information can be multi-faceted, from morphological studies to expression profiling of genes in different tissues. A second, yet equally important value of an animal model is that it allows for the evaluation of antiviral strategies and vaccines against a microbial pathogen, something which would only yield very limited information in a monolayer of cells. Given the urgency of the SARS epidemic and the realization of a definite zoonotic pattern of transmission, the need to study all these aspects of SARS-CoV infection as well as to evaluate novel antivirals and vaccines to prepare against future outbreaks, was of utmost importance.

The first demonstration of SARS pathology in an animal model was made in 2003, when cynomolgus macaques were infected with SARS-associated coronavirus (as it was originally dubbed after isolation from patients) passaged in Vero E6 cells. The infected macaques displayed pulmonary lesions and dysfunction similar to human patients, with the diffuse alveolar damage, necrosis of alveolar epithelium, multinucleated alveolar syncitia, and macrophage/neutrophil-containing proteinaceous lung exudate that was characteristic of the disease in humans. These pathological features allowed for the fulfillment of Koch's postulates, indicating that the SARS-associated coronavirus was the etiological agent of the disease (Fouchier et al 2003). The first attempt at a mouse model was reported shortly afterwards - BALB/C mice were infected with SARS-CoV to determine if the inbred mouse would prove a suitable model. Surprisingly, it was found that the mice showed little sign of pulmonary disease, and peak viral titers were achieved within the first 2 days post-infection before being cleared by day 7. Determination of immune response in the mice showed that neutralizing antibodies were developed, rendering them resistant to reinfection. Transfer of serum into naive mice was also able to confer resistance in these mice to virus challenge (Subbarao et al 2004). The same group also attempted to establish a mouse model in a different inbred mouse strain, C57BL/6. Similar to observations in the BALB/C mice, the virus was cleared within 9 days of infection, with peak titer established at day 3. It was observed that several pro-inflammatory chemokines were upregulated, along with their cognate receptors; however pro-inflammatory cytokines were not observed to be upregulated, and levels of pulmonary dysfunction remained low (Glass et al 2004). A subsequent model of pathogenesis was eventually found in aged BALB/C mice, which was based on the idea that advanced disease was observed in aged patients as compared to other age groups. Infection of aged BALB/C mice showed similarities to human disease, and early upregulation of pro-inflammatory cytokines such as IFNα, IFNγ, and TNFα which the researchers postulated to be responsible for pathological differences between these mice and previous attempts at adolescent BALB/C and B6 mice (Roberts et al 2005a). A second study on these aged mice also demonstrated an interesting pattern of cytokine production in aged mice - while the initial observations of pro-inflammatory cytokine production concur with the original study, at around day 7 post-infection a second wave of pro-inflammatory cytokine production was observed, with concomitant infiltration of T-lymphocytes. This second wave was found to be dependent on CD4+ T cells (Chen et al 2010).

While the various attempts at a mouse model were being worked out, a separate study using both cynomolgus and rhesus macaques found little correlation between pulmonary and systemic disease in these macaques and the previous studies of SARS-CoV infection in cynomolgus macaques which were used to fulfill Koch's postulates (Rowe et al 2004). What was found, though, was that there were pathological differences between rhesus and cynomolgus macaques, with more advanced signs of disease in cynomolgus macaques. The study also highlighted that technical differences in the execution of the animal studies could have an effect on observations of pathology and thereby in the interpretation of these observations in terms of SARS-CoV pathology in these macaques. It was suggested that pathology was more pronounced at the earlier timepoint of 4-6 days post-infection used by other groups, and at later timepoints such as 12-14 days post-infection, the infection (along with pathology) is largely resolved, leading to the interpretation that cynomolgus macaques only display mild lung pathology.

An interesting approach to the generation of a SARS animal model was shown with the report of SARS-CoV infection of a mouse line transgenic for the human ACE-2 receptor. Infection of this transgenic line resulted in consistently higher viral titers than in non-transgenic control mice, and

lethality occurred in almost all mice within 5 days post-infection. Upon examination of mice, it was found that the lungs and brains were the major sites of viral replication. Histologic examination of lungs showed the characteristic diffuse alveolar damage seen in SARS patients, and proinflammatory cytokines and chemokines such as IL-1β, RANTES and MCP-1 were observed to be upregulated in the lungs of these mice (Tseng 2007). But the problems with this transgenic line were evident in the high levels of pathology in the brain, which seemed to make a significant contribution to mortality, and the observation that a similar transgenic line with a lower hACE-2 expression level showed lesser pathology with the eventual recovery of infected mice. The results of this study could simply be interpreted as the consequences of the level to which cell lines are permissive to infection with a particular virus - the mouse line with higher hACE-2 expression underwent a greater level of mortality and a low level of viremia where the line with lower levels of hACE-2 showed no viremia and lower levels of mortality. This study could help explain the results from the previous studies performed with juvenile BALB/C and C57BL/6 nice.

While these animal models proved useful in highlighting aspects of SARS-CoV pathology, their underlying purpose is considerably more important - the evaluation of potential antivirals and vaccines in a mammalian organism. Several different groups have attempted to evaluate vaccine candidates in animal models of SARS-CoV infection in order to arrive at some measure of their efficacy either as therapeutic or prophylactic agents. One of the first uses of animal models to this end was the evaluation of recombinant adenoviruses encoding the SARS-CoV structural proteins S, M and N in evoking an immune response in rhesus macaques. Intramuscular immunization of the macaques with a combination of all three recombinant adenoviruses was observed to generate neutralizing antibodies which were shown to inhibit lysis of SARS-CoV infected Vero E6 cells. No challenge experiment was performed, with the authors citing the need for a clinically relevant animal model (Gao et al 2003). Since then, several groups have attempted to evaluate vaccination strategies and vaccine candidates in different species, chiefly among them inbred mice. Mice immunized with a fusion protein comprised of the receptor-binding domain of the SARS-CoV S protein elicited protective effects in a mouse challenge model (Du et al 2007), and a prime-boost strategy using T-cell-specific S-protein epitopes was found to elicit both CD4+ and CD8+ T lymphocyte responses in mice (Huang et al 2007). Some groups also examined the use of recombinant viruses as vaccine delivery systems, such as modified vaccinia Ankara (Bisht et al 2004) and vesicular stomatitis virus (Kapadia et al 2004) expressing the S protein. One study even compared the protective response elicited by S and N-expressing recombinant adenoviruses against whole killed virus in a mouse challenge model (See et al 2006). While the results of these vaccine experiments are promising, the mouse model used by most of these groups has not been shown to be clinically relevant, as different juvenile mouse models have been observed to show no overt signs of disease (Roberts et al 2008).

In addition to the mouse models, a hamster model of SARS was shown using Golden Syrian hamsters. Infection of hamsters was observed to peak around 2 days post-infection, with eventual clearance of virus about a week later. While no overt signs of clinical disease were observed, lung histology showed similarities to pathological manifestations observed in human patients, and persistence of viral infection was longer than in juvenile mouse models. Hamsters were also shown to produce neutralizing antibodies against the virus, and were resistant to reinfection (Roberts et al 2005b). This model was used to evaluate the therapeutic potential of a human monoclonal antibody against SARS-CoV (Roberts et al 2006), and also to evaluate the immunogenicity and efficacy of a live attenuated virus lacking the E gene (Lamirande et al 2008).

4 RESULTS AND DISCUSSION

4.1 CELLULAR EFFECTS OF THE ORF6 PROTEIN (PAPERS I, III, IV)

The ORF6 protein of SARS-CoV is a relatively small gene of just 63 amino acids. Initial characterization of this protein showed that it was found to be expressed in the lungs and intestinal tracts of SARS patients, and that at the cellular level, this expression was localized to the endoplasmic reticulum, by means of colocalisation studies using a ORF6-GFP fusion protein and a dsRed marker for the ER (Geng et al 2005). Another study performed at around the same time, using reverse genetics to selectively remove accessory genes from the SARS-CoV genome, showed little effect on virus replication in most cells when infected with a recombinant SARS-CoV lacking ORF6, suggesting that the *ORF6* gene encoded for a protein of nonessential function (Yount et al 2005). However, the OR6 protein attracted a lot of interest when it was shown that a recombinant neurotropic mouse hepatitis virus (strain JHM) encoding the ORF6 gene turned an otherwise sublethal infection of the wildtype virus into a fully lethal infection, increasing virus titer by $10^{1.5}$ (Pewe et al 2005). This finding suggested that the ORF6 protein might indeed have a role to play in viral replication. While the effect seen might not be due to a direct effect on viral replication, it might have been due to a virus-host interaction that was beneficial to viral replication. This observation of a stimulatory effect on MHV replication piqued the interest of several groups working on SARS accessory proteins, ourselves included.

We set about to characterize the interaction of ORF6 protein with other SARS proteins to examine the possibility that an interaction between ORF6 and another viral protein might have an effect on replication. In Paper I, a yeast-two-hybrid assay was used to examine a subset of such potential interactions, and found that ORF6 interacted with the nsp8 protein of the virus. In order to further study this interaction, an in vitro, cell-free transcription/translation system expressing His6-nsp8 and myc-ORF6 was set up in rabbit reticulocyte lysates. Using antibodies against both the His6 and myc epitope tags, it was determined that both proteins were co-immunoprecipitated with the use of each of these antibodies, indicating that these 2 proteins did indeed interact. Given that the co-immunoprecipitation experiment was performed in a cell-free system expressing these 2 proteins, the result also indicated that the ORF6 and nsp8 proteins interacted directly. In a system that utilized mammalian cells, such a confirmatory experiment would cast doubt on whether the interaction was direct as the possibility would exist that an intermediary factor could bind both proteins, showing an interaction, albeit not necessarily a direct one.

Next, mammalian expression constructs were made to express ORF6 and nsp8 in mammalian cells. Vero E6 cells were co-transfected with these constructs, which expressed untagged ORF6 and myc-nsp8. Co-immunoprecipitation experiments using a rabbit antibody against the ORF6 protein and a mouse monoclonal antibody against the myc tag fused to nsp8 showed that ORF6 did not co-immunoprecipitate with a control myc-GST protein, but did indeed co-immunoprecipitate with myc-nsp8. Given this, we sought to determine if the 2 proteins interacted when expressed from SARS-CoV during the course of infection. Vero E6 cells were infected with SARS-CoV for 24 hours or uninfected and lysates were subjected to immunoprecipitation using a rabbit polyclonal antibody against the ORF6 protein. Western blotting using a monoclonal antibody against the nsp8 protein showed that ORF6 and nsp8 interacted when expressed from

SARS-CoV, and presumably, therefore, interacted during the course of infection. We also tried to determine if the 2 viral proteins colocalised in infected cells. The same antibodies that were used for the co-immunoprecipitation experiments were also used to examine the colocalisation of the ORF6 and nsp8 proteins in SARS-CoV-infected Vero E6 cells, and it was observed that the 2 proteins did indeed colocalise in infected cells. This colocalisation was particularly interesting – it has been shown that coronavirus replication complexes localize to intracellular double-membrane vesicles which are a subset of the vesicular trafficking system (Jackson et al 2005). The SARS-CoV replication complex has also been shown to localise to punctate structures in infected cells (Prentice et al 2004). Given this, we sought to determine if the site of ORF6-nsp8 colocalisation was indeed the same vesicular structures. According to Jackson et al, Lamp1 is a marker for the replication machinery for coronaviruses, and using a monoclonal Lamp1 antibody, we showed that ORF6 colocalised with Lamp1 in SARS-CoV infected cells. Taken together, these results illustrate that the ORF6 protein might exert its effect on SARS-CoV replication by interaction with the replicase complex of ORF6. The nsp8 protein has been shown to act as a primase, generating short oligonucleotides of less than 6 residues for priming viral RNA synthesis (Imbert et al 2006), and subsequent work has shown that features of the nsp8 protein important to this function are conserved in other coronaviruses, including MHV-A59 (Li et al 2010). Given this, it seems likely that the stimulatory effect of ORF6 on viral replication might rely on its interaction with the nsp8 primase, both in SARS-CoV and MHV infection.

Another function of ORF6 was elucidated by the demonstration that it could function as an interferon antagonist. Using a plasmid construct expressing ORF6, it was shown that 293T cells infected with Sendai virus, a known inducer of the interferon response, failed to synthesis IFNβ. This was subsequently shown to be due to the inhibition of IRF-3 phosphorylation (Kopecky-Bromberg et al 2007). In addition, it was shown that ORF6 could interact with karyopherin α2 (KPNA2), which forms part of the importin-β superfamily of nuclear import factors. This interaction was deemed to have inhibited the nuclear translocation of STAT-1, which is dependent on KPNA1, another import factor that competes with KPNA2 for a crucial KPNB1 factor to achieve nuclear translocation. The nuclear import of STAT1 transduces the IFNβ signal and initiates a transcription cascade of interferon-sensitive response elements (ISREs) in order to initiate the antiviral response (Frieman et al 2007). We had observed, around this time, that the ORF6 protein had an unusual downregulatory effect on the expression of genes from co-transfected plasmids. Transfection experiments in Vero E6 cells coupled with Western Blotting using relevant antibodies against ORF6 and myc-tagged nsp8 or GST showed that 1) ORF6 downregulates the expression of *myc-nsp8* and *flag-GST*, 2) this effect was dose-dependent, and 3) the effect seems to be specific to ORF6 as flag-GST titrated against myc-nsp8 by transfection did not result in a downregulation of myc-nsp8 expression. Given that ORF6 could downregulate the expression of 2 different transgenes with 2 different epitope tags, it was unclear if this effect might be global. In order to address this, we transfected Vero E6 cells with different amounts of ORF6-expressing plasmid or empty plasmid and labeled the cells with ^{35}S at 16 hours post-transfection. Radiolabelled lysates were PAGE-separated and exposed to film. The resulting autoradiographs showed that no significant change was observed in total protein production between cells that had been transfected with ORF6 or cells that had been transfected with empty vector. Therefore the effect of ORF6 on myc-nsp8 was not a global one, yet as the downregulation of flag-GST showed, not specific to nsp8 either.

While the downregulatory effect of ORF6 on co-transfectant expression was clear, it was unclear if this effect manifested itself at the transcriptional, translational or even post-translational level. In

order to address this, we examined *nsp8* mRNA levels in Vero E6 cells that has been transfected with mammalian expression constructs expressing either *ORF6* or *myc-nsp8*. Quantitative realtime PCR analysis of *nsp8* mRNA levels showed a significant reduction, using specific primers targeting *nsp8* and SYBR Green chemistry. This indicated that the effect of ORF6 on transgene expression manifested itself at the transcriptional level. In the context of findings that ORF6 inhibited STAT1 mediated nuclear translocation (Frieman et al 2007), this was very interesting as the promoter used in our mammalian expression constructs was a CMV promoter, and required nuclear translocation in order to drive transgene expression. It might be possible that the CMV promoter required KPN-mediated nuclear translocation (Lischka et al 2003), and given what has been shown with regard to the perturbation of KPN-mediated activity by the ORF6 protein, these results are consistent with such a model. Indeed, it has been observed that ORF6 is able to impede expression of transgenes encoded in constructs requiring nuclear translocation for expression (Hussain et al 2008).

In order to dissect the ability to the ORF6 protein to selectively impede nuclear translocation, we mutated select motifs in the ORF6 protein. Using the CBS prediction server (www.cbs.dtu.dk/services/), a few select regions of interest were identified from the amino acid sequence of the ORF6 protein. 2 of these, a putative lysosomal targeting motif *YSEL* from amino acids 49-52, and a putative diacidic motif *DDEE* from amino acids 53-56, were substituted with alanine residues and resulting mutants were assayed for their ability to impede the nuclear translocation of a mammalian expression plasmid encoding myc-nsp8 and thereby its expression. Western Blotting of lysates from cells co-transfected with *ORF6A53-56*, but not *ORF6A49-52*, showed a decrease in the impedance of nsp8 expression as compared to cells that had been co-transfected with wildtype ORF6 and myc-nsp8. However, this difference in impedance was deemed to be too small to be entirely certain that the ORF6A49-52 mutant did not exhibit a decreased impedance of myc-nsp8 expression when examined by Western Blotting. In order to generate quantitative data that would better highlight the differences in impedance between wildtype ORF6 and its 2 mutants, we employed the use of QPCR to examine the difference in myc-nsp8 mRNA levels between Vero E6 cells that had been co-transfected with myc-nsp8 and either ORF6 or the 2 mutants. It was observed from the QPCR results that the difference, while more evident, was not convincing. In order to strengthen the determination of these differences, we repeated the experiment 5 times and the resulting differences in *myc-nsp8* mRNA levels as compared to cells which were not transfected with ORF6 was subjected to a Student's two-tailed T-test. The T-test showed that the difference in impedance was significantly different in cells transfected with ORF6A53-56, but not in cells that had been transfected with ORF6A49-52, although a discernible difference was also observed in these cells. These results indicated the diacidic motif *DDEE* from amino acids 53-56 in the C-terminal of the ORF6 protein is involved in its ability to impede nuclear translocation.

It has also been shown that the ORF6 protein induces membrane rearrangements in mammalian cells (Zhou et al 2010). We had also previously observed the localization of ORF6, and the np8 replicase protein, to punctate structures in SARS-CoV-infected Vero E6 cells in Paper I of this thesis. To determine if the expression of ORF6 in our system could induce similar membrane rearrangements, we examined the localization of ORF6 in Vero E6 cells transfected with a mammalian expression plasmid expressing ORF6. It was observed that ORF6 did indeed localize to vesicles in these cells, and we determined that these vesicles were positive for Lamp1, as observed in infected cells, as well as CD63, a marker for late endosomes. It was not clear if these vesicles were induced by ORF6, as has been previously suggested (Zhou et al 2010) or simply a

pre-existing site of ORF6 localisation. If these vesicles were indeed induced by ORF6, mutants which might be able to disrupt this putative function would also alter the subcellular localization of ORF6 as well as possibly the morphological characteristics of these vesicles. With this in mind, the same ORF6 alanine substitution mutants *ORF6A49-52* and *ORF6A53-56* were transfected into Vero E6 cells and analysed by confocal microscopy, using a rabbit polyclonal antibody against ORF6. It was observed that in the ORF6A49-52 mutant, which disrupts a putative lysosomal targeting motif, no obvious difference in morphology was observed, only a slightly more diffuse cytoplasmic localization. The ORF6A53-56 mutant, however, showed a more dramatic difference in localization, with clusters of vesicles positively stained for the ORF6 antibody. While this finding suggests that the diacidic motif of the ORF6 protein exerts some influence over its subcellular localization, given that this same mutant was observed to significantly alter the ability of the ORF6 protein to impede nuclear translocation, the finding also suggests that the subcellular localization of the ORF6 protein is linked to its ability to impede nuclear translocation. A previous study which looked at the membrane rearrangement by ORF6 suggested on the basis of N-terminal mutants that the N-terminal was sufficient for this function (Zhou et al 2010). With this study, we show that motifs at both termini of the protein might exert an effect on the same functions, and that the 2 halves of the protein do not necessarily carry out independent functions, as was previously suggested (Zhou et al 2010). More evidence of this comes from the same study that examines the ability of ORF6 to impede the nuclear translocation of STAT1 by interaction with KPNA1 (Frieman et al 2007). It was shown in this study that an alanine substitution mutant, ORF6Ala54-58, had an effect on ORF6-mediated impedance of STAT1 nuclear import. This mutant disrupts the same diacidic motif that was observed in our study to decrease the ORF6-mediate impedance of nuclear import as well as its subcellular localization, suggesting that perhaps the localization, or generation of vesicles the ORF6 protein is linked is some way to its ability to impede nuclear transport. Interestingly, several groups had previously looked at ORF6 subcellular localization (Geng et al 2005, Pewe et al 2005, Frieman et al 2007, Netland et al 2007, Zhou et al 2010). All of these groups reported the localization of the ORF6 protein, in a variety of different conditions and utilizing a variety of cellular/infection systems, to be confined to the ER and Golgi compartments. However, none reported any change in subcellular localization of the ORF6 protein caused by mutating any residues on the protein or by deletion of specific C-terminal regions of the protein. None of these studies have also reported the localization of the ORF6 protein to any compartment other than those in the ER or Golgi, although none had reported the use of any markers for other cellular compartments besides dsRed, giantin or other markers for these compartments. A crucial difference between these studies and ours seems to be that most other studies examining the subcellular localization of ORF6 used a GFP tag fused to the ORF6 protein. In our studies, we used an untagged ORF6 protein in our constructs because it had been determined that a commercially available rabbit polyclonal antibody against ORF6 was suitable for detection by both Western Blotting as well as immunofluorescence. The use of an untagged ORF6 protein might explain the differences between our observations.

The generation or subversion of intracellular vesicular populations is a running theme in the study of virus-host interactions. Various viruses have been observed to utilize vesicular populations in several viral infections. For example, proteins from several picornaviruses have been observed to localize to intracellular vesicles, such as polioviruses and coxsackieviruses. The flavivirus Hepatitis C virus has also been observed to utilize vesicles for replication (Pierini et al 2009). The use of intracellular vesicles presents advantages for viral replication: vesicles could provide a microenvironment for viral RNA synthesis, provide an anchoring point or scaffolding for viral replicase complexes, and aid in concealing viral RNA intermediates, from recognition by the host.

Interestingly, similar observations of subversion of vesicular populations have been observed for coronaviruses. It has been shown that MHV replication complexes localize to double membrane vesicles (Gosert et al 2002) and subsequently it was suggested that these vesicles might have their origins in cellular autophagy (Prentice et al 2004b), although this claim has been contested by others (Zhao et al 2007). One of the earliest studies of SARS replicase proteins showed the colocalisation of nsp8 with the LC3 protein, which is a marker for cellular autophagy (Prentice et al 2004). The implications of this are that like a few other viruses, SARS-CoV might induce autophagy in order to generate vesicles for viral replication. But a later study examined the colocalisation of SARS replicase proteins with GFP-tagged LC3 expressed from a mammalian expression plasmid and found no evidence of colocalisation (Snijder et al 2006). The researchers suggest instead that SARS replication vesicles (the existence of which was confirmed using electron microscopy of SARS-CoV infected Vero E6 cells) are derived from the ER. In this vein, the localization of the ORF6 protein is similarly contentious, with most groups reporting ER/Golgi localization as opposed to our findings of colocalisation with Lamp1 in SARS-CoV infected cells and Lamp1 and CD63 in cells transiently transfected with a plasmid encoding ORF6. The finding that nsp8 was able to colocalise with a marker for the LC3 protein was indeed received with great interest; however, as several groups have pointed out, the LC3 antibody resulted in high background and difficulty in imaging, something which we had also encountered. Our use of a GFP-LC3 plasmid to determine if the ORF6-positive vesicles were of autophagic origin proved inconclusive (data not shown), and identity of the ORF6-positive vesicles remains uncertain. One possible approach to study vesicle generation by the ORF6 protein comes from a recent study that suggests MHV is dependent on EDEMosomes, part of the cell's ER associated degradation pathway (ERAD) for generating a vesicular population for viral synthesis (Reggiori et al 2010). EDEMosomes are positive for nonlipidated LC3 (the pre-autophagic precursor of LC3) and yet do not form part of the cellular autophagic machinery, failing to colocalise with GFP-LC3. The eventual destination of these degradatory vesicles is late endosomes, although this pathway is poorly characterised. This might help to explain the colocalisation of LC3 with SARS nsp8 (Prentice et al 2004) and reconcile this with an apparent lack of autophagic markers colocalising with these viral proteins. Until further experiments can be done, the possibility that this might represent the origin of ORF6-positive vesicles remains just a possibility, albeit an exciting one.

Adding to the plethora of cellular functions attributed to the ORF6 protein, it was demonstrated that ORF6 could induce ER stress in cells, along with JNK- and caspase-dependent apoptosis (Ye et al 2008). A similar, albeit independent observation was made in our group, by employing the use of fluorometric detection kits for caspase activity in Vero E6 cells that had been transiently transfected with ORF6. In order to further characterise the induction of apoptosis by ORF6, in Paper IV of this thesis we decided to examine the differential expression of host apoptotic genes in cells expressing ORF6. Several medium to high throughput technologies exist for the purpose of examining the differential expression of genes in a system, such as microarrays, deep sequencing, and QPCR arrays. The study of differential expression of genes in a system using these technologies allows for the determination of mechanisms leading to changes in cellular physiology at the transcriptional level, although such examination at the protein level is also possible with these systems. In order to identify differentially expressed genes in these systems, it is necessary to achieve a comprehensive background of expression of, in this instance, the ORF6 gene. Typically the introduction of transgenes into mammalian culture systems uses various chemical or electrical transfection systems to transport an expression plasmid encoding the gene of interest across the plasma membrane of the host cell. While this method has enjoyed substantial popularity for its ease of use and reliability, the efficiency of transfection varies from cell line to

cell line, and is typically observed to be around 50-70 percent, which is deemed suboptimal for the requirements of expression profiling of a cell population. One approach to achieving this expression background would be to employ the use of a recombinant virus, which would infect target cells and express a gene of interest. For these purposes, however, the contribution of the virus to host gene changes could potentially complicate the results of the analysis. Keeping this in mind, we prepared a recombinant vaccinia virus encoding the *ORF6* gene, dVV-L-ORF6 in order to create a thorough expression background. This defective vaccinia virus is derived from the Lister strain, and is replication-defective owing to the deletion of a crucial uracil DNA glycosylase from the D4R locus of the virus genome. This D4R locus is replaced with a recombination cassette allowing for genes of interest to be recombined into the virus genome for expression (Holzer and Faulkner 1997). In parallel to the recombinant vaccinia virus expressing ORF6, a second, empty vaccinia virus dVV-L-empty was prepared to serve as a control for vaccinia-induced background.

In order to assess the functionality of virally-expressed ORF6 from this vaccinia system, in particular its ability to induce caspase-dependent apoptosis, we infected Huh7 and Vero E6 cells with either dVV-L-empty or dVV-L-ORF6. A third virus, dVV-L-7a, expressing the known pro-apoptotic 7a gene from SARS-CoV, was used as a positive control for apoptosis. Using a fluorometric assay for caspase activity, we determined that both ORF6 and 7a expressed from recombinant vaccinia viruses were able to induce capase-dependent apoptosis, as compared to the empty virus. This indicated that the ORF6 protein as expressed by the vaccinia system was functionally intact, and allowed us to proceed with characterization. Because of their ability to undergo caspase dependent apoptosis from a much earlier timepoint (12 hours) as opposed to Vero E6 cells which only showed significant caspase activity at 24 hours post-infection, Huh7 cells were infected with dVV-L-ORF6 at an MOI of 5, with total RNA extracted at 6, 12 and 24 hours post-infection. Following reverse transcription, total cDNA was subjected to analysis using a commercially available QPCR array for apoptosis containing primers for 84 human genes involved in either the positive or negative regulation of apoptosis. Analysis of fold changes in these apoptotic genes following a second experiment serving as a biological replicate revealed the differential expression of a total of 14 genes. In order to validate these genes, we employed the use of quantitative realtime PCR (QPCR) using pre-fabricated Taqman-based assays specific to each of the 14 genes. The validation results indicated that a total of 7 genes were reproducibly upregulated or downregulated as a result of ORF6 expression in the host cell population. These genes were observed to fall into 2 categories – *BNIP3*, *CIDEB*, *DAPK1* and *TP53* form part of the intrinsic or mitochondrial death pathway and *GADD45A*, *LTA* and *TNF* form part of the extrinsic pathway of apoptosis. The results here pointed to a possible induction of the apoptotic pathway by the ORF6 protein via the extrinsic pathway, given the upregulation of TNF and the concomitant downregulation of the *TP53* gene, which is considered the master regulator of the mitochondrial death pathway. Indeed, the upregulation of the *TNF* gene is very interesting, as it points to a JNK-dependent mode of apoptotic induction, consistent with previous findings (Ye et al 2008). In order to assess if these observed transcriptional changes were consistent with ORF6-mediated apoptosis in other cell lines, we used the same validation gene assays to examine the differential expression of these genes in Huh7.5 and CaCo2 cells which had been similarly infected with either dVV-L-ORF6 or dVV-L-empty. The results were largely consistent with what we had observed in Huh7 cells, although there were a few interesting differences. Where the *FAS* gene was observed to be downregulated in Huh7, it was observed to be upregulated in Huh7.5 as well as CaCo2 cells. The same extrinsic-pathway genes observed to be upregulated in Huh7 cells were also observed to be upregulated in these cell lines. On the other hand, the *TP53* gene was observed to be upregulated

in CaCo2 cells. While the level of upregulation was low, given the magnitude of downregulation in other cell lines, this result was surprising. However, put together, the results suggest that ORF6 activates the extrinsic pathway of apoptosis, in more than just one cell line.

A previous study of ORF6 apoptosis showed that ORF6 induced JNK-dependent, caspase-3 mediated apoptosis. We have observed from the fluorometric caspase assays that in our vaccinia expression system, ORF6 is able to induce caspase-3 dependent apoptosis as well. The observation that a few genes from the extrinsic pathway of activation were upregulated matches the JNK-dependence observed by others. The *TNF* gene, which has been observed in this study to be upregulated, is a known transcriptional target of both JNK and p38 MAPK, which are both mediators of apoptotic signaling in either direction – pro and anti-apoptotic, but in this case, pro-apoptotic. From here, the binding of TNFα to the TNF receptor initiates the activation of caspase-8, which eventually results in the execution of the death program by the activation of executor caspases such as caspase-3. However, pro-apoptotic signaling by JNK can occur via both the extrinsic or intrinsic pathways. While it was observed that one member of the intrinsic pathway, *BNIP3*, was reproducibly upregulated, a key component of the intrinsic pathway, the *TP53* gene, was observed to be significantly downregulated in cells expressing ORF6. This could mean that ORF6 induces apoptosis exclusively via the extrinsic pathway, but it could also mean that ORF6 could activate the intrinsic pathway of apoptosis independently of *TP53*, along with a concomitant activation of the extrinsic pathway. In order to shed further light on this mode of activation, the protein levels of proteins involved at this stage of apoptotic signaling need to be examined. This especially applies to p53, the protein product of the *TP53* gene, as it cannot be assumed that a lack of *TP53* transcription equates to a loss of p53 activity.

While the QPCR array examining apoptotic genes gives us an idea of the transcriptional changes occurring in these pathways, it is limited in its format (current restrictions of the QPCR plates limits the number of genes to a maximum of 384) and cannot yield information on cellular processes that might be activated upstream of the apoptotic pathway which might lead to ORF6-mediated apoptosis. In order to examine the cellular transcriptional changes in cells expressing ORF6, a portion of total RNA was used from the QPCR array experiments and subjected to microarray analysis using a commercially available microarray chip containing gene-specific probes corresponding to the human genome. Following data normalization and fold change calculations, we sought to compare the microarray data to the QPCR array data by direct comparison of fold changes in the 7 validated apoptotic genes from the QPCR array. It was observed that the fold change trends for these genes from the microarray concurred with those from the QPCR array: *CIDEB*, *DAPK1* and *TP53* were observed to be downregulated and *BNIP3*, *GADD45A*, *LTA* and *TNF* were observed to be upregulated. A fold change threshold of 5 was selected and genes exhibiting fold changes of greater than 5 or lesser than -5 were intersected between 2 biological replicates to arrive at a list of genes which were reproducibly differentially expressed in ORF6-expressing cells relative to cells infected with the empty vaccinia virus. A functional profile of these genes was then obtained using DAVID, an online toolset for gene functional assignment from microarray data ((*http://david.abcc.ncifcrf.gov*) with parameters accordingly set to yield high-level functional assignments for each gene, clustering the results by pathway. Similarities were observed between the clusters for functional assignments of upregulated and downregulated genes, suggesting that ORF6 had an effect on specific cellular pathways. Interestingly, it was observed that 3 candidate genes which were downregulated according the microarray results were annotated as being related to (positive regulation of apoptosis). These genes were not represented in the QPCR array, but remain of interest given their

putative function.

The results of the functional analysis of the microarray study, while yielding a myriad of different pathways, exhibited a very interesting commonality – these were largely calcium-dependent processes. The presence of so many pathways that are calcium-dependent points to a possible upregulation of calcium in cells infected with dVV-L-ORF6. A great deal of published work has implicated calcium levels in the ER as a putative 'trigger' that initiates apoptotic signaling. Such work has also shown that JNK activation in apoptotic cells correlates to sustained elevated ER calcium levels, leading to the transcriptional activation of *TNF*, downstream signaling of the TNF receptor and subsequent caspase recruitment and activation (Brnjic et al 2009). This observation of elevated ER calcium levels corresponds to the activation of the ER stress pathway, which has been observed in the induction of apoptosis by different viral proteins, including the 3a protein of SARS-CoV (Law et al 2005, Minakshi et al 2009). Consistent with this model, we have observed the upregulation of several genes related to calcium influx and the cellular response to calcium such as *CACNA1D*, *CACNA1E*, *CACNA1F*, *CACNA1G*, *and CACNA1S*, which encode for subunits of L-type calcium channels and other genes involved in the transduction of calcium signals such as *CAPN3* (calpain 3). Taking these results together, a putative picture of ORF6-mediated apoptosis begins to emerge: ER stress results in elevated calcium levels in the ER, invoking JNK activation which in turns transcriptionally activates *TNF* and consequently other members of the extrinsic pathway, resulting in caspase-3 dependent apoptosis. However, it must be taken into account that these candidate genes from the microarray have not been validated, and with the gene lists being quite long (>200 genes), candidates for validation should be deliberated. Also, ER stress has not been directly observed in this study, although examining GRP78 or GRP94 protein levels should address this uncertainty. Lastly, and quite importantly, most apoptotic signaling occurs at the protein level and not at the transcriptional level, and involves several protein-modification steps such as phosphorylation and proteolytic cleavage of precursors of apoptotic proteins leading to their activation or inhibition. It would prove quite useful to examine the protein products of genes involved in the induction and regulation of apoptosis in order to arrive at a clearer picture of this process.

4.2 MECHANISMS OF INHIBITION BY NITRIC OXIDE (PAPER II)

Work done by several groups has shown that nitric oxide and its derivatives have an effect on the replication of several viruses that can be either stimulatory or inhibitory. It was shown that SARS-CoV is one such virus that is affected in an inhibitory manner. The use of S-nitroso-N-acetyl penicillamine (SNAP) was observed to cause a dose-dependent reduction in SARS-CoV titer, with a concomitant reduction observed in the expression of viral proteins, as exemplified by an observed reduction in expression of the N protein. It was shown that cytokine-dependent NOS-2 activation reduced viral yield significantly, suggesting that NOS-2 activation held antiviral potential against SARS-CoV (Åkerström et al 2005). Mechanistically, this suggests a potential action of peroxynitrite ($ONOO^-$), which is formed by the rapid reaction of superoxide ($O2^-$) and nitric oxide (NO). The use of increasing concentrations of SIN-1, a peroxynitrite donor, in Vero E6 cells infected with SARS-CoV showed no discernible effect on virus titer, suggesting that peroxynitrite did not have a role to play in the inhibition of SARS-CoV replication by nitric oxide. Moreover, a superoxide scavenger MnTBAP, when used in conjuction with SIN-1, was observed to restore the inhibition of viral replication as determined by virus titer. Because the formation of

peroxynitrite is a reversible reaction, the scavenging of superoxide shifts this reaction in the direction of excess nitrix oxide production. This result indicated therefore that the inhibition was due to nitric oxide or another derivative of this compound, rather than peroxynitrite.

The inhibition of SARS-CoV replication by nitric oxide or its derivatives could manifest itself at several different steps in the viral life cycle, beginning with the process of infection itself, where the S protein of the virus binds to its cognate ACE-2 receptor and undergoes endocytosis into the host cell. To examine the possibility that the S protein might be affected by nitric oxide, we treated cells infected with a replicative recombinant vaccinia virus expressing the S protein (rVV-L-S) and treated these cells with either SNAP or NAP. Nitrotyrosine immunoprecipitation was able to pull down the S protein from lysates, indicating that the S protein was indeed reacting with nitric oxide when infected cells were treated with SNAP. However, there are 2 different residues which can react with nitric oxide or its derivatives. In addition to tyrosine nitration, which allowed for the pulldown of the S protein, cysteine residues on the S protein are also able to react with nitric oxide-based compounds. The S protein of SARS-CoV is known to undergo a few post-translational modifications such as glycosylation and palmitoylation. Of these palmitoylation, which is the addition of a 16-carbon saturated fatty acid chain, is interesting as palmitate links to the S-protein via thiol groups on cysteine residues, and has been implicated in membrane fusion by the S protein after receptor binding (Petit et al 2007). In order to determine if palmitoylation of the S protein was affected by nitric oxide, Vero E6 cells infected with rVV-L-S were treated with SNAP, NAP, SIN-1 or SIN-1 with MnTBAP and labeled with [^{3}H]-palmitic acid. Subsequent pulldown of labeled S using a rabbit polyclonal antibody against this protein showed that the amount of palmitoylated S was noticeably reduced in cells treated with SNAP, as compared to cells which had been treated with NAP or left untreated. SIN-1 treatment was not observed to have an effect on S palmitoylation, an effect that was restored with the combined use of SIN-1 and MnTBAP. These results indicated that the palmitoylation of the S protein was indeed adversely affected by nitric oxide or its derivatives, and additionally, that peroxynitrite did not have a noticeable effect on this modification. The functional consequence of the interference of nitric oxide on this modification was examined using a cell-cell fusion assay based on the fusion of 293T cells stably expressing S with Chinese hamster ovary (CHO) cells stably expressing the ACE-2 receptor (Lip et al 2006). The treatment of S-expressing cells with SNAP was observed to inhibit the formation of syncytia where similar cells treated with NAP were not hindered in terms of cell-cell fusion.

While it had been shown that nitric oxide or its derivatives might have an effect on the post-translational modification of the S protein, it was unclear if this was the extent of the mechanism of nitric oxide-mediated inhibition of SARS-CoV replication. To address this, Vero E6 cells were infected with SARS-CoV and treated with SNAP, NAP or left untreated. QPCR analysis of RNA isolated from these cells using Taqman probes and primers specific to the N gene of SARS showed a significant decrease in cDNA encoding the N gene in cells treated with SNAP. Pre-treatment of Vero E6 cells with SNAP did not result in a further decrease in N amplification. This indicated that nitric oxide had an effect on the production of viral RNA. This finding presented a myriad of possibilities as to the nature of inhibition of viral RNA production by nitric oxide – an effect on the viral replicase proteins seemed a likely explanation for the observed decrease. Additionally, it was known that the replicase proteins of SARS-CoV are expressed as 2 polyproteins pp1a and pp1ab which are then autoproteolytically cleaved by 2 cysteine proteases, PL^{pro} and $3C^{pro}$, encoded within these polyproteins. It has been previously shown that nitric oxide or its derivatives could have an effect on the activity of cysteine proteases by modifying thiol

groups on the cysteine residues at the active sites of these proteases (Saura et al 1999, Cao et al 2003a). In the case of SARS-CoV, modification of the cysteine residues on the replicase polyproteins would likely result in an alteration of the activity of these proteases. In order to study this possibility, Vero E6 cells were infected with SARS-CoV and treated with SNAP, NAP or left untreated for 24 hours and harvested lysates were examined by PAGE separation and Western Blotting using a mouse monoclonal antibody against nsp8 (see Paper I). While no difference was observed in the levels of nsp8 protein, there were observed differences in other bands on the Western Blot. When matched against calculated permutations of replicase polyprotein cleavage intermediates, these bands represented the calculated molecular weights of cleavage intermediates, suggesting that while nitric oxide did not completely inhibit the cleavage of the replicase polyproteins, it may have altered the cleavage patterns produced. Such polyproteins are indicative of a stoichiometric relationship between different proteins, and presumably an alteration in cleavage of this polyprotein could result in a perturbation of this relationship, adversely affecting viral RNA production. A study of 11 unique sites on the SARS-CoV replicase polyprotein cleaved by $3C^{pro}$ suggested that these 11 unique sites were cleaved with different efficiencies (Fan et al 2005). Given that an altered pattern of cleavage was observed with SARS-CoV replicase polyproteins in the face of SNAP treatment, it would be interesting to examine the possibility these efficiencies might accordingly be altered. Also, all these results point to a significant antiviral activity of nitric oxide, or a derivative of nitric oxide. However, it is not known if NOS-2 is activated during SARS-CoV infection, and whether such an effect plays a role in natural infection *in vivo*, or if NOS-2 might be inhibited in some manner by the virus, as has been previously described in the case of adenovirus E1A infection (Cao et al 2003b). These are among the interesting possibilities that might merit further study.

5 ACKNOWLEDGEMENTS

During the course of my PhD studies, I have met several people who have encouraged, assisted, enriched, and supported me in one way or another. I would like to express my gratitude to all of these people, in particular:

My supervisors – **Tan Yee-Joo**, for believing in me, for supporting me, and for being so very patient with me. And of course, thank you for listening every time I waltzed in with another idea. **Ali Mirazimi**, for all your support and through-provoking discussions, and helping to make my stay in Sweden a memorable one.

The Agency for Science, Technology and Research (Singapore) – for giving me this opportunity, and for supporting me throughout.

Collaborators – **Chris Birch** and the rest of his group at the Victorian Infectious Disease Laboratory in Melbourne, and **Sunil Lal** and his group at the International Centre for Genetic Engineering and Biotechnology in New Delhi.

The CAVR group, Institute of Molecular and Cell Biology (Singapore) – **Timothy Tan, Choi Yook-Wah, Scottz Lip, Daphne Chan, Tham Puay Yoke, Janice Oh, Shen Shuo, Bertram Fielding, Sehaam Khan, Chou Chih-Fong, Sujit Dutta, Wee Boon Yu** and **Nur Khairiah Mohd Ismail** - thank you for all the laughter, the arguments, the discussions, the birthday parties, BBQs, the long conversations at the bench and of course, the lunches! And especially to **Keng Choong Tat**, who has been a great friend and colleague for the last 7 years.

The great people at Smittskyddsinstitutet – **Monica Hammarberg**, for all your help in getting me settled in**,** and helping to find my way around. A special thanks to **Jonas 'Master' Klingström, John 'Dinghy' Wahlgren, Shawon 'Minion' Gupta** and **Karin Sundström of the Orkney Islands** – great friends, scientists and co-conspirators. Many thanks also to the virology group at KCB – **Cecilia, Melinda, Annette, Sara, Anne-Marie, Ida, Helen, Gunnel and Caroline**, for all the fikas, lunches, conversations, discussions, assistance, advice, and for being great lab-mates.

Last but not least, my parents, for their unconditional love and support.

6 REFERENCES

Akaike, T, & Maeda, H. (2000). Nitric oxide and virus infection. *Immunology*, *101*(3), 300-8.

Akaike, Takaaki, Noguchi, Y., Ijiri, S., Setoguchi, K., Suga, M., Zheng, Y. M., Dietzschold, B., et al. (1996). Pathogenesis of influenza virus-induced pneumonia: involvement of both nitric oxide and oxygen radicals. *Proceedings of the National Academy of Sciences of the United States of America*, *93*(6), 2448-53.

Akerström, S., Mousavi-Jazi, M., Klingström, J., Leijon, M., Lundkvist, Ake, & Mirazimi, Ali. (2005). Nitric oxide inhibits the replication cycle of severe acute respiratory syndrome coronavirus. *Journal of virology*, *79*(3), 1966-9.

Akerström, S., Tan, Y.-J., & Mirazimi, Ali. (2006). Amino acids 15-28 in the ectodomain of SARS coronavirus 3a protein induces neutralizing antibodies. *FEBS letters*, *580*(16), 3799-803.

Alvarez, C. P., Lasala, F., Carrillo, J., Muñiz, O., Corbí, A. L., & Delgado, R. (2002). C-type lectins DC-SIGN and L-SIGN mediate cellular entry by Ebola virus in cis and in trans. *Journal of virology*, *76*(13), 6841-4. Am Soc Microbiol.

Badorff, C., Fichtlscherer, B., Rhoads, R. E., Zeiher, a M., Muelsch, a, Dimmeler, S., & Knowlton, K. U. (2000). Nitric oxide inhibits dystrophin proteolysis by coxsackieviral protease 2A through S-nitrosylation: A protective mechanism against enteroviral cardiomyopathy. *Circulation*, *102*(18), 2276-81.

Best, S. M. (2008). Viral subversion of apoptotic enzymes: escape from death row. *Annual review of microbiology*, *62*, 171-92.

Bisht, H., Roberts, A., Vogel, L., Bukreyev, A., Collins, P. L., Murphy, B. R., Subbarao, K., et al. (2004). Severe acute respiratory syndrome coronavirus spike protein expressed by attenuated vaccinia virus protectively immunizes mice. *Proceedings of the National Academy of Sciences of the United States of America*, *101*(17), 6641-6.

Booth, C. M., Matukas, L. M., Tomlinson, G. a, Rachlis, A. R., Rose, D. B., Dwosh, H. a, Walmsley, S. L., et al. (2003). Clinical features and short-term outcomes of 144 patients with SARS in the greater Toronto area. *JAMA : the journal of the American Medical Association*, *289*(21), 2801-9.

Bordi, L., Castilletti, C., Falasca, L., Ciccosanti, F., Calcaterra, S., Rozera, G., Di Caro, a, et al. (2006). Bcl-2 inhibits the caspase-dependent apoptosis induced by SARS-CoV without affecting virus replication kinetics. *Archives of virology*, *151*(2), 369-77.

Boscá, L., & Hortelano, S. (1999). Mechanisms of nitric oxide-dependent apoptosis: involvement of mitochondrial mediators. *Cellular signalling*, *11*(4), 239-44.

Brnjic, S., Olofsson, M. H., Havelka, A. M., & Linder, S. (2010). Chemical biology suggests a role for calcium signaling in mediating sustained JNK activation during apoptosis. *Molecular bioSystems*, *6*(5), 767-74.

Cao, W., Baniecki, M. L., McGrath, W. J., Bao, C., Deming, C. B., Rade, J. J., Lowenstein, Charles J, et al. (2003a). Nitric oxide inhibits the adenovirus proteinase in vitro and viral infectivity in vivo. *The FASEB journal : official publication of the Federation of American Societies for Experimental Biology*, *17*(15), 2345-6.

Cao, W., Bao, C., & Lowenstein, Charles J. (2003b). Inducible nitric oxide synthase expression inhibition by adenovirus E1A. *Proceedings of the National Academy of Sciences of the United States of America*, *100*(13), 7773-8.

Chambers, R., & Takimoto, T. (2010). Trafficking of Sendai virus nucleocapsids is mediated by intracellular vesicles. *PLoS One*, *5*(6), e10994.

Chan, C.-M., Tsoi, H., Chan, W.-M., Zhai, S., Wong, C.-O., Yao, X., Chan, W.-Y., et al. (2009). The ion channel activity of the SARS-coronavirus 3a protein is linked to its pro-apoptotic function. *The international journal of biochemistry & cell biology*, *41*(11), 2232-9.

Chan, V. S. F., Chan, K. Y. K., Chen, Y., Poon, Leo L M, Cheung, A. N. Y., Zheng, B., Chan, K.-H., et al. (2006). Homozygous L-SIGN (CLEC4M) plays a protective role in SARS coronavirus infection. *Nature genetics*, *38*(1), 38-46.

Chau, T.-N., Lee, K.-C., Yao, H., Tsang, T.-Y., Chow, T.-C., Yeung, Y.-C., Choi, K.-W., et al. (2004). SARS-associated viral hepatitis caused by a novel coronavirus: report of three cases. *Hepatology (Baltimore, Md.)*, *39*(2), 302-10.

Chen, C.-Y., Ping, Y.-H., Lee, H.-C., Chen, K.-H., Lee, Y.-M., Chan, Y.-J., Lien, T.-C., et al. (2007). Open reading frame 8a of the human severe acute respiratory syndrome coronavirus not only promotes viral replication but also induces apoptosis. *The Journal of infectious diseases*, *196*(3), 405-15.

Chen, Jun, Lau, Y. F., Lamirande, E. W., Paddock, C. D., Bartlett, J. H., Zaki, S. R., & Subbarao, K. (2010). Cellular immune responses to severe acute respiratory syndrome coronavirus (SARS-CoV) infection in senescent BALB/c mice: CD4+ T cells are important in control of SARS-CoV infection. *Journal of virology*, *84*(3), 1289-301.

Cheung, Chung Y, Poon, Leo L M, Ng, I. H. Y., Luk, W., Sia, S.-F., Wu, M. H. S., Chan, K.-H., et al. (2005). Cytokine responses in severe acute respiratory syndrome coronavirus-infected macrophages in vitro: possible relevance to pathogenesis. *Journal of virology*, *79*(12), 7819-26.

Cinatl, J, Morgenstern, B., Bauer, G., Chandra, P., Rabenau, H, & Doerr, H W. (2003). Treatment of SARS with human interferons. *Lancet*, *362*(9380), 293-4.

Cohen, J. R., Lin, L. D., & Machamer, C. E. (2011). Identification of a Golgi complex-targeting signal in the cytoplasmic tail of the severe acute respiratory syndrome coronavirus envelope protein. *Journal of virology*, *85*(12), 5794-803.

Cui, W., Fan, Y., Wu, W., Zhang, F., Wang, J.-ying, & Ni, A.-ping. (2003). Expression of lymphocytes and lymphocyte subsets in patients with severe acute respiratory syndrome. *Clinical infectious diseases : an official publication of the Infectious Diseases Society of America*, *37*(6), 857-9.

Devaraj, S. G., Wang, N., Chen, Zhongbin, Chen, Zihong, Tseng, M., Barretto, N., Lin, R., et al. (2007). Regulation of IRF-3-dependent innate immunity by the papain-like protease domain of the severe acute respiratory syndrome coronavirus. *The Journal of biological chemistry*, *282*(44), 32208-21.

Diemer, C., Schneider, M., Seebach, J., Quaas, J., Frösner, G., Schätzl, H. M., & Gilch, S. (2008). Cell type-specific cleavage of nucleocapsid protein by effector caspases during SARS coronavirus infection. *Journal of molecular biology*, *376*(1), 23-34.

Drosten, C., Günther, S., Preiser, W., van der Werf, S., Brodt, H.-R., Becker, S., Rabenau, Holger, et al. (2003). Identification of a novel coronavirus in patients with severe acute respiratory syndrome. *The New England journal of medicine*, *348*(20), 1967-76.

Du, L., Zhao, G., He, Yuxian, Guo, Y., Zheng, B.-J., Jiang, Shibo, & Zhou, Y. (2007). Receptor-binding domain of SARS-CoV spike protein induces long-term protective immunity in an animal model. *Vaccine*, *25*(15), 2832-8.

Fan, K., Ma, L., Han, X., Liang, H., Wei, P., Liu, Y., & Lai, L. (2005). The substrate specificity of SARS coronavirus 3C-like proteinase. *Biochemical and biophysical research communications*, *329*(3), 934-40.

Fielding, B. C., Gunalan, V., Tan, T. H. P., Chou, C.-F., Shen, S., Khan, S., Lim, S. G., et al. (2006). Severe acute respiratory syndrome coronavirus protein 7a interacts with hSGT. *Biochemical and biophysical research communications*, *343*(4), 1201-8.

Fouchier, R. A. M., Kuiken, T., Schutten, M., van Amerongen, G., van Doornum, G. J. J., van den Hoogen, B. G., Peiris, M., et al. (2003). Aetiology: Koch's postulates fulfilled for SARS virus. *Nature*, *423*(6937), 240.

Freundt, E. C., Yu, L., Goldsmith, C. S., Welsh, S., Cheng, A., Yount, B., Liu, W., et al. (2010). The open reading frame 3a protein of severe acute respiratory syndrome-associated coronavirus promotes membrane rearrangement and cell death. *Journal of virology*, *84*(2), 1097-109.

Frieman, M., Yount, B., Heise, M., Kopecky-Bromberg, S. a, Palese, P., & Baric, R. S. (2007). Severe acute respiratory syndrome coronavirus ORF6 antagonizes STAT1 function by sequestering nuclear import factors on the rough endoplasmic reticulum/Golgi membrane. *Journal of virology*, *81*(18), 9812-24.

Galluzzi, L., Brenner, C., Morselli, E., Touat, Z., & Kroemer, G. (2008). Viral control of mitochondrial apoptosis. *PLoS pathogens*, *4*(5), e1000018.

Gao, W., Tamin, A., Soloff, A., D'Aiuto, L., Nwanegbo, E., Robbins, P. D., Bellini, W. J., et al. (2003). Effects of a SARS-associated coronavirus vaccine in monkeys. *Lancet*, *362*(9399), 1895-6.

Gardner, J. P., Durso, R. J., Arrigale, R. R., Donovan, G. P., Maddon, P. J., Dragic, T., & Olson, W. C. (2003). L-SIGN (CD 209L) is a liver-specific capture receptor for hepatitis C virus. *Proceedings of the National Academy of Sciences of the United States of America*, *100*(8), 4498-503.

Geng, H., Liu, Y.-M., Chan, W.-S., Lo, A. W.-I., Au, D. M.-Y., Waye, M. M.-Y., & Ho, Y.-Y. (2005). The putative protein 6 of the severe acute respiratory syndrome-associated coronavirus: expression and functional characterization. *FEBS letters*, *579*(30), 6763-8.

Glass, W. G., Subbarao, K., Murphy, B., & Murphy, P. M. (2004). Mechanisms of host defense following severe acute respiratory syndrome-coronavirus (SARS-CoV) pulmonary infection of mice. *Journal of immunology (Baltimore, Md. : 1950)*, *173*(6), 4030-9.

Goldsmith, C. S., Tatti, K. M., Ksiazek, T. G., Rollin, P. E., Comer, J. a, Lee, W. W., Rota, P. a, et al. (2004). Ultrastructural characterization of SARS coronavirus. *Emerging infectious diseases*, *10*(2), 320-6.

Gorbalenya, A. E., Snijder, E. J., & Spaan, W. J. M. (2004). Severe acute respiratory syndrome coronavirus phylogeny: toward consensus. *Journal of virology*, *78*(15), 7863-6.

Gosert, R., Kanjanahaluethai, A., Egger, D., Bienz, K., & Baker, S. C. (2002). RNA replication of mouse hepatitis virus takes place at double-membrane vesicles. *Journal of virology*, *76*(8), 3697-708.

Guan, M., Chen, H. Y., Foo, S. Y., Tan, Y.-J., Goh, P.-Y., & Wee, S. H. (2004a). Recombinant protein-based enzyme-linked immunosorbent assay and immunochromatographic tests for detection of immunoglobulin G antibodies to severe acute respiratory syndrome (SARS) coronavirus in SARS patients. *Clinical and diagnostic laboratory immunology*, *11*(2), 287-91.

Guan, M., Chen, H. Y., Tan, P. H., Shen, S., Goh, P.-yee, Tan, Y.-joo, Pang, P. H., et al. (2004b). Use of viral lysate antigen combined with recombinant protein in Western immunoblot assay as confirmatory test for serodiagnosis of severe acute respiratory syndrome. *Clinical and diagnostic laboratory immunology*, *11*(6), 1148-53.

Gunalan, V., Mirazimi, Ali, & Tan, Y.-J. (2011). A putative diacidic motif in the SARS-CoV ORF6 protein influences its subcellular localization and suppression of expression of co-transfected expression constructs. *BMC Research Notes*, *(in press)*.

Guo, J.-P., Petric, M., Campbell, W., & McGeer, P. L. (2004). SARS coronavirus peptides recognized by antibodies in the sera of convalescent cases. *Virology*, *324*(2), 251-6.

He, L., Ding, Y., Zhang, Q., Che, X., He, Y, Shen, H., Wang, H., et al. (2006). Expression of elevated levels of pro-inflammatory cytokines in SARS-CoV-infected + cells in SARS patients: relation to the acute lung injury and pathogenesis of SARS. *The Journal of pathology*, *210*(3), 288-97.

He, Z., Zhao, C., Dong, Q., Zhuang, H., Song, S., Peng, G., & Dwyer, D. E. (2005). Effects of severe acute respiratory syndrome (SARS) coronavirus infection on peripheral blood lymphocytes and their subsets. *International journal of infectious diseases : IJID : official publication of the International Society for Infectious Diseases*, *9*(6), 323-30.

Holzer, G. W., & Falkner, F G. (1997). Construction of a vaccinia virus deficient in the essential DNA repair enzyme uracil DNA glycosylase by a complementing cell line. *Journal of virology*, *71*(7), 4997-5002.

Hortelano, S., Alvarez, a M., & Boscá, L. (1999). Nitric oxide induces tyrosine nitration and release of cytochrome c preceding an increase of mitochondrial transmembrane potential in macrophages. *The FASEB journal : official publication of the Federation of American Societies for Experimental Biology*, *13*(15), 2311-7.

Huang, C., Ito, N., Tseng, C.-T. K., & Makino, S. (2006). Severe acute respiratory syndrome coronavirus 7a accessory protein is a viral structural protein. *Journal of virology*, *80*(15), 7287-94.

Huang, C., Peters, C J, & Makino, S. (2007). Severe acute respiratory syndrome coronavirus accessory protein 6 is a virion-associated protein and is released from 6 protein-expressing cells. *Journal of virology*, *81*(10), 5423-6.

Huang, J., Cao, Y., Du, J., Bu, X., Ma, R., & Wu, C. (2007). Priming with SARS CoV S DNA and boosting with SARS CoV S epitopes specific for CD4+ and CD8+ T cells promote cellular immune responses. *Vaccine*, *25*(39-40), 6981-91.

Hussain, S., & Gallagher, Tom. (2010). SARS-coronavirus protein 6 conformations required to impede protein import into the nucleus. *Virus research*, *153*(2), 299-304.

Imbert, I., Guillemot, J.-C., Bourhis, J.-M., Bussetta, C., Coutard, B., Egloff, M.-P., Ferron, F., et al. (2006). A second, non-canonical RNA-dependent RNA polymerase in SARS coronavirus. *The EMBO journal*, *25*(20), 4933-42.

Ito, N., Mossel, E. C., Narayanan, K., Popov, V. L., Huang, C., Inoue, T., Peters, Clarence J, et al. (2005). Severe acute respiratory syndrome coronavirus 3a protein is a viral structural protein. *Journal of virology*, *79*(5), 3182-6.

Jackson, W. T., Giddings, T. H., Taylor, M. P., Mulinyawe, S., Rabinovitch, M., Kopito, R. R., & Kirkegaard, K. (2005). Subversion of cellular autophagosomal machinery by RNA viruses. *PLoS biology*, *3*(5), e156.

Jeffers, S. a, Tusell, S. M., Gillim-Ross, L., Hemmila, E. M., Achenbach, J. E., Babcock, G. J., Thomas, W. D., et al. (2004). CD209L (L-SIGN) is a receptor for severe acute respiratory syndrome coronavirus. *Proceedings of the National Academy of Sciences of the United States of America*, *101*(44), 15748-53.

Kaiser, L., Fritz, R. S., Straus, S. E., Gubareva, L., & Hayden, F. G. (2001). Symptom pathogenesis during acute influenza: interleukin-6 and other cytokine responses. *Journal of medical virology*, *64*(3), 262-8.

Kapadia, S. U., Rose, J. K., Lamirande, E., Vogel, L., Subbarao, K., & Roberts, A. (2005). Long-term protection from SARS coronavirus infection conferred by a single immunization with an attenuated VSV-based vaccine. *Virology*, *340*(2), 174-82.

Karjee, S., Minhas, A., Sood, V., Ponia, S. S., Banerjea, A. C., Chow, V. T. K., Mukherjee, S. K., et al. (2010). The 7a accessory protein of severe acute respiratory syndrome coronavirus acts as an RNA silencing suppressor. *Journal of virology*, *84*(19), 10395-401.

Keng, C.-T., Akerström, S., Leung, C. S.-W., Poon, Leo L M, Peiris, J S Malik, Mirazimi, Ali, & Tan, Y.-J. (2011). SARS coronavirus 8b reduces viral replication by down-regulating E via an ubiquitin-independent proteasome pathway. *Microbes and infection / Institut Pasteur*, *13*(2), 179-88.

Keng, C.-T., Choi, Y.-W., Welkers, M. R. a, Chan, D. Z. L., Shen, S., Gee Lim, S., Hong, W., et al. (2006). The human severe acute respiratory syndrome coronavirus (SARS-CoV) 8b protein is distinct from its counterpart in animal SARS-CoV and down-regulates the expression of the envelope protein in infected cells. *Virology*, *354*(1), 132-42.

Khan, S., Fielding, B. C., Tan, T. H. P., Chou, C.-F., Shen, S., Lim, S. G., Hong, W., et al. (2006). Over-expression of severe acute respiratory syndrome coronavirus 3b protein induces both apoptosis and necrosis in Vero E6 cells. *Virus research*, *122*(1-2), 20-7.

Klingström, J., Akerström, S., Hardestam, J., Stoltz, M., Simon, Melinda, Falk, Kerstin I, Mirazimi, Ali, et al. (2006). Nitric oxide and peroxynitrite have different antiviral effects against hantavirus replication and free mature virions. *European journal of immunology*, *36*(10), 2649-57.

Knoops, K., Kikkert, M., Worm, S. H. E. V. D., Zevenhoven-Dobbe, J. C., van der Meer, Y., Koster, A. J., Mommaas, a M., et al. (2008). SARS-coronavirus replication is supported by a reticulovesicular network of modified endoplasmic reticulum. *PLoS biology*, *6*(9), e226.

Kopecky-Bromberg, S. A., Martinez-Sobrido, L., & Palese, P. (2006). 7a protein of severe acute respiratory syndrome coronavirus inhibits cellular protein synthesis and activates p38 mitogen-activated protein kinase. *Journal of virology*, *80*(2), 785-93.

Kopecky-Bromberg, S. a, Martínez-Sobrido, L., Frieman, M., Baric, R. a, & Palese, P. (2007). Severe acute respiratory syndrome coronavirus open reading frame (ORF) 3b, ORF 6, and nucleocapsid proteins function as interferon antagonists. *Journal of virology*, *81*(2), 548-57.

Ksiazek, T. G., Erdman, D., Goldsmith, C. S., Zaki, S. R., Peret, T., Emery, S., Tong, Suxiang, et al. (2003). A novel coronavirus associated with severe acute respiratory syndrome. *The New England journal of medicine*, *348*(20), 1953-66. Massachusetts Medical Society.

Kuhn, J. H., Li, W., Choe, H., & Farzan, M. (2004). Angiotensin-converting enzyme 2: a functional receptor for SARS coronavirus. *Cellular and molecular life sciences : CMLS*, *61*(21), 2738-43.

Kumar, P., Gunalan, V., Liu, B., Chow, V. T. K., Druce, J., Birch, C., Catton, M., et al. (2007). The nonstructural protein 8 (nsp8) of the SARS coronavirus interacts with its ORF6 accessory protein. *Virology*, *366*(2), 293-303.

Kuri, T., Zhang, X., Habjan, M., Martínez-Sobrido, L., García-Sastre, A., Yuan, Z., & Weber, F. (2009). Interferon priming enables cells to partially overturn the SARS coronavirus-induced block in innate immune activation. *The Journal of general virology*, *90*(Pt 11), 2686-94.

Lamirande, E. W., DeDiego, M. L., Roberts, A., Jackson, J. P., Alvarez, E., Sheahan, Tim, Shieh, W.-J., et al. (2008). A live attenuated severe acute respiratory syndrome coronavirus is immunogenic and efficacious in golden Syrian hamsters. *Journal of virology*, *82*(15), 7721-4.

Lang, Z., Zhang, L., Zhang, S., Meng, X., Li, Junqiang, Song, C., Sun, L., et al. (2003). Pathological study on severe acute respiratory syndrome. *Chinese medical journal*, *116*(7), 976-80.

Law, H. K. W., Cheung, Chung Yan, Ng, H. Y., Sia, S. F., Chan, Y. O., Luk, W., Nicholls, John M, et al. (2005). Chemokine up-regulation in SARS-coronavirus-infected, monocyte-derived human dendritic cells. *Blood*, *106*(7), 2366-74.

Law, P. T. W., Wong, C.-H., Au, T. C. C., Chuck, C.-P., Kong, S.-K., Chan, Paul K S, To, K.-F., et al. (2005). The 3a protein of severe acute respiratory syndrome-associated coronavirus induces apoptosis in Vero E6 cells. *The Journal of general virology*, *86*(Pt 7), 1921-30.

Lee, M. C. S., Miller, E. a, Goldberg, J., Orci, L., & Schekman, R. (2004). Bi-directional protein transport between the ER and Golgi. *Annual review of cell and developmental biology*, *20*, 87-123.

Lee, N., & Sung, Joseph J.Y. (2003). Nosocomial Transmission of SARS. *Current infectious disease reports*, *5*(6), 473-476.

Lee, N., Chan, P K S, Ip, M., Wong, E., Ho, J., Ho, C., Cockram, C. S., et al. (2006). Anti-SARS-CoV IgG response in relation to disease severity of severe acute respiratory syndrome. *Journal of clinical virology : the official publication of the Pan American Society for Clinical Virology*, *35*(2), 179-84.

Lew, T. W. K., Kwek, T.-K., Tai, D., Earnest, A., Loo, S., Singh, K., Kwan, K. M., et al. (2003). Acute respiratory distress syndrome in critically ill patients with severe acute respiratory syndrome. *JAMA : the journal of the American Medical Association*, *290*(3), 374-80.

Li, S., Zhao, Q., Zhang, Yinjie, Zhang, Yang, Bartlam, M., Li, X., & Rao, Z. (2010). New nsp8 isoform suggests mechanism for tuning viral RNA synthesis. *Protein & cell*, *1*(2), 198-204.

Lip, K.-M., Shen, S., Yang, X., Keng, C.-T., Zhang, A., Oh, H.-L. J., Li, Z.-hong, et al. (2006). Monoclonal antibodies targeting the HR2 domain and the region immediately upstream of the HR2 of the S protein neutralize in vitro infection of severe acute respiratory syndrome coronavirus. *Journal of virology*, *80*(2), 941-50. Am Soc Microbiol.

Lischka, P., Sorg, G., Kann, M., Winkler, M., & Stamminger, T. (2003). A nonconventional nuclear localization signal within the UL84 protein of human cytomegalovirus mediates nuclear import via the importin alpha/beta pathway. *Journal of virology*, *77*(6), 3734-48.

Loutfy, M. R., Blatt, L. M., Siminovitch, K. a, Ward, S., Wolff, B., Lho, H., Pham, D. H., et al. (2003). Interferon alfacon-1 plus corticosteroids in severe acute respiratory syndrome: a preliminary study. *JAMA : the journal of the American Medical Association*, *290*(24), 3222-8.

Lowenstein, Charles J, & Padalko, E. (2004). iNOS (NOS2) at a glance. *Journal of cell science*, *117*(Pt 14), 2865-7.

Lu, W., Zheng, B.-J., Xu, K., Schwarz, W., Du, L., Wong, C. K. L., Chen, Jiadong, et al. (2006). Severe acute respiratory syndrome-associated coronavirus 3a protein forms an ion channel and modulates virus release. *Proceedings of the National Academy of Sciences of the United States of America*, *103*(33), 12540-5.

Marra, M. a, Jones, S. J. M., Astell, C. R., Holt, R. a, Brooks-Wilson, A., Butterfield, Y. S. N., Khattra, J., et al. (2003). The Genome sequence of the SARS-associated coronavirus. *Science (New York, N.Y.)*, *300*(5624), 1399-404.

McBride, C. E., Li, Jie, & Machamer, C. E. (2007). The cytoplasmic tail of the severe acute respiratory syndrome coronavirus spike protein contains a novel endoplasmic reticulum retrieval signal that binds COPI and promotes interaction with membrane protein. *Journal of virology*, *81*(5), 2418-28.

Meier, C., Aricescu, a R., Assenberg, R., Aplin, R. T., Gilbert, R. J. C., Grimes, J. M., & Stuart, D. I. (2006). The crystal structure of ORF-9b, a lipid binding protein from the SARS coronavirus. *Structure (London, England : 1993)*, *14*(7), 1157-65.

Minakshi, R., Padhan, K., Rani, M., Khan, N., Ahmad, F., & Jameel, S. (2009). The SARS Coronavirus 3a protein causes endoplasmic reticulum stress and induces ligand-independent downregulation of the type 1 interferon receptor. *PloS one*, *4*(12), e8342.

Miranda-Saksena, M., Boadle, R. a, Aggarwal, A., Tijono, B., Rixon, F. J., Diefenbach, R. J., & Cunningham, A. L. (2009). Herpes simplex virus utilizes the large secretory vesicle pathway for anterograde transport of tegument and envelope proteins and for viral exocytosis from growth cones of human fetal axons. *Journal of virology*, *83*(7), 3187-99.

Mizutani, T., Fukushi, S., Saijo, M., Kurane, I., & Morikawa, S. (2004). Phosphorylation of p38 MAPK and its downstream targets in SARS coronavirus-infected cells. *Biochemical and biophysical research communications*, *319*(4), 1228-34.

Moshynskyy, I., Viswanathan, S., Vasilenko, N., Lobanov, V., Petric, M., Babiuk, L. a, & Zakhartchouk, A. N. (2007). Intracellular localization of the SARS coronavirus protein 9b: evidence of active export from the nucleus. *Virus research*, *127*(1), 116-21.

Nakamura, T., Wang, L., Wong, C. C. L., Scott, F. L., Eckelman, B. P., Han, X., Tzitzilonis, C., et al. (2010). Transnitrosylation of XIAP regulates caspase-dependent neuronal cell death. *Molecular cell*, *39*(2), 184-95. Elsevier Ltd.

Nakauchi, M., Kariwa, H., Kon, Y., Yoshii, K., Maeda, A., & Takashima, I. (2008). Analysis of severe acute respiratory syndrome coronavirus structural proteins in virus-like particle assembly. *Microbiology and immunology*, *52*(12), 625-30.

Netland, J., Ferraro, D., Pewe, L., Olivares, H., Gallagher, Thomas, & Perlman, S. (2007). Enhancement of murine coronavirus replication by severe acute respiratory syndrome coronavirus protein 6 requires the N-terminal hydrophobic region but not C-terminal sorting motifs. *Journal of virology*, *81*(20), 11520-5.

Ng, L. F. P., Hibberd, M. L., Ooi, Eng-Eong, Tang, K.-F., Neo, S.-Y., Tan, J., Murthy, K. R. K., et al. (2004). A human in vitro model system for investigating genome-wide host responses to SARS coronavirus infection. *BMC infectious diseases*, *4*, 34.

Ng, M.-L., Tan, S.-H., See, E.-E., Ooi, E-E, & Ling, A-E. (2003). Proliferative growth of SARS coronavirus in Vero E6 cells. *The Journal of general virology*, *84*(Pt 12), 3291-303.

Nicholls, John M, Poon, Leo L M, Lee, K. C., Ng, W. F., Lai, Sik T, Leung, C. Y., Chu, Chung M, et al. (2003). Lung pathology of fatal severe acute respiratory syndrome. *Lancet*, *361*(9371), 1773-8.

Nie, Y., Wang, P., Shi, X., Wang, G., Chen, Jianguo, Zheng, A., Wang, W., et al. (2004). Highly infectious SARS-CoV pseudotyped virus reveals the cell tropism and its correlation with receptor expression. *Biochemical and biophysical research communications*, *321*(4), 994-1000.

O'Donnell, R., Tasker, R. C., & Roe, M. F. E. (2003). SARS: understanding the coronavirus: apoptosis may explain lymphopenia of SARS. *BMJ (Clinical research ed.)*, *327*(7415), 620.

Pacher, P., Beckman, J. S., & Liaudet, L. (2007). Nitric oxide and peroxynitrite in health and disease. *Physiological reviews*, *87*(1), 315-424.

Padhan, K., Minakshi, R., Towheed, M. A. B., & Jameel, S. (2008). Severe acute respiratory syndrome coronavirus 3a protein activates the mitochondrial death pathway through p38 MAP kinase activation. *The Journal of general virology*, *89*(Pt 8), 1960-9.

Panesar, N. S. (2008). What caused lymphopenia in SARS and how reliable is the lymphokine status in glucocorticoid-treated patients? *Medical hypotheses*, *71*(2), 298-301.

Peiris, J S M, Chu, C M, Cheng, V. C. C., Chan, K. S., Hung, I. F. N., Poon, L L M, Law, K. I., et al. (2003a). Clinical progression and viral load in a community outbreak of coronavirus-associated SARS pneumonia: a prospective study. *Lancet*, *361*(9371), 1767-72.

Peiris, J S M, Lai, S T, Poon, L L M, Guan, Y, Yam, L. Y. C., Lim, W, Nicholls, J., et al. (2003b). Coronavirus as a possible cause of severe acute respiratory syndrome. *Lancet*, *361*(9366), 1319-25.

Peng, H., Yang, L.-tao, Li, Jian, Lu, Z.-qiang, Wang, L.-yun, Koup, R. a, Bailer, R. T., et al. (2006a). Human memory T cell responses to SARS-CoV E protein. *Microbes and infection / Institut Pasteur*, *8*(9-10), 2424-31.

Peng, H., Yang, L.-tao, Wang, L.-yun, Li, Jian, Huang, J., Lu, Z.-qiang, Koup, R. a, et al. (2006b). Long-lived memory T lymphocyte responses against SARS coronavirus nucleocapsid protein in SARS-recovered patients. *Virology*, *351*(2), 466-75.

Petit, C. M., Chouljenko, V. N., Iyer, A., Colgrove, R., Farzan, M., Knipe, D. M., & Kousoulas, K. G. (2007). Palmitoylation of the cysteine-rich endodomain of the SARS-coronavirus spike glycoprotein is important for spike-mediated cell fusion. *Virology*, *360*(2), 264-74.

Pewe, L., Zhou, H., Netland, J., Tangudu, C., Olivares, H., Shi, L., Look, D., et al. (2005). A severe acute respiratory syndrome-associated coronavirus-specific protein enhances virulence of an attenuated murine coronavirus. *Journal of virology*, *79*(17), 11335-42.

Pfefferle, S., Krähling, V., Ditt, V., Grywna, K., Mühlberger, E., & Drosten, C. (2009). Reverse genetic characterization of the natural genomic deletion in SARS-Coronavirus strain Frankfurt-1 open reading frame 7b reveals an attenuating function of the 7b protein in-vitro and in-vivo. *Virology journal*, *6*, 131.

Pierini, R., Cottam, E., Roberts, R., & Wileman, T. (2009). Modulation of membrane traffic between endoplasmic reticulum, ERGIC and Golgi to generate compartments for the replication of bacteria and viruses. *Seminars in cell & developmental biology*, *20*(7), 828-33.

Poutanen, S. M., Low, D. E., Henry, B., Finkelstein, S., Rose, D., Green, K., Tellier, R., et al. (2003). Identification of severe acute respiratory syndrome in Canada. *The New England journal of medicine*, *348*(20), 1995-2005.

Prentice, E., Jerome, W. G., Yoshimori, T., Mizushima, N., & Denison, Mark R. (2004a). Coronavirus replication complex formation utilizes components of cellular autophagy. *The Journal of biological chemistry*, *279*(11), 10136-41.

Prentice, E., McAuliffe, J., Lu, X., Subbarao, K., & Denison, Mark R. (2004b). Identification and characterization of severe acute respiratory syndrome coronavirus replicase proteins. *Journal of virology*, *78*(18), 9977-86.

Reggiori, F., Monastyrska, I., Verheije, M. H., Calì, T., Ulasli, M., Bianchi, S., Bernasconi, R., et al. (2010). Coronaviruses Hijack the LC3-I-positive EDEMosomes, ER-derived vesicles exporting short-lived ERAD regulators, for replication. *Cell host & microbe*, *7*(6), 500-8.

Ren, L., Yang, R., Guo, L., Qu, J., Wang, J., & Hung, T. (2005). Apoptosis induced by the SARS-associated coronavirus in Vero cells is replication-dependent and involves caspase. *DNA and cell biology*, *24*(8), 496-502.

Roberts, A., Lamirande, E. W., Vogel, L., Jackson, J. P., Paddock, C. D., Guarner, J., Zaki, S. R., et al. (2008). Animal models and vaccines for SARS-CoV infection. *Virus research*, *133*(1), 20-32. Elsevier.

Roberts, A., Paddock, C., Vogel, L., Butler, E., Zaki, S., & Subbarao, K. (2005a). Aged BALB/c mice as a model for increased severity of severe acute respiratory syndrome in elderly humans. *Journal of virology*, *79*(9), 5833-8. Am Soc Microbiol.

Roberts, A., Thomas, W. D., Guarner, J., Lamirande, E. W., Babcock, G. J., Greenough, T. C., Vogel, L., et al. (2006). Therapy with a severe acute respiratory syndrome-associated coronavirus-neutralizing human monoclonal antibody reduces disease severity and viral burden in golden Syrian hamsters. *The Journal of infectious diseases*, *193*(5), 685-92.

Roberts, A., Vogel, L., Guarner, J., Hayes, N., Murphy, B., Zaki, S., & Subbarao, K. (2005b). Severe acute respiratory syndrome coronavirus infection of golden Syrian hamsters. *Journal of virology*, *79*(1), 503-11. Am Soc Microbiol.

Rota, P. a, Oberste, M. S., Monroe, S. S., Nix, W. A., Campagnoli, R., Icenogle, J. P., Peñaranda, S., et al. (2003). Characterization of a novel coronavirus associated with severe acute respiratory syndrome. *Science (New York, N.Y.)*, *300*(5624), 1394-9.

Rowe, T., Gao, G., Hogan, R. J., Crystal, R. G., Voss, T. G., Grant, R. L., Bell, P., et al. (2004). Macaque model for severe acute respiratory syndrome. *Journal of virology*, *78*(20), 11401-4.

Ruan, Y. J., Wei, C. L., Ee, A. L., Vega, V. B., Thoreau, H., Su, S. T. Y., Chia, J.-M., et al. (2003). Comparative full-length genome sequence analysis of 14 SARS coronavirus isolates and common mutations associated with putative origins of infection. *Lancet*, *361*(9371), 1779-85.

Saura, M., Zaragoza, C., McMillan, A., Quick, R. a, Hohenadl, C., Lowenstein, J. M., & Lowenstein, C J. (1999). An antiviral mechanism of nitric oxide: inhibition of a viral protease. *Immunity*, *10*(1), 21-8.

Sawicki, S. G., Sawicki, D. L., & Siddell, S. G. (2007). A contemporary view of coronavirus transcription. *Journal of virology*, *81*(1), 20-9.

Saxena, S. K., Mathur, A., & Srivastava, R. C. (2001). Induction of nitric oxide synthase during Japanese encephalitis virus infection: evidence of protective role. *Archives of biochemistry and biophysics*, *391*(1), 1-7.

Schaecher, S. R., Touchette, E., Schriewer, J., Buller, R. M., & Pekosz, A. (2007). Severe acute respiratory syndrome coronavirus gene 7 products contribute to virus-induced apoptosis. *Journal of virology*, *81*(20), 11054-68.

See, R. H., Zakhartchouk, A. N., Petric, M., Lawrence, D. J., Mok, C. P. Y., Hogan, R. J., Rowe, T., et al. (2006). Comparative evaluation of two severe acute respiratory syndrome (SARS) vaccine candidates in mice challenged with SARS coronavirus. *The Journal of general virology*, *87*(Pt 3), 641-50.

Sha, Y., & Marshall, H. E. (2011). S-nitrosylation in the regulation of gene transcription. *Biochimica et biophysica acta*. Elsevier B.V.

Sharma, K., Åkerström, S., Sharma, A. K., Chow, V. T. K., Teow, S., Abrenica, B., Booth, S. A., et al. (2011). SARS-CoV 9b protein diffuses into nucleus, undergoes active Crm1 mediated nucleocytoplasmic export and triggers apoptosis when retained in the nucleus. *PloS one*, *6*(5), e19436.

Shen, S., Lin, P.-S., Chao, Y.-C., Zhang, A., Yang, X., Lim, S. G., Hong, W., et al. (2005). The severe acute respiratory syndrome coronavirus 3a is a novel structural protein. *Biochemical and biophysical research communications*, *330*(1), 286-92.

da Silva, R. C., Segat, L., & Crovella, S. (2011). Role of DC-SIGN and L-SIGN receptors in HIV-1 vertical transmission. *Human immunology*, *72*(4), 305-11. Elsevier Inc.

Simon, M, Falk, K I, Lundkvist, A, & Mirazimi, A. (2006). Exogenous nitric oxide inhibits Crimean Congo hemorrhagic fever virus. *Virus research*, *120*(1-2), 184-90.

Sims, a C., Ostermann, J., & Denison, M R. (2000). Mouse hepatitis virus replicase proteins associate with two distinct populations of intracellular membranes. *Journal of virology*, *74*(12), 5647-54.

Siu, Y. L., Teoh, K. T., Lo, J., Chan, C. M., Kien, F., Escriou, N, Tsao, S. W., et al. (2008). The M, E, and N structural proteins of the severe acute respiratory syndrome coronavirus are required for efficient assembly, trafficking, and release of virus-like particles. *Journal of virology*, *82*(22), 11318-30.

Snijder, E. J., Bredenbeek, P. J., Dobbe, J. C., Thiel, V., Ziebuhr, J., Poon, Leo L M, Guan, Yi, et al. (2003). Unique and conserved features of genome and proteome of SARS-coronavirus, an early split-off from the coronavirus group 2 lineage. *Journal of molecular biology*, *331*(5), 991-1004.

Snijder, E. J., van der Meer, Y., Zevenhoven-Dobbe, J., Onderwater, J. J. M., van der Meulen, J., Koerten, H. K., & Mommaas, a M. (2006). Ultrastructure and origin of membrane vesicles associated with the severe acute respiratory syndrome coronavirus replication complex. *Journal of virology*, *80*(12), 5927-40.

Stamler, J. S., Simon, D. I., Osborne, J. a, Mullins, M. E., Jaraki, O., Michel, T., Singel, D. J., et al. (1992). S-nitrosylation of proteins with nitric oxide: synthesis and characterization of biologically active compounds. *Proceedings of the National Academy of Sciences of the United States of America*, *89*(1), 444-8.

Stertz, S., Reichelt, M., Spiegel, M., Kuri, T., Martínez-Sobrido, L., García-Sastre, A., Weber, F., et al. (2007). The intracellular sites of early replication and budding of SARS-coronavirus. *Virology*, *361*(2), 304-15.

Subbarao, K., McAuliffe, J., Vogel, L., Fahle, G., Fischer, S., Tatti, K., Packard, M., et al. (2004). Prior infection and passive transfer of neutralizing antibody prevent replication of severe acute respiratory syndrome coronavirus in the respiratory tract of mice. *Journal of virology*, *78*(7), 3572-7.

Tan, Y.-J., Fielding, B. C., Goh, P.-Y., Shen, S., Tan, T. H. P., Lim, S. G., & Hong, W. (2004). Overexpression of 7a, a protein specifically encoded by the severe acute respiratory syndrome coronavirus, induces apoptosis via a caspase-dependent pathway. *Journal of virology*, *78*(24), 14043-7.

Tan, Y.-J., Goh, P.-Y., Fielding, B. C., Shen, S., Chou, C.-F., Fu, J.-L., Leong, H. N., et al. (2004). Profiles of antibody responses against severe acute respiratory syndrome coronavirus recombinant proteins and their potential use as diagnostic markers. *Clinical and diagnostic laboratory immunology*, *11*(2), 362-71.

Tan, Y.-J., Tham, P.-yoke, Chan, D. Z. L., Chou, C.-fong, Shen, S., Fielding, B. C., Tan, T. H. P., et al. (2005). The severe acute respiratory syndrome coronavirus 3a protein up-regulates expression of fibrinogen in lung epithelial cells. *Journal of virology*, *79*(15), 10083-7.

Tan, Y.-X., Tan, T. H. P., Lee, M. J.-R., Tham, P.-Y., Gunalan, V., Druce, J., Birch, C., et al. (2007). Induction of apoptosis by the severe acute respiratory syndrome coronavirus 7a protein is dependent on its interaction with the Bcl-XL protein. *Journal of virology*, *81*(12), 6346-55.

Tangudu, C., Olivares, H., Netland, J., Perlman, S., & Gallagher, Thomas. (2007). Severe acute respiratory syndrome coronavirus protein 6 accelerates murine coronavirus infections. *Journal of virology*, *81*(3), 1220-9.

Thiel, V., Ivanov, K. A., Putics, A., Hertzig, T., Schelle, B., Bayer, S., Weissbrich, B., et al. (2003). Mechanisms and enzymes involved in SARS coronavirus genome expression. *The Journal of general virology*, *84*(Pt 9), 2305-15.

Tsang, K. W., Ho, P. L., Ooi, G. C., Yee, W. K., Wang, T., Chan-Yeung, M., Lam, W. K., et al. (2003). A cluster of cases of severe acute respiratory syndrome in Hong Kong. *The New England journal of medicine*, *348*(20), 1977-85.

Tseng, C.-T. K., Huang, C., Newman, P., Wang, N., Narayanan, K., Watts, D. M., Makino, S., et al. (2007). Severe acute respiratory syndrome coronavirus infection of mice transgenic for the human Angiotensin-converting enzyme 2 virus receptor. *Journal of virology*, *81*(3), 1162-73.

Tseng, Y.-T., Wang, S.-M., Huang, K.-J., Lee, A. I.-R., Chiang, C.-C., & Wang, C.-T. (2010). Self-assembly of severe acute respiratory syndrome coronavirus membrane protein. *The Journal of biological chemistry*, *285*(17), 12862-72.

Tsui, P. T., Kwok, M. L., Yuen, H., & Lai, Sik To. (2003). Severe acute respiratory syndrome: clinical outcome and prognostic correlates. *Emerging infectious diseases*, *9*(9), 1064-9.

Varshney, B., & Lal, S. K. (2011). SARS-CoV accessory protein 3b induces AP-1 transcriptional activity through activation of JNK and ERK pathways. *Biochemistry*, *50*(24), 5419-25.

Vasilenko, N., Moshynskyy, I., & Zakhartchouk, A. (2010). SARS coronavirus protein 7a interacts with human Ap4A-hydrolase. *Virology journal*, *7*, 31.

Wang, P., Chen, Jian, Zheng, A., Nie, Y., Shi, X., Wang, W., Wang, G., et al. (2004). Expression cloning of functional receptor used by SARS coronavirus. *Biochemical and biophysical research communications*, *315*(2), 439-44.

Wei, L., Sun, S., Xu, C.-H., Zhang, Jing, Xu, Y., Zhu, H., Peh, S.-C., et al. (2007). Pathology of the thyroid in severe acute respiratory syndrome. *Human pathology*, *38*(1), 95-102.

Wong, R. S. M., Wu, A., To, K. F., Lee, N., Lam, C. W. K., Wong, C K, Chan, Paul K S, et al. (2003). Haematological manifestations in patients with severe acute respiratory syndrome: retrospective analysis. *BMJ (Clinical research ed.)*, *326*(7403), 1358-62.

Xu, K., Zheng, B.-J., Zeng, R., Lu, W., Lin, Y.-P., Xue, L., Li, L., et al. (2009). Severe acute respiratory syndrome coronavirus accessory protein 9b is a virion-associated protein. *Virology*, *388*(2), 279-85. Elsevier Inc.

Yan, H., Xiao, G., Zhang, Jiamin, Hu, Y., Yuan, F., Cole, D. K., Zheng, C., et al. (2004). SARS coronavirus induces apoptosis in Vero E6 cells. *Journal of medical virology*, *73*(3), 323-31.

Yang, L.-T., Peng, H., Zhu, Z.-L., Li, G., Huang, Z.-T., Zhao, Z.-X., Koup, R. a, et al. (2006). Long-lived effector/central memory T-cell responses to severe acute respiratory syndrome coronavirus (SARS-CoV) S antigen in recovered SARS patients. *Clinical immunology (Orlando, Fla.)*, *120*(2), 171-8.

Yang, L.-T., Peng, H., Zhu, Z., Li, G., Huang, Z., Zhao, Zhixin, Koup, R. a, et al. (2007). Persistent memory CD4+ and CD8+ T-cell responses in recovered severe acute respiratory syndrome (SARS) patients to SARS coronavirus M antigen. *The Journal of general virology*, *88*(Pt 10), 2740-8.

Ye, Z., Wong, Chung Kai, Li, P., & Xie, Y. (2008). A SARS-CoV protein, ORF-6, induces caspase-3 mediated, ER stress and JNK-dependent apoptosis. *Biochimica et biophysica acta*, *1780*(12), 1383-7.

Yen, Y.-T., Liao, F., Hsiao, C.-hsiang, Kao, C.-L., Chen, Y.-C., & Wu-Hsieh, B. A. (2006). Modeling the early events of severe acute respiratory syndrome coronavirus infection in vitro. *Journal of virology*, *80*(6), 2684-93.

Yount, B., Curtis, K. M., Fritz, E. a, Hensley, L. E., Jahrling, P. B., Prentice, E., Denison, Mark R, et al. (2003). Reverse genetics with a full-length infectious cDNA of severe acute respiratory syndrome coronavirus. *Proceedings of the National Academy of Sciences of the United States of America*, *100*(22), 12995-3000.

Yuan, X., Shan, Y., Zhao, Zhenhu, Chen, Jiapei, & Cong, Y. (2005). G0/G1 arrest and apoptosis induced by SARS-CoV 3b protein in transfected cells. *Virology journal*, *2*, 66.

Yuan, X., Wu, J., Shan, Y., Yao, Z., Dong, B., Chen, B., Zhao, Zhenhu, et al. (2006). SARS coronavirus 7a protein blocks cell cycle progression at G0/G1 phase via the cyclin D3/pRb pathway. *Virology*, *346*(1), 74-85.

Yuan, X., Yao, Z., Shan, Y., Chen, B., Yang, Z., Wu, J., Zhao, Zhenhu, et al. (2005). Nucleolar localization of non-structural protein 3b, a protein specifically encoded by the severe acute respiratory syndrome coronavirus. *Virus research*, *114*(1-2), 70-9.

Yuan, X., Yao, Z., Wu, J., Zhou, Y., Shan, Y., Dong, B., Zhao, Zhenhu, et al. (2007). G1 phase cell cycle arrest induced by SARS-CoV 3a protein via the cyclin D3/pRb pathway. *American journal of respiratory cell and molecular biology*, *37*(1), 9-19.

Zhao, Jincun, Falcón, A., Zhou, H., Netland, J., Enjuanes, L., Pérez Breña, P., & Perlman, S. (2009a). Severe acute respiratory syndrome coronavirus protein 6 is required for optimal replication. *Journal of virology*, *83*(5), 2368-73.

Zhao, Jincun, Zhao, Jingxian, & Perlman, S. (2010). T cell responses are required for protection from clinical disease and for virus clearance in severe acute respiratory syndrome coronavirus-infected mice. *Journal of virology*, *84*(18), 9318-25.

Zhao, Jincun, Zhao, Jingxian, Van Rooijen, N., & Perlman, S. (2009b). Evasion by stealth: inefficient immune activation underlies poor T cell response and severe disease in SARS-CoV-infected mice. *PLoS pathogens*, *5*(10), e1000636.

Zhao, Zijiang, Thackray, L. B., Miller, B. C., Lynn, T. M., Becker, M. M., Ward, E., Mizushima, N. N., et al. (2007). Coronavirus replication does not require the autophagy gene ATG5. *Autophagy*, *3*(6), 581-5.

Zhong, X., Guo, Zufeng, Yang, H., Peng, L., Xie, Y., Wong, T.-Y., Lai, S.-T., et al. (2006). Amino terminus of the SARS coronavirus protein 3a elicits strong, potentially protective humoral responses in infected patients. *The Journal of general virology*, *87*(Pt 2), 369-73.

Zhou, H., Ferraro, D., Zhao, Jincun, Hussain, S., Shao, J., Trujillo, J., Netland, J., et al. (2010). The N-terminal region of severe acute respiratory syndrome coronavirus protein 6 induces membrane rearrangement and enhances virus replication. *Journal of virology*, *84*(7), 3542-51.

I

Available online at www.sciencedirect.com
ScienceDirect
Virology 366 (2007) 293–303
VIROLOGY
www.elsevier.com/locate/yviro

The nonstructural protein 8 (nsp8) of the SARS coronavirus interacts with its ORF6 accessory protein

Purnima Kumar [a,1], Vithiagaran Gunalan [b,1], Boping Liu [c], Vincent T.K. Chow [c], Julian Druce [d], Chris Birch [d], Mike Catton [d], Burtram C. Fielding [b], Yee-Joo Tan [b], Sunil K. Lal [a,*]

[a] *Virology Group, International Centre for Genetic Engineering and Biotechnology, P. O. Box: 10504, Aruna Asaf Ali Road, New Delhi 110067, India*
[b] *Collaborative Anti-Viral Research Group, Institute of Molecular and Cell Biology, 61 Biopolis Drive, Proteos, Singapore 138673, Singapore*
[c] *Microbiology Department, National University of Singapore, Kent Ridge, Singapore 117597, Singapore*
[d] *Victorian Infectious Diseases Reference Laboratory, North Melbourne, Victoria, Australia*

Received 20 February 2007; returned to author for revision 14 March 2007; accepted 21 April 2007
Available online 25 May 2007

Abstract

Severe acute respiratory syndrome (SARS) coronavirus (SARS-CoV) caused a severe outbreak in several regions of the world in 2003. The SARS-CoV genome is predicted to contain 14 functional open reading frames (ORFs). The first ORF (1a and 1b) encodes a large polyprotein that is cleaved into nonstructural proteins (nsp). The other ORFs encode for four structural proteins (spike, membrane, nucleocapsid and envelope) as well as eight SARS-CoV-specific accessory proteins (3a, 3b, 6, 7a, 7b, 8a, 8b and 9b). In this report we have cloned the predicted nsp8 gene and the ORF6 gene of the SARS-CoV and studied their abilities to interact with each other. We expressed the two proteins as fusion proteins in the yeast two-hybrid system to demonstrate protein–protein interactions and tested the same using a yeast genetic cross. Further the strength of the interaction was measured by challenging growth of the positive interaction clones on increasing gradients of 2-amino trizole. The interaction was then verified by expressing both proteins separately in-vitro in a coupled-transcription translation system and by coimmunoprecipitation in mammalian cells. Finally, colocalization experiments were performed in SARS-CoV infected Vero E6 mammalian cells to confirm the nsp8–ORF6 interaction. To the best of our knowledge, this is the first report of the interaction between a SARS-CoV accessory protein and nsp8 and our findings suggest that ORF6 protein may play a role in virus replication.

Keywords: SARS coronavirus; Protein–protein interaction; Yeast two-hybrid system; Non structural protein; Accessory protein; Immunoprecipitation

Introduction

Severe acute respiratory syndrome (SARS) is a newly emerging infectious disease. The etiologic agent of SARS has been identified as a novel coronavirus, namely SARS-associated coronavirus (SARS-CoV) (Ksiazek et al., 2003; Marra et al., 2003; Peiris et al., 2003; Rota et al., 2003). As of June 30th, 2003, 8447 probable SARS cases including 811 deaths were reported by the World Health Organization (WHO) from 32 countries or regions worldwide. The significant morbidity and mortality, and the potential for re-emergence, makes SARS-CoV a continued worldwide public health threat.

Like other known coronaviruses, SARS-CoV is an enveloped, plus-strand RNA virus that features the largest RNA genomes currently known. The SARS viral genome comprises approximately 30,000 nucleotides, which are organized into 14 functional open reading frames (ORFs) (Rota et al., 2003; Thiel et al., 2003). Analysis of the nucleotide sequence of this novel coronavirus revealed a similar pattern of gene organization typical of coronaviruses (Marra et al., 2003; Rota et al., 2003). Two large, 5′-terminal overlapping ORFs, 1a and 1b of the replicase gene encode two polyproteins, pp1a and pp1ab (Fig. 1) (Rota et al., 2003; Thiel et al., 2003). Like other coronaviruses, the nascent SARS-CoV replicase polyproteins are processed by

Abbreviations: AD, activation domain; BD, binding domain; 3-AT, 3-amino trizole; N, nucleocapsid.

* Corresponding author. Fax: +91 11 26162316.
E-mail address: sunillal@icgeb.res.in (S.K. Lal).
[1] Contributed equally.

0042-6822/$ - see front matter © 2007 Elsevier Inc. All rights reserved.
doi:10.1016/j.virol.2007.04.029

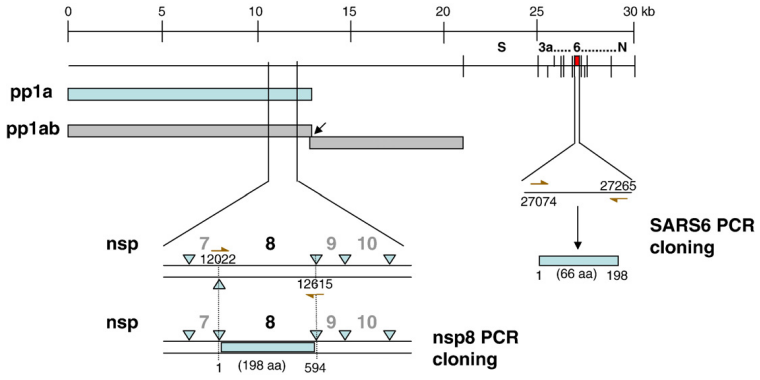

Fig. 1. Cloning of the putative nsp8 and ORF6 genes from the SARS CoV genome. The full-length nsp8 (198 amino acids) and ORF6 (66 amino acids) genes of the SARS coronavirus (Tor2 isolate) were PCR-amplified from a genomic construct of clone NC_004718 and cloned into the pCR-XL-TOPO vector (Invitrogen) as described in Table 1. The scale on top shows genomic region.

virus-encoded proteinases, and in this case, two proteinases have been identified: a 3C-like proteinase (3CLpro) and a papain-like proteinase (PLP) (Denison et al., 1992; Snijder et al., 2003; Ziebuhr, 2004). The processed end products of pp1a are designated nonstructural proteins (nsp) 1 to nsp11 and those of pp1ab are designated nsp1 to nsp16. Cleavage by the viral main protease, $3CL^{pro}$ results in generating the nsp8 protein which is currently of undesignated function. The nsp8 protein has been shown to associate with several other nsps and to colocalize with these nsps in cytoplasmic complexes that are important for viral RNA synthesis (Prentice et al., 2004a, 2004b; Sutton et al., 2004; Zhai et al., 2005). The +RNA coronavirus usually encode a non-structural protein (nsp12 for SARS-CoV) that includes an RdRp domain, conserved in all RNA viruses. The SARS-CoV uniquely encodes a second RdRp residing in nsp8, responsible for initiation of the synthesis of complementary oligonucleotides smaller than 6 residues long, at relatively low fidelity. These nsp8 RdRp produced primers are postulated to be utilized by the primer-dependent nsp12 RdRp for replication (Imbert et al., 2006).

The remaining 12 ORFs encode the four structural proteins, spike (S), membrane (M), nucleocapsid (N) and envelope (E), and eight accessory proteins (3a, 3b, 6, 7a, 7b, 8a, 8b and 9b). These accessory proteins are postulated to be non-essential in tissue culture but may provide a selective advantage in the infected host. The ORF3a protein has been studied to some details (Tan et al., 2006) and has been shown to be expressed in infected cells (Tan et al., 2004c; Yu et al., 2004; Zeng et al., 2004). ORF3a protein has been shown to bind the spike protein (Zeng et al., 2004; Tan et al., 2004c) and recent work demonstrated that it is a novel structural protein (Ito et al., 2005). The ORF7a protein was also detected in infected cells and has been found to localize in the ER-Golgi intermediate compartments where coronaviruses are known to assemble (Fielding et al., 2004; Nelson et al., 2005). In addition, ORF3a, ORF3b and ORF7a proteins have been shown to induce apoptosis (Tan et al., 2004a; Law et al., 2005; Yuan et al., 2005). Two recent papers on the ORF6 accessory protein also demonstrated its expression during infection and have showed that it may be important for viral pathogenesis (Geng et al., 2005; Pewe et al., 2005). Most recently the ORF6 protein has been shown to accelerate replication of a related mouse virus, a property that may contribute towards its increased in vivo virulence (Tangudu et al., 2007).

In this study, the nsp8 and ORF6 proteins were tested for interaction in a yeast cellular environment using the yeast two-hybrid system. These interactions were further verified by in-vitro coimmunoprecipitation experiments using proteins expressed by a coupled-transcription/translation system or in mammalian cells by lipid-mediated transfection of DNA. Finally, the nsp8–ORF6 interaction was confirmed by colocalization of the two proteins in SARS-CoV infected mammalian cells (Vero E6). This unique SARS-CoV accessory protein 6 interacting with a non-structural protein, nsp8, suggests that ORF6 may have a role in SARS virus replication.

Results and discussion

The nsp8 protein of the SARS coronavirus was cloned from the Tor2 Singapore isolate and expressed using the yeast two-hybrid vectors resulting in an N-terminal in-frame fusion protein with the GAL4 activation domain (AD). Similarly the ORF6 protein was PCR cloned and expressed in yeast two-hybrid vectors resulting in an N-terminal in-frame fusion protein with the GAL4 DNA binding domain (BD). In order to check for correct reading-frame constructs, the final plasmids were sequenced and checked for in-vitro protein expression. *Saccharomyces cerevisiae* AH109 cells were transformed with single plasmids, or co-transformed with the GAL4 BD- and AD-vectors containing SARS Co-V ORF6 and/or nsp8, respectively. The AH109 host strain containing pAS2-N and pACT2-N were used as positive controls (Surjit et al., 2004).

AH109 contains integrated copies of both HIS3 and *lacZ* reporter genes under the control of GAL4 binding sites. The results of the two-hybrid assay are shown in Fig. 2A. Single transformants used in this assay were yeast (AH109) cells containing BD-ORF6, and host cells containing AD-nsp8, also yeast cells containing only the BD- and only the AD-vectors, were also used as negative controls. All these transformants and co-transformants grew well on the unrestricted YPD plate (non-

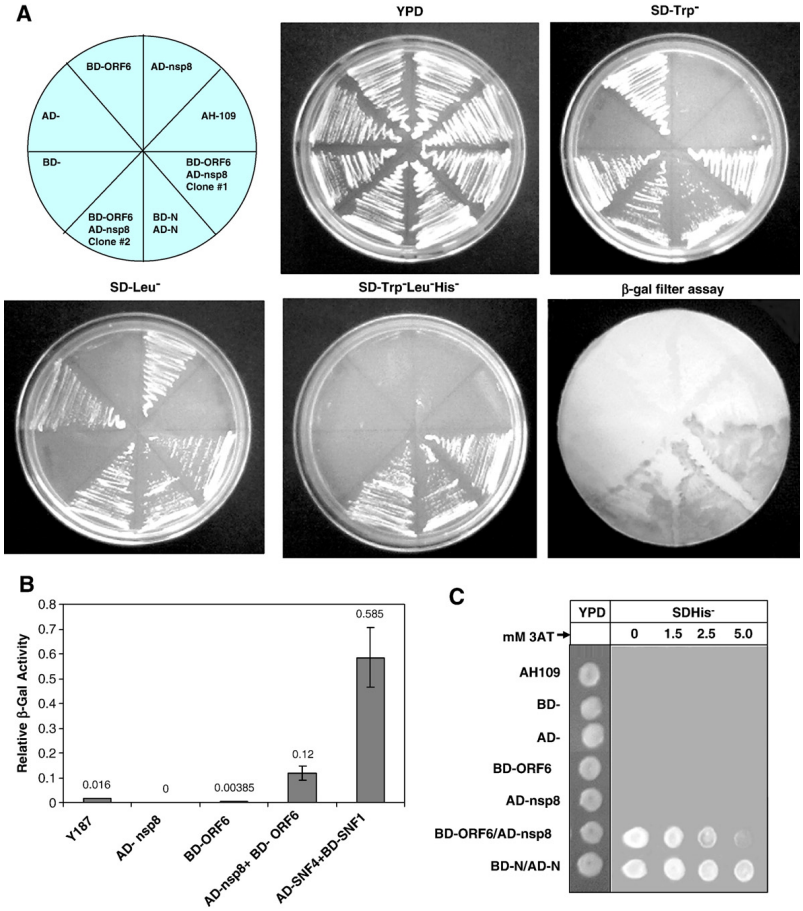

Fig. 2. Yeast two-hybrid results showing that nsp8 and ORF6 proteins interact with each other. (A) AD-nsp8 fusion protein and BD-ORF6 fusion protein tested as single and co-transformants on various synthetic growth media lacking specific amino-acids. YPD media shows uninhibited growth of all transformants and host strain. SDTrp⁻ and SD-Leu⁻ selective media have Tryptophan and Leucine missing, respectively. SD Trp⁻Leu⁻His⁻ media are triple dropout plates lacking Tryptophan, Leucine and Histidine. Growth on the SD Trp⁻Leu⁻His⁻ plate and blue color (shown here in shades of grey) on the β-gal filter assay represents a positive interaction. BD-N:AD-N combination was used as a positive control in these yeast two-hybrid experiments (Surjit et al., 2004). (B) Liquid β-galactosidase assay results of the nsp8–ORF6 protein–protein interactions. Single transformants and co-transformants were analyzed in a liquid β-galactosidase assay and compared with each other. Values given are in arbitrary units. The numbers above each bar represent the mean from five independent transformants. Y187 corresponds to the untransformed host strain. Transformants with more than one plasmid are separated by a slash. Positive controls used in this assay are denoted by BD-SNF1/AD-SNF4 (Harper et al., 1993). (C) Measurement of strength of the nsp8–ORF6 interactions on an increasing 3-AT gradient. Activation of the *HIS3* reporter was determined for the host AH109 strain, single transformants (BD, AD, BD-ORF6 and AD-nsp8), and co-transformants (BD-ORF6/AD-nsp8 and BD-N/AD-N). Hundred-fold serial dilutions of all of the above-mentioned log-phase cultures were plated on YPD (left) followed by SD-His-plus 50 mM 3-AT in increasing concentrations (0 mM to 5 mM 3-AT).

selective media). Also, the untransformed host cells were plated as a negative control. Single transformants containing the BD-by itself or as a fusion with the ORF6 protein, showed growth on the synthetic dextrose Trp^- plate ($SDTrp^-$). Correspondingly, single transformants containing the AD- by itself or as a fusion with nsp8 showed growth on the synthetic dextrose Leu^- plate ($SDLeu^-$). The co-transformants were similarly plated on YPD and synthetic dextrose medium lacking Trp or Leu or Trp, Leu and upon positive growth on these was subsequently plated on His^- medium ($SD\ Trp^-Leu^-His^-$) to test for His prototrophy. Growth of the co-transformants, containing the BD-ORF6 and AD-nsp8 constructs, in both $SDTrp^-$ and $SDLeu^-$ plates simply showed that both plasmids were present in the transformed cells. Growth of these clones on the $SD\ Trp^-Leu^-His^-$ media showed that the transcription of the HIS3 gene was turned on by the reconstitution of the GAL4 transactivator due to a specific ORF6–nsp8 interaction. Colonies were transferred on to nitrocellulose filters and a β-galactosidase filter assay was performed as described in methods. The co-transformants containing both the BD-ORF6 and AD-nsp8 constructs along with all positive and negative controls were used in this assay. Results obtained from the β-galactosidase filter assay were in agreement with the results obtained from the $SDHis^-$ growth experiments.

The liquid β-galactosidase assay was conducted and the activity determined using the substrate chlorophenol red-β-D-galactopyranoside (CPRG) as described in methods. The host strain alone, along with single transformants containing either AD-nsp8 or BD-ORF6 and co-transformants containing AD-/BD- without a fusion protein was tested. Negative controls (host untransformed cells) showed almost no liquid β-galactosidase activity. BD-SNF1/AD-SNF4 was the positive control whereas the clones containing BD-ORF6/AD-nsp8 were the test samples in this experiment (Fig. 2B). Relative enzymatic activity was determined in five independent transformants from each group. Our results from this assay indicate a moderate strength protein–protein interaction between the AD-nsp8 and BD-ORF6 proteins. This observation was further confirmed by the use of a 3-AT gradient on which the His^+ phenotype was tested (Fig. 2C). 3-AT is known to be a competitive inhibitor of HIS3 protein, thus enhancing the stringency of selection, it reduces the background signal by inhibiting the product of the HIS3 reporter. This result clearly showed that the interaction of nsp8 with ORF6 was not as strong as the N–N dimerization positive control interaction. On plates with increasing concentrations of 3-AT, the growth ability of the His^+ colonies diminished and was almost undetectable at 5 mM 3-AT concentrations.

To further confirm these interactions we performed a coimmunoprecipitation assay using proteins expressed by a cell-free coupled transcription–translation system. The rabbit reticulocyte lysates expressing His6-nsp8 and myc-ORF6 proteins separately were tested for expression (Fig. 3A). For detection of the expressed proteins, the lysates were immunoprecipitated using the respective antibodies i.e. anti-His antibody was used for detection of the nsp8 protein and anti-myc antibody was used for the detection of the ORF6 protein. When the two cell lysates were mixed in equal proportions, one of the two antibodies was added and subsequently pulled out using Protein A Sepharose beads, we observed the interacting protein to be present in the gel as well. This procedure was repeated conversely to show the other corresponding antibody pull out the interacting protein partner as well (Fig. 3B). When

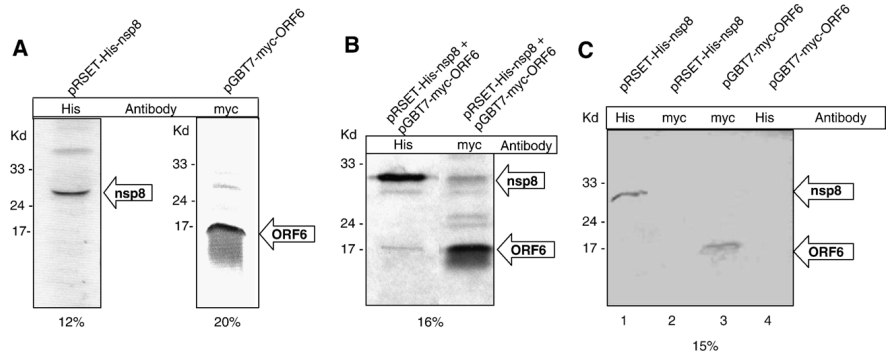

Fig. 3. Confirmation of the nsp8–ORF6 interaction using an in-vitro cell-free coupled transcription/translation coimmunoprecipitation assay. (A) The His_6-tagged nsp8 and myc-tagged ORF6 proteins were produced by coupled transcription–translation in the presence of ^{35}S-Met and detected using their corresponding antibodies (Anti-His and anti-myc, respectively). Both nsp8 and ORF6 proteins were visible and corresponded to their correct molecular sizes on 12% and 20% SDS-PAGE, respectively. (B) The ^{35}S-Met-His-nsp8 and ^{35}S-Met-myc-ORF6 proteins were detected by autoradiography. The nsp8–ORF6 complex was detected by both anti-His and anti-myc antibodies on 16% SDS-PAGE. When nsp8 was probed for using anti-His antibody, the ORF6 protein was visible and when ORF6 protein was probed using myc antibody, the nsp8 protein was visible. (C) In a control reaction, the ^{35}S-Met-His_6-nsp8 and ^{35}S-Met-myc-ORF6 proteins showed no cross-reactivity with the other antibody used in the pull-down experiments. Also this control experiment shows that the proteins do not non-specifically bind to the beads used in the results shown in panel B. Lane 1 shows the nsp8 protein immunoprecipitated by anti-His, lane 2 does not show nsp8 protein band when immunoprecipitated by anti-myc. Similarly, lane 3 shows myc-tagged ORF6 protein immunoprecipitated by anti-myc and lane 4 does not show ORF6 protein where it was immunoprecipitated using anti-His.

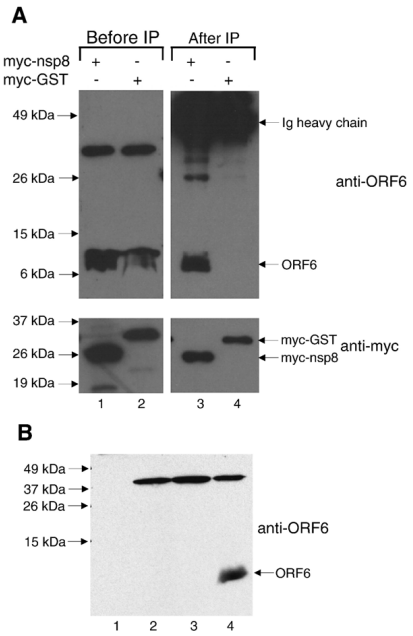

Fig. 4. (A) Cell lysates were obtained from Vero E6 cells expressing ORF6 and myc-nsp8 or ORF6 and myc-GST (negative control) and subjected to Western blot analysis with either anti-ORF6 polyclonal (upper panel, lanes 1 and 2) or anti-myc monoclonal antibodies (lower panel, lanes 1 and 2). Equal amounts of lysates were subjected to immunoprecipitation using anti-myc polyclonal antibodies and protein A beads. The immuno-complexes were subjected to Western blot with either anti-ORF6 polyclonal (upper panel, lanes 3 and 4) or anti-myc monoclonal antibodies (lower panel, lanes 3 and 4). (B) Equal amounts of total cellular protein from Vero E6 cells either uninfected (lane 1) or infected with wildtype Dryvax (lane 2), a recombinant vaccinia virus expressing the SARS-CoV S protein (lane 3), or the recombinant vaccinia virus expressing the ORF6 protein used in this study (lane 4) were subjected to Western blot and probed with anti-ORF6 rabbit polyclonal antibody. This demonstrates that the ~37 kDa band seen in lanes 1 and 2 of panel A is a cross-reacting protein that is probably a vaccinia virus protein or an up-regulated cellular protein which is detected by the rabbit anti-ORF6 antibody used in this study.

anti-His antibody was used to pull out the nsp8 protein from the mixture of proteins, it also pulled out the ORF6 protein. Similarly, when anti-myc antibody was used to pull out the ORF6 protein, the nsp8 protein was also observed to be pulled out as an interaction partner of ORF6. In a control experiment we observed no ORF6 protein binding directly to the anti-His antibody Sepharose-A complex and similarly observed no binding of the nsp8 protein to the anti-myc antibody Separose-A complex (Fig. 3C). These results clearly showed that the two proteins nsp8 and ORF6 interacted with each other.

In order to verify the interaction between nsp8 and ORF6 in mammalian cells, co-immunoprecipitation experiments were performed using lysates obtained from Vero E6 cells expressing transiently transfected myc-tagged nsp8 and untagged ORF6 proteins carried by a replicative recombinant vaccinia virus. Myc-polyclonal antibody conjugated to protein A Sepharose beads was used to pull-down myc-nsp8 or myc-GST (negative control), and any ORF6 protein that co-immunoprecipitated was detected using a rabbit polyclonal antibody raised against a peptide of ORF6 (Abgent). This antibody specifically detected the ORF6 protein (~7 kDa) in cells that were infected with ORF6 recombinant vaccinia virus (Fig. 4, lanes 1 and 2). As shown in Fig. 4, ORF6 was co-immunoprecipitated by myc-nsp8 (lane 3) but not by myc-GST (lane 4), showing that the ORF6 and nsp8 proteins can interact in Vero E6 cells.

In order to confirm that the interaction between nsp8 and ORF6 occurs during SARS-CoV infection, co-immunoprecipitation experiments were performed with lysates obtained from SARS-CoV infected cells. Infection of Vero E6 cells with an isolate of SARS-CoV (strain HKU 39849) was carried out in a physical containment level 4 (PC4) laboratory as previously described (Kaye et al., 2006). The cells were harvested at 0 or 24 h post-infection (h.p.i.) and the lysates were subjected to Western blot analysis to determine the expression of nsp8 and ORF6 proteins (Fig. 5). Two specific proteins in the cells at 24 h. p.i. were detected with purified supernatant from hybridomas producing monoclonal antibodies against the nsp8 protein (see Materials and methods) and these were not found in the cells harvested at 0 h.p.i. (upper panel, lanes 1 and 2). The protein that

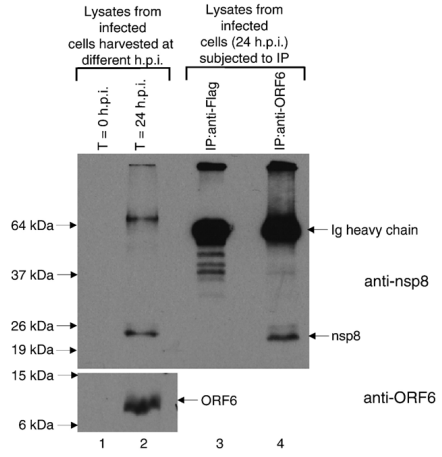

Fig. 5. Lysates were obtained from SARS-CoV infected Vero E6 cells harvested at 0 or 24 h post infection (h.p.i.) and Western blot analyses were performed to determine the expression of SARS-CoV proteins using mouse anti-nsp8 monoclonal antibody (upper panel, lanes 1 and 2) and rabbit anti-ORF6 polyclonal antibody (lower panel, lanes 1 and 2). Cell lysates obtained at 24 h.p.i. were then subjected to immunoprecipitation using anti-Flag (irrelevant antibody as negative control) or anti-ORF6 rabbit polyclonal antibodies and protein A beads. The immuno-complexes were subjected to Western blot analysis with mouse anti-nsp8 monoclonal antibody (upper panel, lanes 3 and 4).

migrated at ~24 kDa matched the predicted molecular mass of nsp8 while the slower migrating protein (~65 kDa) may be an aggregated form of nsp8. As expected, the ORF6 protein was also detected at 24 h.p.i. and not at 0 h.p.i. (lower panel, lanes 1 and 2). Cell lysates obtained at 24 h.p.i. were then subjected to immunoprecipitation with either an irrelevant antibody (rabbit anti-Flag polyclonal antibody, lane 3) or rabbit anti-ORF6 polyclonal antibody (lane 4) and protein-A agarose beads. Western blot analyses showed that nsp8 protein (~24 kDa) was co-immunoprecipitated when anti-ORF6 antibody was used but not when an irrelevant antibody was used, indicating that the nsp8 interacts specifically with ORF6 in SARS-CoV infected cells (upper panel, lanes 3 and 4).

Indirect immunofluorescence analysis of ORF6 expression in SARS-CoV-infected cells (Fig. 6, middle panel) showed that, consistent with previous publications (Geng et al., 2005; Pewe et al., 2005), ORF6 was found in the cytoplasm. Most of the ORF6 protein seen in infected cells were observed in a punctate staining pattern consistent with a vesicle-associated intracellular distribution. Using the rabbit polyclonal antibody against ORF6 (Abgent) and purified supernatant from hybridomas producing monoclonal antibodies against the nsp8 protein (see Materials and methods), cells infected with an isolate of SARS-CoV (strain HKU39849) were examined by indirect immunofluorescence to determine if the two proteins colocalized, as their interaction would suggest. The extent of colocalization seen between the two proteins was significant, both localizing to the same set of punctate structures (Fig. 6, middle panel, D). The punctate distribution of nsp8 has been previously described (Prentice et al., 2004a) and the colocalization of ORF6 protein with nsp8 suggests that ORF6 could be associated with the SARS-CoV replicase complex, localized to a subset of the vesicular trafficking complex in mammalian cells. These ORF6-containing vesicular structures did not colocalize with AP-1 and LAMP-2 (data not shown), which are present in early and late endosomes respectively. However, the ORF6 protein does colocalize with LAMP-1 (Fig. 7), which is a lysosomal marker. LAMP-1 has been used as a marker for characteristic double-membrane vesicles seen in infections by other viruses (Jackson et al., 2005) and it has been shown that at least one other coronavirus induces these double-membrane vesicles, presumably as a site for the assembly of virus replication complexes (Prentice et al., 2004b). Given this, the ORF6 protein might localize to these vesicles which have been suggested to be derived from the cellular autophagosomal machinery, but further study will be required. A recent structural study of the nsp8 protein has suggested a role for the

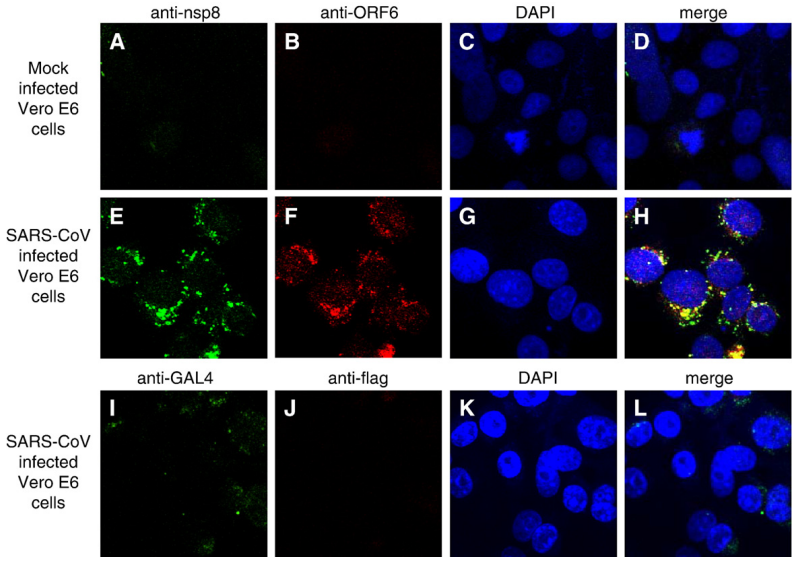

Fig. 6. Indirect immunofluorescence used to study cellular localization of nsp8 and ORF6 in SARS-CoV infected Vero E6 cells. (Upper panel) Mouse anti-nsp8 (A) and rabbit anti-ORF6 (B) antibodies were used against uninfected cells to determine if the antibodies showed any unspecific staining. Nuclei are represented by means of a DAPI stain (C). (Middle panel) Vero E6 cells infected with SARS-CoV were examined by indirect immunofluorescence using the same antibodies. The expression of nsp8 is represented by FITC staining (E), while the expression of ORF6 is represented by Rhodamine staining (F). Nuclei are represented by means of a DAPI stain (G). The merged image showed that the nsp8 and ORF6 proteins colocalize to punctuate structures in the cytoplasm (H). (Lower panel) Irrelevant antibodies (mouse anti-GAL4TA (I) and rabbit anti-flag (J)) were used to probe SARS-CoV infected cells at the same final concentrations as their counterparts in the middle panel to show the specificity of the antibodies used in detecting the ORF6 and nsp8 proteins.

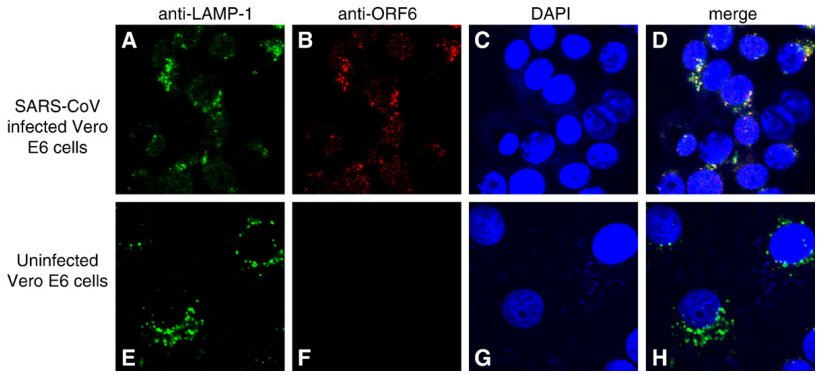

Fig. 7. Indirect immunofluorescence was used to probe for LAMP-1 (A, E) and ORF6 (B, F) staining in SARS-CoV infected cells (upper panel) and uninfected Vero E6 cells (lower panel). Nuclei are represented by means of a DAPI stain (C, G). The merged image showed that there is colocalization between the LAMP-1 protein and ORF6 proteins in SARS-CoV infected cells (D, upper panel).

nsp8–nsp7 hexadecamer in binding dsRNA intermediates in the viral replication cycle (Zhai et al., 2005), further lending impetus to such a study.

This is the first report describing the interaction between the ORF6 accessory protein and the nsp8 protein. We demonstrated the strength and specificity of this interaction by three independent methods, i.e. by yeast-2-hybrid, co-immunoprecipitation using in-vitro translated proteins in a cell-free system and co-immunoprecipitation using lysates from Vero E6 cells. Interestingly, two previous publications on ORF6 have shed some light on its possible function in viral pathogenesis. Geng and co-workers detected ORF6 protein in lung and intestine of SARS patients and showed that it could stimulate cellular DNA synthesis when over-expressed (Geng et al., 2005). Pewe et al. (2005) showed that when SARS-CoV ORF gene was introduced into an attenuated murine coronavirus, the recombinant virus grew faster in cell culture and also exhibited enhanced lethality of infection in mice. In contrast, Yount and co-workers reported that the SARS-CoV virus with ORF6 deleted has the same viral replication kinetics as the wild-type virus in cell-culture and mice (Yount et al., 2005). Hence, ORF6 is non-essential for viral replication in these models although it cannot rule out that ORF6 (and/or the other accessory proteins of SARS-CoV) contributes to the virulence and pathogenesis of SARS coronavirus infection in its natural host. Further experiments in more robust animal models, like non-human primates that demonstrate clinical disease upon SARS-CoV infection, will be needed to determine the actual function of ORF6 during SARS infection in vivo. Since our data shows that ORF6 interacts with nsp8 which is part of the replicase complex (Prentice et al., 2004a, 2004b), it will be important in future studies to determine if the interaction between ORF6 and nsp8 can modulate the viral synthesis process and to determine how ORF6 modulates viral pathogenesis in these animal models.

Materials and methods

Growth media, yeast strains and plasmid constructs

All strains, plasmids and plasmid constructs used in this study are described in Table 1. The full-length nsp8 and ORF6 genes of the SARS coronavirus (Tor2 isolate) were PCR-amplified from a genomic construct of clone NC_004718 (Fig. 1), and cloned into the pCR-XL-TOPO vector (Invitrogen). The full-length nsp8 and ORF6 genes were subjected to DNA sequencing and the inserts were verified against the corresponding region of the SARS coronavirus complete genome NC_004718. The nsp8 gene was excised from the pCR-XL-TOPO-nsp8 construct using the restriction enzymes *Nco*I and *Eco*RI, and ligated into the yeast two-

Table 1
Yeast strains, plasmids and recombinant plasmid constructs used in this study

Strain/plasmid/ construct	Genotype/description/reference
Strains	
AH109	MATa *trp1-901* his3 leu2-3, 112 ura3-52 ade2 gal4 gal80URA3: :GAL-lacZ LYS2: :GAL-HIS3
Y187	MATα, ura3-52, his3-200, ade2-101, trp1-901, leu2-3, 112, gal4Δ, met-, gal80Δ, URA3: :$GAL1_{UAS}$- $GAL1_{TATA}$-lacZ
Plasmids	
pGADT7/pACT2	*GAL4* AD vector [*GAL4(768–881)*]; *LEU2*, 2 μm, Amp^r
pGBKT7/pAS2	GAL4 DNA-BD vector [*GAL4(1–147)*]; *TRP1*, 2 μm, Amp^r
Constructs	
pACT2-nsp8	pCR-XL-TOPO-nsp8-easy-nsp8 digested with *Nco*I and *Eco*RI, fragment ligated into pACT2
pGBKT7-ORF6	pCR-XL-TOPO-ORF6 digested with *Nco*I and *Eco*RI, fragment ligated into pGBKT7
pRSET-nsp8	pGEMT-nsp8 digested with *Nco*I and *Eco*RI, fragment ligated into pRSET

hybrid Activation Domain vector, pACT2 to generate an N-terminal in-frame fusion with the GAL4 activation domain (AD). The ORF6 gene was excised from the pCR-XL-TOPO-ORF6 construct using the restriction enzymes *Eco*RI and *Pst*I, and cloned into the yeast two-hybrid DNA Binding Domain (BD) vector pGBKT7 in fusion with the GAL4 DNA-binding domain to express an N-terminal fusion protein. Similarly the *Nco*I and *Eco*RI sites were used to clone the nsp8 gene into the pRSET vector to give the construct pRSET-nsp8. All DNA manipulations were performed as described by Sambrook et al. (1989). All constructs were verified by restriction digestion and DNA sequencing.

Yeast two-hybrid techniques

The GAL4-based two-hybrid system, kindly provided by Dr. Stephen Elledge (Harper et al., 1993), containing pGBKT7 (DNA-binding domain vector) and pACT2 (activation domain vector), together with the yeast reporter strain *S. cerevisiae* AH109 (*trp1-901* his3 leu2-3, 112 ura3-52 ade2 gal4 gal80URA3∷GAL-lacZ LYS2∷GAL-HIS3) were employed. The host strain containing the Nucleocapsid protein (N) of SARS virus fusion constructs pACT2-N and pAS2-N, shown previously to form a homodimer (Surjit et al., 2004) was used as a positive control. The AH109 host contains integrated copies of both *HIS3* and *lacZ* reporter genes under the control of GAL4 binding sites. The AH109 yeast strain was transformed with the appropriate plasmids, using the lithium acetate procedure and grown on SD plates in the absence of Trptophane (Trp) and Leucine (Leu); ($SDTrp^-$ and $SDLeu^-$). Protein interaction was tested on SD plates without Leu, Trp and Histidine ($SDLeu^-$ Trp^- His^-). After 3 days at 30 °C, individual colonies were streaked out and tested for liquid and filter-lift β-galactosidase activity, 5 mM 3-amino-1,2,3-trizole assay (3AT) and the liquid β-galactosidase assay (Ober et al., 2002; Peiris et al., 2003; Pewe et al., 2005). The filter β-galactosidase assay, a parameter directly reflecting the strength of protein–protein interactions, was performed by streaking doubly transformed yeast colonies onto filter paper and allowing them to grow for 2 days on selection medium. Yeast was permeabilized by freezing yeast-impregnated filters in liquid nitrogen, and thawing at room temperature. This filter was placed over a second filter that was pre-soaked in Z buffer (pH 7.0) containing 10 mg/ml 5-bromo-4-chloro-3-indolyl-β-D-galactopyranoside (X-gal) and 0.27% β-mercaptoethanol. Filters were left for 18 h to develop a blue color, which indicated a positive protein–protein interaction. The liquid β-galactosidase activity was determined using the substrate CPRG as described previously (Tyagi et al., 2001, 2002). Relative enzymatic activity was determined in five independent transformants. Data for quantitative assays were collected for yeast cell number and are the mean ± S.E.M. of triplicate assays. Appropriate positive/negative controls and buffer blanks were used. The yeast Y187 host strain containing BD-1111 and AD-1112 were used as positive controls for these assays.

In-vitro cell-free coupled transcription/translation binding analysis

The ^{35}[S]-methionine labeled full-length pRSET-His6-nsp8 protein (198 amino acids nsp8 with N-terminal His_6-tag) and radiolabelled ^{35}[S]-methionine full-length ORF6 accessory protein (66 amino acids with an N-terminal myc tag), were expressed in separate reactions using a coupled in-vitro transcription–translation system (TNT coupled reticulocyte lysate system; Promega) as per manufacturer's instructions. 10 μl of the His6-nsp8 labeled protein lysate was mixed with 10 μl of myc-ORF6 protein lysate. This mixture was incubated on ice for 2 h and the primary antibody (either anti-His or anti-myc) was added to the mixture. Subsequently the mixture was incubated at 4 °C for 1 overnight. Sepharose-A beads were added to the mixture and incubated at 4 °C with gentle shaking for 1 h. The beads were washed three times with PBS, resuspended in 10 μl of SDS-PAGE loading buffer and boiled for 5 min to dissociate the bound proteins and detected by autoradiography. Appropriate control reactions were performed to validate the data.

Mammalian cell cultures

The CV-1 (African Green monkey kidney) cell-line was a kind gift from Baxter Vaccines, Orth/Donau, Austria. The Vero E6 cell-line was purchased from the American Type Culture Collection (Manassas, VA, USA). All cells were cultured at 37 °C in 5% CO_2 in DMEM containing 1 g/l glucose, 2 mM L-glutamine, 1.5 g/l sodium bicarbonate, 0.1 mM non-essential amino acids, 0.1 mg/ml streptomycin and 100 U penicillin, and 10% FBS (HyClone, Utah, USA).

Generation of ORF6 recombinant replicating vaccinia virus

ORF6 recombinant replicating vaccinia virus was generated using the system developed by Baxter Vaccine (Orth/Donau, Austria). The vector, cell-lines and viruses used here were kind gifts from Baxter Vaccine. ORF6 was amplified from cDNA prepared from SARS-CoV infected cells as previously described (Tan et al., 2004b) and the pair of primers used is ORF6_forward (5′-GCAAGCTTATGTTTCATCTTGTTGA-3′) and ORF6_reverse (5′-CCGGCGGCCGCTTATGGATAATC-TAACACC-3′). The amplicon was digested with *Hin*dIII and *Not*I and cloned into the compatible sites of the pDD4-mh5 vector to create plasmid pDD4-mh5/ORF6. The pDD4-mh5 vector can be used to generate growth-competent recombinants expressing foreign genes in the D4 locus via a rescue method as previously described (Holzer and Falkner, 1997). Essentially, the parental virus lacking the D4 gene is replication negative in the usual permissive host lines and only the reintegration of D4 into the virus genome allows for growth in these lines. This is in contrast to classical drug-based screening approaches which have previously been well established in the generation of vaccinia recombinants.

CV-1 cells were grown to 70–80% confluence in 60 mm dishes. Confluent monolayers were washed once with PBS,

followed by a two washes with 1 ml DME containing no FBS or antibiotics. The culture medium was removed and overlaid with 0.2 ml defective vaccinia virus (dVVL) (~multiplicity of infection is 1 pfu/cell) diluted in 0.6 ml DMEM for 1 h at 37 °C in CO_2, with shaking every 15 min. dVVL is derived from the vaccinia virus Lister strain (ATCC VR-862; Ober et al., 2002, and was titered in the complementing cell line RK44.20; Holzer and Falkner, 1997). The supernatant was removed, replaced with 2 ml DMEM containing no FBS or antibiotics and cells were transfected with 5 μg pDD4-mh5/ORF6 using lipofectamine reagent (Invitrogen, Carlsbad, CA, USA), according to the manufacturer's protocol. After 3 days, advanced cytopathic effect was evident and the cells were harvested and subjected to Western blot analysis (see below) for determining ORF6 expression. Alternatively, the cells and culture supernatant were harvested together and then subjected to three rounds of freeze-thawing and clarified by centrifugation at 1500 rpm for 5 min. The supernatant, which constitute the P1 viral stock, was used to infect fresh CV-1 cells after which the P2 viral stock was harvested in the same manner and stored at −80 °C before use. The P2 viral stock was titered in CV-1 cells. This approach of dominant host range selection provides a stringent and time-saving method for obtaining vaccinia recombinants carrying foreign genes and has been described previously (Holzer et al., 1998). The recombinant vaccinia virus expressing the SARS-CoV S protein was previously generated using the same methods (Lip et al., 2006).

Expression of viral proteins in mammalian cells and co-immuoprecipitation experiments

The nsp8 gene was PCR amplified from the pRSET-nsp8 plasmid with the following pair of primers: nsp8_forward (5′-CGGGATCCGGCACCATGGCTATTGCTTCAG-3′) and nsp8_reverse (5′-CCGCTCGAGTCACTGTAGTTTAA-CAGCTG-3′). The amplicon was digested with *Bam*HI and *Xho*I and cloned into compatible sites in the mammalian expression pXJ40myc vector which contains a myc-tag at the N-terminus for ease of detection. Typically, ~1×10^6 cells Vero E6 were plated on 6 cm dish and allowed to attach overnight and then infected with ORF6 recombinant vaccinia virus at a multiplicity of infection of 1. Infection media was replaced 1 h post-infection and the cells were transfected with 1 ug of pXJ40myc-nsp8 using lipofectamine reagent as described above. The cells were harvested ~16 h later and lysed in IP buffer (50 mM Tris (pH 8.0), 150 mM NaCl, 0.5% NP40, 0.5% deoxycholic acid, 0.005% SDS) and used in co-immunoprecipitation experiments as previously described (Tan et al., 2004c). Briefly, the lysate was incubated with an anti-myc polyclonal antibody (A14, Santa Cruz Biotechnology, Santa Cruz, CA, USA) overnight at 4 °C, followed by adsorption onto a 50 μl suspension of protein A-sepharose beads (Roche Molecular Biochemicals). Beads were then washed 3 times with cold IP buffer and subjected to Western blot analysis as previously described. Primary antibodies used here were anti-myc monoclonal (9E10, Santa Cruz Biotechnology) and rabbit anti-ORF6 (PUP3, Abgent, San Diego, CA, USA).

For co-immunoprecipitation experiments performed with SARS-CoV infected Vero E6 cells, Vero E6 cells were plated in 25 cm^2 flasks and infected with an isolate of SARS-CoV (strain HKU39849) as previously described (Kaye et al., 2006). The cells were harvest at 0 or 24 h.p.i. and the lysates were then subjected to Western blot analysis and co-immunoprecipitation experiments as described above. Anti-nsp8 monoclonal (described below) and rabbit anti-ORF6 antibodies were used for Western blot while rabbit anti-flag polyclonal (Sigma) or rabbit anti-ORF6 antibodies were used for immunoprecipitation.

Immunofluorescence analysis

Indirect immunofluorescence was performed using SARS-CoV infected Vero E6 cells as previously described (Tan et al., 2004c). Briefly, Vero E6 cells were plated onto 4-well chamber slides (Lab-Tek) and infected with an isolate of SARS-CoV (strain HKU39849) as previously described (Kaye et al., 2006). 42 h post-infection, chamber slides were washed twice in phosphate-buffered saline (PBS); cells were then fixed and permeabilized with methanol for 5 min and subsequently subjected to gamma-irradiation to neutralize infectivity of the virus. Cells were then refixed with 4% paraformaldehyde and permeabilized with 0.2% Triton X100. Blocking was done using PBS with 1% bovine serum albumin (Sigma) and each chamber was incubated with relevant and irrelevant control antibodies before being washed with PBS+1% BSA several times. Chamber slides were then incubated using FITC-conjugated goat anti-mouse and rhodamine-conjugated goat anti-rabbit secondary antibodies (1:200; Santa Cruz) before being washed again and mounted using glass coverslips and a mixture of Fluorsave mounting medium (Calbiochem) and Vectashield mounting medium with DAPI (Vector Laboratories). Imaging was done with an Olympus Fluoview upright confocal microscope (Olympus).

Antibodies for detecting endogenous AP-1 and the FLAG epitope were purchased from Sigma and antibodies against LAMP-1 and LAMP-2 were purchased from Abcam plc. The anti-GAL4TA antibody was purchased from Santa Cruz. Monoclonal antibody against the nsp8 protein was prepared as follows: bacterially expressed glutathione *S*-transferase (GST)-nsp8 fusion protein was used to immunize BALB/c mice as previously described (Fielding et al., 2004). The spleen was excised from a mouse that showed strong antibody response and hybridoma fusion was performed to generate hybridomas producing monoclonal anti-nsp8 antibodies as previously described (Lip et al., 2006). All procedures on the use of laboratory animals were performed by trained personnel in accordance with the regulations and guidelines of the National Advisory Committee for Laboratory Animal Research (NACLAR), Singapore. The culture supernatants from several of these hybridoma clones were pooled and purified using a HiTrap protein G HP column (Amersham) and verified by immunofluoresence assay to be specific to the nsp8 protein.

The mouse monoclonal primary antibodies (mouse anti-nsp8 and anti-GAL4TA) were used at concentrations of 0.2 mg/ml

and the rabbit polyclonal antibodies (anti-ORF6 and anti-flag) were used at concentrations of 0.0025 mg/ml. Identical dilutions of secondary antibodies were used for all samples.

Acknowledgments

This work was supported by internal funds from the International Centre for Genetic Engineering and Biotechnology (India), Institute of Molecular and Cell Biology (Agency for Science, Technology and Research (A∗STAR), Singapore), and Microbiology Department, National University of Singapore and a research grant from the Department of Biotechnology, Government of India. We thank Baxter Vaccine (Orth/Donau, Austria) for sharing their proprietary vaccinia virus expression system, and personnel at the Biological Resource Centre (Agency for Science, Technology and Research (A∗STAR), Singapore), Monoclonal Antibody Unit (Institute of Molecular and Cell Biology, Singapore) and PC4 laboratory (Victorian Infectious Diseases Reference Laboratory, Australia) for technical assistance.

References

Denison, M.R., Zoltick, P.W., Hughes, S.A., Giangreco, B., Olson, A.L., Perlman, S., Leibowitz, J.L., Weiss, S.R., 1992. Intracellular processing of the N-terminal ORF 1a proteins of the coronavirus MHV-A59 requires multiple proteolytic events. Virology 189 (1), 274–284.

Fielding, B.C., Tan, Y.J., Shuo, S., Tan, T.H., Ooi, E.E., Lim, S.G., Hong, W., Goh, P.Y., 2004. Characterization of a unique group-specific protein (U122) of the severe acute respiratory syndrome coronavirus. J. Virol. 78 (14), 7311–7318.

Geng, H., Liu, Y.M., Chan, W.S., Lo, A.W., Au, D.M., Waye, M.M., Ho, Y.Y., 2005. The putative protein 6 of the severe acute respiratory syndrome-associated coronavirus: expression and functional characterization. FEBS Lett. 579 (30), 6763–6768.

Harper, J.W., Adami, G.R., Wei, N., Keyomarsi, K., Elledge, S.J., 1993. The p21 Cdk-interacting protein Cip1 is a potent inhibitor of G1 cyclin-dependent kinases. Cell 75 (4), 805–816.

Holzer, G.W., Falkner, F.G., 1997. Construction of a vaccinia virus deficient in the essential DNA repair enzyme uracil DNA glycosylase by a complementing cell line. J. Virol. 71 (7), 4997–5002.

Holzer, G.W., Gritschenberger, W., Mayrhofer, J.A., Wieser, V., Dorner, F., Falkner, F.G., 1998. Dominant host range selection of vaccinia recombinants by rescue of an essential gene. Virology 249 (1), 160–166.

Imbert, I., Guillemot, J.C., Bourhis, J.M., Bussetta, C., Coutard, B., Egloff, M.P., Ferron, F., Gorbalenya, A.E., Canard, B., 2006. A second, non-canonical RNA-dependent RNA polymerase in SARS coronavirus. EMBO J. 25 (20), 4933–4942.

Ito, N., Mossel, E.C., Narayanan, K., Popov, V.L., Huang, C., Inoue, T., Peters, C.J., Makino, S., 2005. Severe acute respiratory syndrome coronavirus 3a protein is a viral structural protein. J. Virol. 79 (5), 3182–3186.

Jackson, W.T., Ginddings J.r., T.H., Taylor, M.P., Mulinyawe, S., Rabinovitch, M., Kopito, R.R., Kirkegaard, K., 2005. Subversion of cellular autophagosomal machinery by RNA viruses. PLoS Biology 3 (5), e156.

Kaye, M., Druce, J., Tran, T., Kostecki, R., Chibo, D., Morris, J., Catton, M., Birch, C., 2006. SARS-associated coronavirus replication in cell lines. Emerg. Infect. Dis. 12 (1), 128–133.

Ksiazek, T.G., Erdman, D., Goldsmith, C.S., Zaki, S.R., Peret, T., Emery, S., Tong, S., Urbani, C., Comer, J.A., Lim, W., Rollin, P.E., Dowell, S.F., Ling, A.E., Humphrey, C.D., Shieh, W.J., Guarner, J., Paddock, C.D., Rota, P., Fields, B., DeRisi, J., Yang, J.Y., Cox, N., Hughes, J.M., LeDuc, J.W., Bellini, W.J., Anderson, L.J., 2003. A novel coronavirus associated with severe acute respiratory syndrome. N. Engl. J. Med. 348 (20), 1953–1966.

Law, P.T., Wong, C.H., Au, T.C., Chuck, C.P., Kong, S.K., Chan, P.K., To, K.F., Lo, A.W., Chan, J.Y., Suen, Y.K., Chan, H.Y., Fung, K.P., Waye, M.M., Sung, J.J., Lo, Y.M., Tsui, S.K., 2005. The 3a protein of severe acute respiratory syndrome-associated coronavirus induces apoptosis in Vero E6 cells. J. Gen. Virol. 86 (Pt. 7), 1921–1930.

Lip, K.M., Shen, S., Yang, X., Keng, C.T., Zhang, A., Oh, H.L., Li, Z.H., Hwang, L.A., Chou, C.F., Fielding, B.C., Tan, T.H., Mayrhofer, J., Falkner, F.G., Fu, J., Lim, S.G., Hong, W., Tan, Y.J., 2006. Monoclonal antibodies targeting the HR2 domain and the region immediately upstream of the HR2 of the S protein neutralize in vitro infection of severe acute respiratory syndrome coronavirus. J. Virol. 80, 941–950.

Marra, M.A., Jones, S.J., Astell, C.R., Holt, R.A., Brooks-Wilson, A., Butterfield, Y.S., Khattra, J., Asano, J.K., Barber, S.A., Chan, S.Y., Cloutier, A., Coughlin, S.M., Freeman, D., Girn, N., Griffith, O.L., Leach, S.R., Mayo, M., McDonald, H., Montgomery, S.B., Pandoh, P.K., Petrescu, A.S., Robertson, A.G., Schein, J.E., Siddiqui, A., Smailus, D.E., Stott, J.M., Yang, G.S., Plummer, F., Andonov, A., Artsob, H., Bastien, N., Bernard, K., Booth, T.F., Bowness, D., Czub, M., Drebot, M., Fernando, L., Flick, R., Garbutt, M., Gray, M., Grolla, A., Jones, S., Feldmann, H., Meyers, A., Kabani, A., Li, Y., Normand, S., Stroher, U., Tipples, G.A., Tyler, S., Vogrig, R., Ward, D., Watson, B., Brunham, R.C., Krajden, M., Petric, M., Skowronski, D.M., Upton, C., Roper, R.L., 2003. The Genome sequence of the SARS-associated coronavirus. Science 300 (5624), 1399–1404.

Nelson, C.A., Pekosz, A., Lee, C.A., Diamond, M.S., Fremont, D.H., 2005. Structure and intracellular targeting of the SARS-coronavirus Orf7a accessory protein. Structure 13 (1), 75–85.

Ober, B.T., Bruhl, P., Schmidt, M., Wieser, V., Gritschenberger, W., Coulibaly, S., Savidis-Dacho, H., Gerencer, M., Falkner, F.G., 2002. Immunogenicity and safety of defective vaccinia virus lister: comparison with modified vaccinia virus Ankara. J. Virol. 76 (15), 7713–7723.

Peiris, J.S., Lai, S.T., Poon, L.L., Guan, Y., Yam, L.Y., Lim, W., Nicholls, J., Yee, W.K., Yan, W.W., Cheung, M.T., Cheng, V.C., Chan, K.H., Tsang, D.N., Yung, R.W., Ng, T.K., Yuen, K.Y., 2003. Coronavirus as a possible cause of severe acute respiratory syndrome. Lancet. 361 (9366), 1319–1325.

Pewe, L., Zhou, H., Netland, J., Tangudu, C., Olivares, H., Shi, L., Look, D., Gallagher, T., Perlman, S., 2005. A severe acute respiratory syndrome-associated coronavirus-specific protein enhances virulence of an attenuated murine coronavirus. J. Virol. 79 (17), 11335–11342.

Prentice, E., McAuliffe, J., Lu, X., Subbarao, K., Denison, M.R., 2004a. Identification and characterization of severe acute respiratory syndrome coronavirus replicase proteins. J. Virol. 78 (18), 9977–9986.

Prentice, E., Jerome, W.G., Yoshimori, T., Mizushima, N., Denison, M.R., 2004b. Coronavirus replication complex formation utilizes components of cellular autophagy. J. Biol. Chem. 279 (11), 10136–10141.

Rota, P.A., Oberste, M.S., Monroe, S.S., Nix, W.A., Campagnoli, R., Icenogle, J.P., Penaranda, S., Bankamp, B., Maher, K., Chen, M.H., Tong, S., Tamin, A., Lowe, L., Frace, M., DeRisi, J.L., Chen, Q., Wang, D., Erdman, D.D., Peret, T.C., Burns, C., Ksiazek, T.G., Rollin, P.E., Sanchez, A., Liffick, S., Holloway, B., Limor, J., McCaustland, K., Olsen-Rasmussen, M., Fouchier, R., Gunther, S., Osterhaus, A.D., Drosten, C., Pallansch, M.A., Anderson, L.J., Bellini, W.J., 2003. Characterization of a novel coronavirus associated with severe acute respiratory syndrome. Science 300 (5624), 1394–1399.

Sambrook, J., Fritsch, E.F., Maniatis, T., 1989. Molecular Cloning: A Laboratory Manual, 2nd Ed., Cold Spring Harbor Laboratory, Cold Spring Harbor, NY.

Snijder, E.J., Bredenbeek, P.J., Dobbe, J.C., Thiel, V., Ziebuhr, J., Poon, L.L., Guan, Y., Rozanov, M., Spaan, W.J., Gorbalenya, A.E., 2003. Unique and conserved features of genome and proteome of SARS-coronavirus, an early split-off from the coronavirus group 2 lineage. J. Mol. Biol. 331 (5), 991–1004.

Surjit, M., Liu, B., Kumar, P., Chow, V.T., Lal, S.K., 2004. The nucleocapsid protein of the SARS coronavirus is capable of self-association through a C-terminal 209 amino acid interaction domain. Biochem. Biophys. Res. Commun. 317 (4), 1030–1036.

Sutton, G., Fry, E., Carter, L., Sainsbury, S., Walter, T., Nettleship, J., Berrow, N., Owens, R., Gilbert, R., Davidson, A., Siddell, S., Poon, L.L., Diprose, J., Alderton, D., Walsh, M., Grimes, J.M., Stuart, D.I., 2004. The nsp9 replicase

protein of SARS-coronavirus, structure and functional insights. Structure 12 (2), 341–353.

Tan, Y.J., Fielding, B.C., Goh, P.Y., Shen, S., Tan, T.H., Lim, S.G., Hong, W., 2004a. Overexpression of 7a, a protein specifically encoded by the severe acute respiratory syndrome coronavirus, induces apoptosis via a caspase-dependent pathway. J. Virol. 78 (24), 14043–14047.

Tan, Y.J., Goh, P.Y., Fielding, B.C., Shen, S., Chou, C.F., Fu, J.L., Leong, H.N., Leo, Y.S., Ooi, E.E., Ling, A.E., Lim, S.G., Hong, W., 2004b. Profiles of antibody responses against severe acute respiratory syndrome coronavirus recombinant proteins and their potential use as diagnostic markers. Clin. Diagn. Lab. Immunol. 11 (2), 362–371.

Tan, Y.J., Teng, E., Shen, S., Tan, T.H., Goh, P.Y., Fielding, B.C., Ooi, E.E., Tan, H.C., Lim, S.G., Hong, W., 2004c. A novel severe acute respiratory syndrome coronavirus protein, U274, is transported to the cell surface and undergoes endocytosis. J. Virol. 78 (13), 6723–6734.

Tan, Y.J., Lim, S.G., Hong, W., 2006. Understanding the accessory viral proteins unique to the severe acute respiratory syndrome (SARS) coronavirus. Antivir. Res. 72 (2), 78–88.

Tangudu, C., Olivares, H., Netland, J., Perlman, S., Gallagher, T., 2007. Severe acute respiratory syndrome coronavirus protein 6 accelerates murine coronavirus infections. J. Virol. 81 (3), 1220–1229.

Thiel, V., Ivanov, K.A., Putics, A., Hertzig, T., Schelle, B., Bayer, S., Weissbrich, B., Snijder, E.J., Rabenau, H., Doerr, H.W., Gorbalenya, A.E., Ziebuhr, J., 2003. Mechanisms and enzymes involved in SARS coronavirus genome expression. J. Gen. Virol. 84 (Pt. 9), 2305–2315.

Tyagi, S., Jameel, S., Lal, S.K., 2001. Self-association and mapping of the interaction domain of hepatitis E virus ORF3 protein. J. Virol. 75 (5), 2493–2498.

Tyagi, S., Salier, J.P., Lal, S.K., 2002. The liver-specific human alpha(1)-microglobulin/bikunin precursor (AMBP) is capable of self-association. Arch. Biochem. Biophys. 399 (1), 66–72.

Yount, B., Roberts, R.S., Sims, A.C., Deming, D., Frieman, M.B., Sparks, J., Denison, M.R., Davis, N., Baric, R.S., 2005. Severe acute respiratory syndrome coronavirus group-specific open reading frames encode nonessential functions for replication in cell cultures and mice. J. Virol. 79 (23), 14909–14922.

Yu, C.J., Chen, Y.C., Hsiao, C.H., Kuo, T.C., Chang, S.C., Lu, C.Y., Wei, W.C., Lee, C.H., Huang, L.M., Chang, M.F., Ho, H.N., Lee, F.J., 2004. Identification of a novel protein 3a from severe acute respiratory syndrome coronavirus. FEBS Lett. 565 (1–3), 111–116.

Yuan, X., Shan, Y., Zhao, Z., Chen, J., Cong, Y., 2005. G0/G1 arrest and apoptosis induced by SARS-CoV 3b protein in transfected cells. Virol. J. 2, 66.

Zeng, R., Yang, R.F., Shi, M.D., Jiang, M.R., Xie, Y.H., Ruan, H.Q., Jiang, X.S., Shi, L., Zhou, H., Zhang, L., Wu, X.D., Lin, Y., Ji, Y.Y., Xiong, L., Jin, Y., Dai, E.H., Wang, X.Y., Si, B.Y., Wang, J., Wang, H.X., Wang, C.E., Gan, Y.H., Li, Y.C., Cao, J.T., Zuo, J.P., Shan, S.F., Xie, E., Chen, S.H., Jiang, Z.Q., Zhang, X., Wang, Y., Pei, G., Sun, B., Wu, J.R., 2004. Characterization of the 3a protein of SARS-associated coronavirus in infected vero E6 cells and SARS patients. J. Mol. Biol. 341 (1), 271–279.

Zhai, Y., Sun, F., Li, X., Pang, H., Xu, X., Bartlam, M., Rao, Z., 2005. Insights into SARS-CoV transcription and replication from the structure of the nsp7-nsp8 hexadecamer. Nat. Struct. Mol. Biol. 12 (11), 980–986.

Ziebuhr, J., 2004. Molecular biology of severe acute respiratory syndrome coronavirus. Curr. Opin. Microbiol. 7 (4), 412–419.

II

Virology 395 (2009) 1–9

Contents lists available at ScienceDirect

Virology

journal homepage: www.elsevier.com/locate/yviro

Dual effect of nitric oxide on SARS-CoV replication: Viral RNA production and palmitoylation of the S protein are affected

Sara Åkerström [a,b,1], Vithiagaran Gunalan [a,b,c,1], Choong Tat Keng [c], Yee-Joo Tan [c,*], Ali Mirazimi [a,b,*]

[a] Centre for Microbiological Preparedness, Swedish Institute for Infectious Disease Control, SE-171 82 Solna, Sweden
[b] Department of Microbiology, Tumor and Cell Biology, Karolinska Institute, 17177 Solna, Sweden
[c] Institute of Molecular and Cell Biology, 61 Biopolis Drive, Proteos Bldg, 138673 Singapore, Singapore

ARTICLE INFO

Article history:
Received 2 April 2009
Returned to author for revision
7 May 2009
Accepted 8 September 2009
Available online 1 October 2009

Keywords:
SARS-CoV
Palmitoylation
Nitric oxide
Spike protein

ABSTRACT

Nitric oxide is an important molecule playing a key role in a broad range of biological process such as neurotransmission, vasodilatation and immune responses. While the anti-microbiological properties of nitric oxide-derived reactive nitrogen intermediates (RNI) such as peroxynitrite, are known, the mechanism of these effects are as yet poorly studied. Severe Acute Respiratory Syndrome coronavirus (SARS-CoV) belongs to the family *Coronaviridae*, was first identified during 2002-2003. Mortality in SARS patients ranges from between 6 to 55%. We have previously shown that nitric oxide inhibits the replication cycle of SARS-CoV *in vitro* by an unknown mechanism. In this study, we have further investigated the mechanism of the inhibition process of nitric oxide against SARS-CoV. We found that peroxynitrite, an intermediate product of nitric oxide in solution formed by the reaction of NO with superoxide, has no effect on the replication cycle of SARS-CoV, suggesting that the inhibition is either directly effected by NO or a derivative other than peroxynitrite. Most interestingly, we found that NO inhibits the replication of SARS-CoV by two distinct mechanisms. Firstly, NO or its derivatives cause a reduction in the palmitoylation of nascently expressed spike (S) protein which affects the fusion between the S protein and its cognate receptor, angiotensin converting enzyme 2. Secondly, NO or its derivatives cause a reduction in viral RNA production in the early steps of viral replication, and this could possibly be due to an effect on one or both of the cysteine proteases encoded in Orf1a of SARS-CoV.

Introduction

Severe acute respiratory syndrome coronavirus (SARS-CoV) belongs to the family *Coronaviridae* and was first identified as a novel coronavirus after the first known outbreak in the fall of 2002 in southern part of China (Resh, 2006; Tan et al., 2006). SARS-CoV is a positive-sense RNA virus with a genome of ~30 kb in length that forms a distinct group within the *Coronaviridae* family. Common to all known coronaviruses are the four structural proteins: spike (S), membrane (M), envelope (E) and nucleocapsid (N) protein (Marra et al., 2003; Rota et al., 2003). The S protein protrudes from the envelope of the virus, which results in its characteristic crown-like appearance. The S protein binds to specific receptors on the cell surface; in the case of SARS-CoV, it is the angiotensin-converting enzyme 2 (ACE2). The S protein has two regions, S1 and S2, where S1 is involved in receptor binding and S2 in membrane fusion (Li et al., 2005, 2006).

In order to achieve its functionality, the S protein has to undergo numerous post-translational modifications like glycosylation (Keng et al., 2005). In addition, Petit et al. (2007) recently showed the importance of S-palmitoylation of the endodomain of the spike protein for the mediation of cell fusion. Palmitoylation involves the addition of palmitate, which is a 16-carbon saturated fatty acid, and a wide range of proteins have been shown to carry this specific modification (Resh, 2006). The addition of palmitate can influence the interaction between protein and membrane, protein trafficking, and protein–protein interactions (Resh, 2006; Smotrys and Linder, 2004; Thorp et al., 2006). In S-palmitoylation, the fatty acids are linked through thioester linkages to thiol groups on cysteine residues (Greaves and Chamberlain, 2007; Resh, 2006; Smotrys and Linder, 2004).

Nitric oxide (NO) is involved in a broad range of processes and act as an important signaling molecule between cells (Adler et al., 1997; Zhang et al., 2003). NO is produced in mammalian cells by three enzymes, neuronal (nNOS), endothelial (eNOS) and inducible nitric oxide synthase (iNOS) and these catalyze the oxidation of L-arginine to NO and L-citrulline (Boucher et al., 1999). Inducible nitric oxide in the host cells is commonly elevated during infection by viruses and this can lead to either inhibition or stimulation of viral replication (Adler et al., 1997;

* Corresponding authors. A. Mirazimi is to be contacted at Centre for Microbiological Preparedness, Swedish Institute for Infectious Disease Control, Nobels Väg 18, SE-171 82 Solna, Sweden. Fax: +46 8 3079 57. Y.-J. Tan, Collaborative Antiviral Research Group, Cancer and Developmental Cell Biology Division, Institute of Molecular and Cell Biology, 61 Biopolis Drive, Proteos Building, Singapore 138673.
E-mail addresses: mcbtanyj@imcb.a-star.edu.sg (Y.-J. Tan), Ali.Mirazimi@smi.se (A. Mirazimi).
[1] These authors contributed equally to the work.

0042-6822/$ – see front matter © 2009 Elsevier Inc. All rights reserved.
doi:10.1016/j.virol.2009.09.007

Akarid et al., 1995; Akerstrom et al., 2005; Fang, 2004; Klingstrom et al., 2006; Pope et al., 1998; Saxena et al., 2001; Thorp et al., 2006).

In our previous study, we showed that NO inhibits the replication cycle of SARS-CoV (Akerstrom et al., 2005). We clearly showed that the progeny viruses were inhibited in a concentration-dependent manner, using the exogenous NO donor S-nitroso-N-acetyl-penicillamine (SNAP). We also demonstrated that endogenously generated NO can inhibit the replication cycle of SARS-CoV. Another host defence against microbes is superoxide (O_2^-) which can be induced when cells are stressed, for example during an infection (Akaike and Maeda, 2000). If NO and O_2^- are elevated at the same time, they will react rapidly to form peroxynitrite ($ONOO^-$), which has also been shown to have an inhibitory effect on viruses (Akaike, 2001). Hantaviruses are one group of viruses known to be adversely affected by peroxynitrite (Klingstrom et al., 2006). Hence, it is unclear if the effect of NO on SARS-CoV replication is caused by peroxynitrite or another derivative of nitric oxide. In this study we show that peroxynitrite does not play a significant role in the NO-mediated inhibition of the SARS-CoV replication cycle. Most interestingly, our data suggest that the effect of NO or its derivatives on the replication cycle of SARS-CoV is twofold: Firstly, NO or its derivatives causes a reduction in the palmitoylation of the S protein which results in the inhibition of membrane fusion mediated by the interaction between S protein and the ACE2 receptor. Secondly, NO or its derivatives have an inhibitory effect on the production of viral RNA, which can be observed as early as 3 h post-infection.

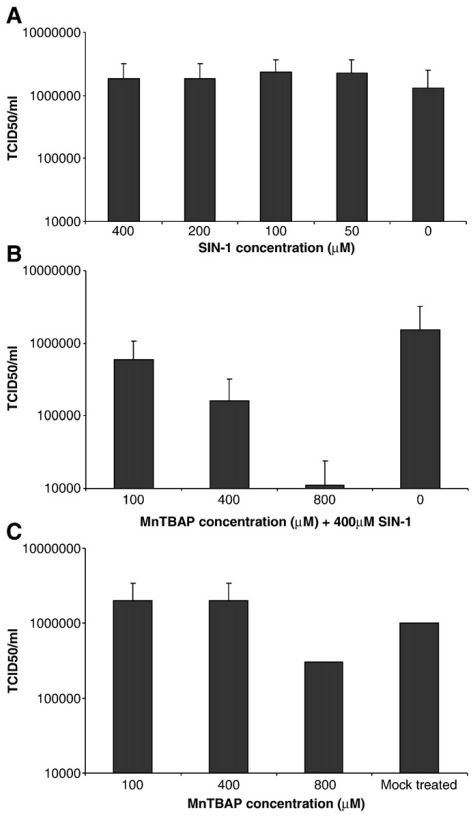

Fig. 1. SIN-1 treatment has no antiviral effect on SARS-CoV infected Vero E6 cells. Vero E6 cells were infected with SARS-CoV at an MOI of 1.0, at 1 hpi cells were treated with different concentrations of SIN-1 and/or MnTBAP. (A) Cells treated with different concentrations of SIN-1. 24 hpi, virus was harvested and titers determined. (B) Cells treated with 400 μM SIN-1 and different concentrations of MnTBAP. Virus was harvested 24 hpi and titers determined. (C) Cells treated with different concentrations of MnTBAP, virus was harvested 24 hpi and titers determined.

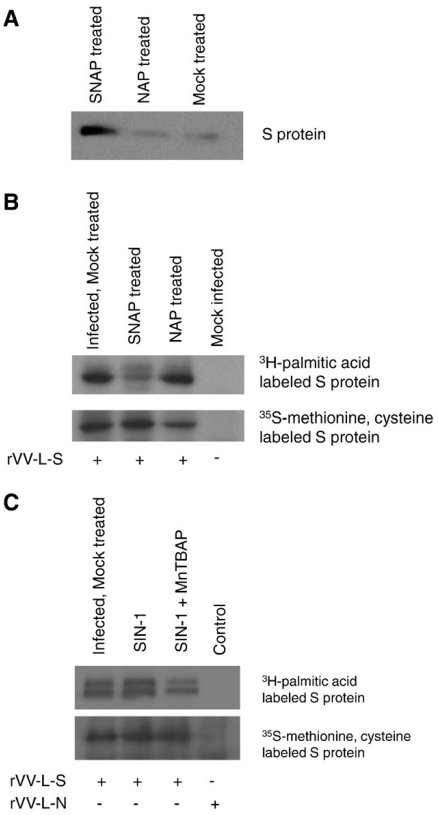

Fig. 2. Effect of SNAP on nitration and palmitoylation of S protein. Vero E6 cells were infected with rVV-L-S at an MOI of 0.1. At 1 hpi cells were treated with 400 μM SNAP or NAP. (A) At 24 h post-infection, the cells were lysed and immunoprecipitation was performed with nitrotyrosine affinity sorbent. Western blot was then performed using rabbit anti-S polyclonal antibody. (B, C) At 24 h post-infection, cells were labelled with 400 μCi of [^{3}H]-palmitic acid for 2 h, or starved with methionine-cysteine (Met-Cys)-free medium for 30 min before being labelled with 22 μCi of [^{35}S]-methionine-cysteine for 2 h. The cells were then lysed and imunoprecipitation was performed with rabbit S polyclonal antibody to detect the amount of radiolabelled S protein.

Results

Peroxynitrite has no effect on SARS-CoV

SIN-1, which produces peroxynitrite, was used in conjunction with a superoxide scavenger, MnTBAP, to determine if peroxynitrite was

involved in the inhibition of SARS-CoV replication. SARS-CoV infected Vero E6 cells were treated with different concentrations of SIN-1, and it was observed that no significant inhibition of viral replication occurred. This suggested that SIN-1 administration had no effect on the replication cycle of SARS-CoV.

Next, we treated the SARS-CoV infected Vero E6 cells with different concentrations of MnTBAP together with SIN-1. MnTBAP removes the superoxide, resulting in a reduction in the amount of peroxynitrite and an increase in the amount of free NO. The results in Fig. 1B clearly demonstrate that with increasing amount of MnTBAP in presence of SIN-1 (400 μM), there is an inhibition in the production of progeny virus in a concentration-dependent manner. Although a slight reduction on the production of progeny virus was observed when the cells were treated with the highest concentration of MnTBAP used in this study (800 μM, Fig. 1C), the reduction of virus replication in cells treated with both SIN-1 and MnTBAP is significantly higher than those treated with MnTBAP alone. This slight reduction might be explained by the possibility that the use of the superoxide scavenger would have resulted in an increase in intracellular free NO, which could then, directly or through an intermediary compound, exert an inhibitory effect.

Treatment with NO donor leads to the nitration of the S protein of SARS-CoV and a reduction in its palmitoylation

In order to determine whether nitric oxide or its derivatives were reacting with the SARS-CoV S protein, Vero E6 cells were infected with recombinant vaccinia virus carrying the S gene (rVV-L-S) and treated with 400 μM of SNAP or NAP. Following immunoprecipitation with nitrotyrosine affinity sorbent (Cayman), which specifically binds nitrated proteins, and detection of S by Western blotting, it was clearly demonstrated that S had been nitrated after stimulation with SNAP but not with NAP (Fig. 2A).

To determine whether the palmitoylation of S was affected by nitric oxide, cells infected with rVV-L-S were treated with either SNAP, NAP, SIN-1 or SIN-1 and MnTBAP and then labelled with [^{3}H]-palmitic acid. After immunoprecipitation of the S protein with an anti-S rabbit polyclonal antibody, the amount of palmitoylated S protein detected in the SNAP-treated cells was found to be noticeably reduced when compared to the mock-treated or NAP-treated ones (Fig. 2B). Treatment with the peroxynitrite donor SIN-1 did not cause a reduction in the palmitoylation of S (Fig. 2C), confirming other results that showed a lack of effect by peroxynitrite treatment on SARS-CoV titer. On the other hand, if [^{35}S]-methionine-cysteine labelling was used, there was no difference in the amount of total S protein immunoprecipitated for all treatments, indicating that the SNAP and SIN-1 treatments did not affect the expression of S (Figs. 2B, C).

Nitric oxide reduces the cell–cell fusion activity of the S protein

An *in vitro* assay was used to examine the effect of nitric oxide on the cell–cell fusion activity of the S protein (Lip et al., 2006). In this case, the S-expressing cells were treated with SNAP or NAP before they were mixed with CHO-ACE2 cells stably expressing the ACE2 receptor. The formation of syncytia was observed 6 h later. Cells treated with SNAP showed no fusion (Fig. 3B), whereas cell–cell fusion was clearly visible in the NAP (Fig. 3C) or mock-treated cells (Fig. 3A). As expected, the mock-infected cells showed no fusion as the S protein was not expressed (Fig. 3D).

SARS-CoV S pseudotyped virus produced in the presence of nitric oxide is less efficient in viral entry

In order to investigate the effect of SNAP on the S-mediated entry of SARS CoV into cells, we used the HIV pseudotyped virus system to produce pseudotyped viruses with S on the surface. Pseudotyped viruses were produced from untreated cells or cells treated with SNAP (200 μM or 400 μM) or NAP (200 μM or 400 μM). SNAP and NAP

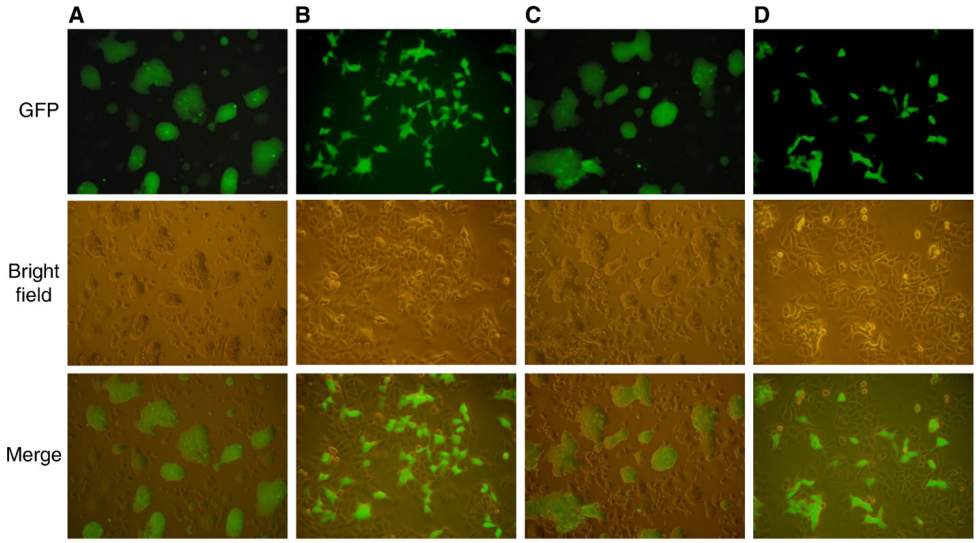

Fig. 3. SNAP interferes with cell–cell membrane fusion. A 293T-GFP stable cell line was infected with rVV-L-S and treated with SNAP or NAP 1 h post-infection. At 24 hpi cells were trypsinized and mixed with pre-plated CHO-ACE2 cells. 6 h after mixing the cell lines, syncytium formation was observed. (A) Infected cells, mock-treated (B) Infected cells, treated with 400 μM SNAP (C) Infected cells, treated with 400 μM NAP (D) Mock-infected cells.

treatments did not affect the assembly of S on the pseudotyped viruses as Western blot analysis showed that similar amounts of S were incorporated into the pseudotyped viruses (Fig. 4A). Similar to our previous observation (Keng et al., 2005), two forms of S were detected and these correspond to the unglycosylated and glycosylated forms of the protein.

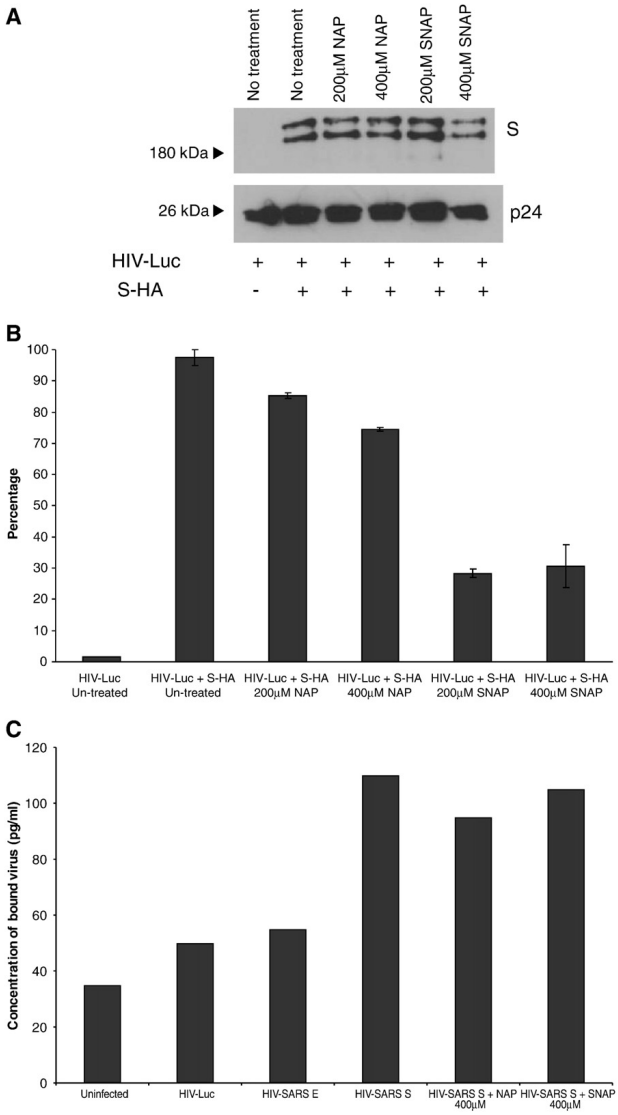

Fig. 4. SARS-CoV S pseudotyped virus produced in the presence of SNAP is less efficient in viral entry. Pseudotyped viruses produced under different conditions were purified and concentrated using ultra-centrifugation through a 20% sucrose bed. (A) The presence of S and HIV-1 p24 proteins in the purified viruses were determined by Western blot analysis. (B) Purified viruses were used for the transduction of CHO-ACE2 cells and the degrees of viral entry were determined by measuring the luciferase activities. Percentages of infectivity were computed by normalizing the entry of untreated S-bearing pseudotyped viruses to 100%. Means and standard deviation from duplicate readings were shown. (C) Nitric oxide or its derivatives do not exert a noticeable effect on the binding of the SARS S protein to ACE2. Cells were infected with pseudotyped virus bearing the S protein, produced under SNAP or NAP treatment. A p24 ELISA kit was used to measure p24 concentration and concentration of bound virus was derived from a standard graph.

The entry of the pseudotyped virus into CHO-ACE2, which is stably expressing the S receptor ACE2 on the surface of the cells, was reflected by the luciferase activity in the CHO-ACE2 cells at 72 h after infection. As shown in Fig. 4B, the luciferase activity in the cells infected with pseudotyped virus bearing S was significantly higher than those without S as the latter contained no viral envelope protein and could not enter the CHO-ACE2 cells. The reading from the cells infected with pseudotyped virus bearing S was normalized to 100% to calculate percentage of infectivity. Treatment with 200 μM and 400 μM of NAP caused appropriately 15% and 25% reduction in infectivity, respectively. However, treatment with 200 μM and 400 μM of SNAP resulted in a significantly higher reduction, appropriately 70%, in infectivity. In order to exclude any effect on the binding of the S protein to the ACE2 receptor, a p24 ELISA kit (Perkin Elmer) was used to determine the concentration of virus bound to cells infected with the HIV pseudotyped virus which had been produced in cells either treated with 400 μM SNAP or 400 μM NAP. As shown in Fig. 4C, SNAP and NAP treatment had no significant effect on the concentration of bound virus, indicating that the primary effect of SNAP treatment on the S protein occurs post-binding, possibly during entry.

SNAP treatment reduces the production of positive-stranded viral RNA

In order to determine if the effect of nitric oxide on SARS-CoV was limited to the post-translational modification of the S protein, we examined the production of viral RNA by realtime PCR analysis. RNA isolated from SARS-CoV infected Vero E6 cells at different time points post-infection in the presence of SNAP, NAP or mock treatment was reverse transcribed and quantitated using primers specific for the N gene of SARS-CoV. An identical amount of each RNA sample was also reverse transcribed and quantitated using primers specific for GAPDH, which served as a housekeeping control. The results showed that SNAP treatment of Vero E6 cells resulted in a reduction in the amount of total positive-stranded viral RNA produced. This effect was observed as early as 3 h post-infection and viral RNA levels remained low at 24 h post-infection (Fig. 5). In order to determine if this observed effect could be exaggerated by pretreating Vero E6 cells with nitric oxide, another experiment was run in parallel which included an additional SNAP treatment step an hour before infection. The effect observed was approximately the same as in cells treated post-infection, suggesting that the pretreatment of Vero E6 cells with nitric oxide did not significantly increase the effects of nitric oxide on the production of viral RNA (Fig. 5). The possibility that the pretreatment had an effect on SARS-CoV particles before infection was excluded by titrating SARS-CoV that had been incubated in SNAP-containing media, which showed that the TCID50 of the virus was unchanged (data not shown). It has been previously shown by others that nitric oxide or its derivatives can exert an effect on the activity of cysteine proteases (Cao et al., 2003; Saura et al., 1999). As SARS-CoV encodes two different cysteine proteases, PL^{pro} and $3C^{pro}$, we tried to determine if the effect seen on production of positive/stranded viral RNA might involve a loss or reduction of the function of one or both of these proteases, which serve to cleave the different replicase proteins from the pp1ab polyprotein expressed from Orfs 1a and 1b of the viral genome (Thiel et al., 2003). One simple way to study this effect would be to look at the cleavage of replicase proteins by Western blotting. A previously described monoclonal antibody (Kumar et al., 2007) targeting the nsp8 protein was used against SDS-PAGE-separated lysates from SARS-CoV infected Vero E6 cells which had been treated with either SNAP, NAP or untreated. Surprisingly, there was no significant difference in nsp8 levels at 24 h post-infection (Fig. 6). Interestingly though, two other peptide species, detected by the nsp8 antibody in infected cells, showed differences in their respective expression levels in SNAP-treated lysates. These high molecular weight species could possibly represent cleavage intermediates of the ORF1a replicase polyprotein from which nsp8 is cleaved. In order to ascertain that NO was acting in these cells, the same lysates were probed for the SARS N protein using a monoclonal antibody against N (Zymed Laboratories). It was observed that N expression was significantly reduced in the same lysates. This was consistent with earlier work (Akerstrom et al., 2005) and showed that the SNAP treatment was working within the Vero E6 cells.

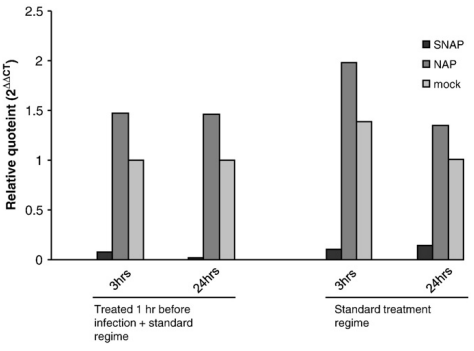

Fig. 5. SNAP treatment causes a reduction in the production of positive-stranded viral RNA. Vero E6 cells were either treated with 400 μM SNAP, NAP or mock-treated and infected with SARS-CoV at an MOI of 1. A parallel set of cells were additionally treated an hour before infection. Cells were harvested from all sets of treatments at 3 h and 24 h post infection and subjected to reverse transcription and realtime PCR using primers and probes specific for the N gene of SARS-CoV and GAPDH. Ct values obtained for N in each sample was normalized against GAPDH control values and plotted for each time point and treatment.

Discussion

NO can either inhibit or stimulate viral replication during an infection (Adler et al., 1997; Fang, 2004; Akarid et al., 1995; Akerstrom et al., 2005; Greaves and Chamberlain, 2007; Klingstrom et al., 2006; Pope et al., 1998; Saxena et al., 2001; Thorp et al., 2006). However, there are only a few reports demonstrating the inhibition mechanism of NO. NO has been shown to affect Epstein–Barr virus (EBV) by downregulation of the Zta protein, an immediate early transactivator. The downregulation of Zta helps to maintain latency of the virus. In the same study, it was also shown that apoptosis in B cell lines were L-arginine dependent and that NO can inhibit apoptosis in B cells (Mannick et al., 1994). In a previous study we have shown that NO inhibits the replication cycle of SARS-CoV. The administration of the exogenous NO donor, SNAP, and endogenous cytokine inducers of NO reduced the amount of progeny virus in a concentration-dependent manner. In tissues that are stressed or inflamed, both NO and O_2^- are elevated. Although SNAP predominantly increases the NO level in the cell, peroxynitrite may also become elevated after SNAP treatment as NO can react with endogenous O_2^- to form peroxynitrite. However, if SIN-1 is used instead, both NO and O_2^- are produced simultaneously and peroxynitrite is rapidly formed. Our results show that unlike SNAP, treatment of SARS-CoV infected Vero E6 cells with SIN-1 has no significant effect on the production of progeny virus (Fig. 1A), suggesting that peroxynitrite does not inhibit SARS-CoV replication. Moreover, if a superoxide scavenger (MnTBAP) is used to remove the O_2^- and allow more NO to accumulate inside the SIN-1-treated cells, a significant inhibition of the virus replication was observed (Fig. 1B). These results clearly demonstrate that peroxynitrite has no effect on the replication of SARS-CoV and that it is NO, or a derivative of NO, that inhibits the virus.

Palmitoylation is an important post-translational modification of proteins. Petit et al. (2007) have demonstrated that palmitoylation of the SARS-CoV S protein plays a role in S-mediated cell–cell fusion. By

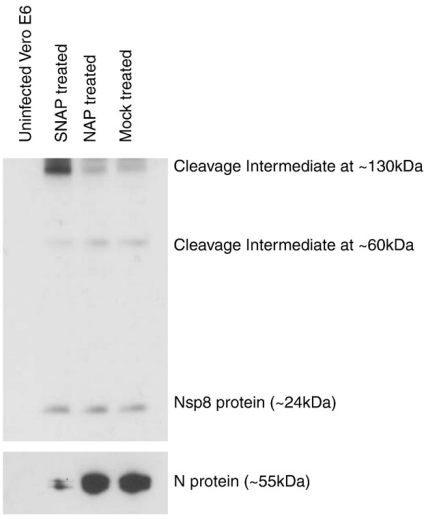

Fig. 6. SNAP treatment causes a difference in observed levels of replicase polyprotein cleavage products. Lysates from either uninfected or SARS-CoV infected Vero E6 cells which had either been treated with SNAP, NAP or mock-treated harvested 24 h post-infection were subjected to Western blot analysis using a monoclonal antibody targeting the nsp8 protein.

substituting select cysteine clusters at the carboxyl terminus of the S protein for alanines, it was shown that palmitoylation of at least two cysteine clusters at the C-terminus was important in membrane fusion that occurred after binding of the S protein to its cognate ACE2 receptor, critical to the infectivity of SARS-CoV. It has also been previously shown that NO or its derivatives have an effect on the palmitoylation of the rat myelin protein (Bizzozero et al., 2001). In agreement with both of these findings, our results in this work indicate that NO or its derivatives reduce the palmitoylation of the S protein and consequently exerts an effect downstream of the S protein binding to ACE2, which is shown by the cell–cell fusion assay. While cell–cell fusion remains an unobserved phenomenon in SARS-CoV infection, in this paper the cell–cell fusion assay has proved useful in examining the interaction of the S protein and its cognate ACE2 receptor. However, the cell–cell fusion assay does not address the question of whether the underpalmitoylation of the S protein affects its expression, folding or incorporation into the mature virus particle. To this end we have created a pseudotyped virus based on HIV which incorporates the S protein and shown that SNAP treatment of cells does not affect the expression or incorporation of the S protein and it is only the infectivity of the pseudovirus, as shown by the luciferase assay, that is affected. It is known that treatment of mammalian cells with NO donors results in at least two different types of post-translational modifications—nitration of tyrosine residues (Ischiropoulos et al., 1992) and S-nitrosylation of cysteine residues (Stamler et al., 1992). We demonstrate that nitric oxide or a derivative compound is interacting with the S protein by means of the tyrosine nitration assay. However, as tyrosine nitration depends on the presence of peroxynitrite (Ischiropoulos et al., 1992), which has been excluded from having an effect on the replication cycle of SARS-CoV in this work, this indicates that either (a) the tyrosine residues which have been nitrated have little or no role to play in the binding between the S protein and ACE2, or (b) that the nitration of these tyrosine residues do not impair their role in the S-protein. The true effect of NO on the binding process might then manifest itself at the cysteine residues on the S protein which may have been palmitoylated, in particular the clusters at the carboxy terminal that have been demonstrated to play a role in cell–cell fusion. But what needs to be determined is whether these residues have simply been under-palmitoylated as a result of an effect on palmitoyl-acyl transferases in the host cell or whether, given that these are cysteine residues, competitively nitrosylated. S-nitrosylation motifs have been previously described as an acid–base motif flanking cysteine residues (Ascenzi et al., 2000, Stamler et al., 1997), and a search of the S-protein amino acid sequence for previously described motifs yielded no results. Further studies will have to be done to answer these questions.

While the palmitoylation of the S protein has been shown to be affected by the administration of SNAP as an NO donor, this is an effect that is seen in the later steps of infection, after the expression of viral proteins. However, nitric oxide and its derivatives have been shown in the case of several micro-organisms to have an effect on the early steps of replication, in both bacterial and viral infections. The work done by several groups has demonstrated that cysteine proteases are particularly susceptible to nitric oxide, as has been described for coxsackieviruses (Saura et al., 1999) and adenoviruses (Cao et al., 2003). The use of realtime PCR directed against positive-stranded RNA species encoded by SARS-CoV showed that SNAP treatment of Vero E6 cells caused a significant decrease in viral RNA production which could be observed as early as 3 h post-infection compared to NAP-treated and mock-treated controls. This observation is interesting as SARS-CoV encodes 2 cysteine proteases, the papain-like protease ($PL2^{pro}$) and the 3C-like protease($3CL^{pro}$) (Thiel et al., 2003). These cleave the pp1ab replicase polyprotein at non-overlapping sites to yield 15 replicase proteins, termed nsp1 to nsp15. $PL2^{pro}$ is predicted to cleave the polyprotein at 3 sites, and the rest of the non-structural proteins have been predicted to be cleaved by $3CL^{pro}$. Hence, in order to examine a possible effect of NO on the activity of these proteases, a monoclonal antibody directed against the nsp8 protein was used to look at the relative amounts of cleavage products being formed in SARS-CoV infected Vero E6 cells treated with either SNAP, NAP or in mock-treated cells. If NO or its derivatives exerted a discrete effect on the activity of $3CL^{pro}$, one might expect to see a reduction in the amount of nsp8 protein as determined by Western blotting. Surprisingly, no difference was seen in the levels of cleaved nsp8 amongst the different treatments. However, 2 bands of higher molecular weight (of around 60 kDa and 130 kDa) was seen to exhibit altered intensities in SARS-CoV infected cells treated with SNAP. As these bands are specific to infection and are detected by the nsp8 antibody, they might represent cleavage intermediates of the replicase polyprotein. In a 2004 study, Fan and coworkers expressed and purified the SARS-CoV $3CL^{pro}$ in order to study its activity. Using an HPLC-based peptide cleavage assay, they found that the 11 unique $3CL^{pro}$ cleavage sites on the pp1ab replicase polyprotein were cleaved with different efficiencies (Fan et al., 2005). In light of this information, the differences seen in the amounts of cleavage products might make more sense to the observer. It could be possible that the effect of NO or its derivatives on $3CL^{pro}$ might have altered its substrate specificities, resulting in a different pattern of cleavage efficiencies from that previously observed. This might account, then, for the lack of a difference in nsp8 levels while an accumulation is observed for a different intermediate cleavage product which might have had its cleavage efficiency altered more detrimentally. In order to confirm that NO was actually working in these samples, we performed a Western blot using a monoclonal antibody specific to the N protein of SARS-CoV (Fig. 6). It was observed that the expression of the N protein was reduced, in agreement with previous findings (Akerstrom et al., 2005). This showed the intended effect of SNAP treatment and therefore that the observed differences in cleavage product intensities was being observed in cells which were being affected by SNAP treatment.

From the results presented here, we suggest that the effect of nitric oxide on the replication of SARS-CoV is at least twofold: an effect on the production of viral RNA in the early steps of replication and a reduction in the palmitoylation of the S protein later in the replication cycle. What remains to be elucidated is whether both of these effects arise strictly from a direct effect of nitric oxide or its derivatives on viral proteins, or strictly from an effect on host factors which are subverted in the course of infection, or a combination of both.

Materials and methods

Peroxynitrite and superoxide dismutase treatment

Vero E6 cells grown in 24-well plates were infected with SARS-CoV Frankfurt strain 1 at an MOI of 1. At 1 hpi, cells were washed twice with PBS, and medium with or without 3-morpholinosydnonimine hydrochloride (SIN-1; Sigma-Aldrich) was added. 50, 100, 200 or 400 μM of SIN-1 were added 3 times with 4-h intervals. After 24 h, the virus was harvested and titration of progeny virus was titrated out on a 96-well plate containing Vero E6 cells as described previously (Akerstrom et al., 2005). At 48 hpi, the amount of virus ($TCID_{50}$) was calculated from the cytopathic effect (CPE) induced in cell culture by serial tenfold dilutions of the harvested virus.

Similarly, SARS-CoV infected Vero E6 cells were treated with a superoxide scavenger, Mn(III)tetrakis(4-Benzoic acid)porphyrin chloride (MnTBAP; Calbiochem), in the absence or presence of 400 μM SIN-1. 100, 400 or 800 μM of MnTBAP with or without 400 μM SIN-1 were added 3 times with 4-h intervals. The amount of progeny virus was measured as described above. All SARS-CoV infection work (described here and elsewhere in the manuscript) was carried out at the BSL4 facility at the Swedish Institute for Infectious Disease Control in Solna, Sweden.

Radiolabelled immunoprecipitation

Vero E6 cells grown in 60 mm dishes were infected with recombinant vaccinia virus carrying the S gene (rVV-L-S), at a MOI of 0.1. For mock-infected cells, a recombinant vaccinia virus carrying the N gene (rVV-L-N) was used. Both rVV-L-S and rVV-L-N are kind gifts from Baxter Vaccine (Orth/Donau, Austria) and have been previously described (Lip et al., 2006). At 1 h post-infection, the cells were treated with 400 μM of SNAP (Sigma, St. Louis, Mo.), 400 μM N-acetylpenicillamine (NAP; Sigma), 400 μM of SIN-1 (Sigma, St. Louis, Mo) or 400 μM of SIN-1 and 400 μM of MnTBAP (Calbiochem). Treatments were repeated 4 times with 2-h intervals. At 24 h post-infection, cells were labelled with 400 μCi of [^{3}H]-palmitic acid (Perkin Elmer, USA) for 2 h or starved with methionine-cysteine (Met-Cys)-free medium for 30 min before being labelled with 22 μCi of [^{35}S]-methionine-cysteine for 2 h. The labelled cells were washed 3 times with cold PBS and lysed in 1 ml TES lysis buffer (20 mM Tris–HCl [pH 7.5], 100 mM NaCl, 1 mM EDTA, 1% Triton X-100 and 2 mM PMSF). Cell debris was removed from the lysates by centrifugation at 13,000 rpm for 10 min. Immunoprecipitation was carried out by adding rabbit anti-SΔ10 antibody (Keng et al., 2005) to the lysates and rotating at 4 °C for 1 h, followed by overnight incubation with protein A-Sepharose beads (Roche Diagnostics). The beads were washed 3 times with lysis buffer and boiled in 20 μl of 2× Laemmli's SDS loading buffer. Samples were separated in a 7.5% SDS-PAGE gel, fixed for 30 min using fixing solution (10% acetic acid, 45% methanol), and treated with Amplify Fluorographic Reagent (Amersham Biosciences) according to protocol. Visualization was done by autoradiography.

Cell–cell membrane fusion assay

An *in vitro* cell fusion assay that can be used to study S-mediated membrane fusion has been previously developed (Lip et al., 2006). Briefly a 293T cell-line stably expressing GFP was infected with rVV-L-S in order to express the S protein and then treated with SNAP or NAP as described above. Another stable cell line stably expressing ACE2, CHO-ACE2, was plated in a 12-well plate in DMEM containing 1 mg/ml porcine trypsin (JRH Biosciences Inc.). Infected 293T-GFP cells were mixed with the CHO-ACE2 cells in a 1:1 ratio per well and syncytium formation was observed 6 h later.

Pseudotyped virus entry assay

To produce HIV pseudotyped virus bearing the SARS-CoV S protein, 9 μg of HIV-1 luciferase reporter vector pNL4.3.Luc.R-E- (HIV-luc) and 4.5 μg of SARS-CoV S protein expression plasmid (pXJ3′-S-HA) were co-transfected into 293T cells in a 100-mm dish using Lipofectamine2000 reagent (Invitrogen) following manufacturer's instructions. For the negative control, the cells were transfected with pNL4-3.Luc.R-E-alone. The construction of the plasmids has been described previously (Connor et al., 1995; He et al., 1995; Tan et al., 2004). The virus-containing medium was harvested after 72 h of incubation and centrifuged at 2000 rpm for 5 min to remove any cell debris. Virus in the supernatant was subsequently concentrated through a 20% sucrose cushion for 3 h at 30,000 rpm and 4 °C by using an SW41 rotor, and subsequently resuspended in DMEM. In order to normalize the amount of pseudotyped virus used, 10 μl of each sample was used to measure p24 content using a p24 ELISA kit (Perkin Elmer), according to the manufacturer's protocol. Absorbance readings were made at 492 nm in a plate reader (Tecan) and sample concentrations were determined from a standard graph. Appropriate volumes corresponding to 16 ng of pseudotyped virus were then used to infect CHO-ACE2 cells (Chou et al., 2005). At 72 hpi, supernatant was removed and the cells were washed and harvested in trypsin and washed again in PBS. Cell pellet was lysed using the Promega lysis buffer and luciferase activity was determined using a luciferase assay kit, following manufacturer's instructions (Promega). Luciferase readings were measured using a Veritus microplate luminometer (Turner Biosystems).

Pseudotyped virus binding assay

HIV pseudotyped virus bearing the SARS-S protein was produced as described in the pseudotyped virus entry assay (see above). Virus-containing medium was harvested after 24 h of incubation and centrifuged at 3000 rpm for 5 min to remove any cell debris. 10 μl of the medium were diluted 20× using DMEM and used to measure virus concentration using a P24 ELISA kit (Perkin Elmer), according to the manufacturer's protocol. Virus concentration was determined from a standard graph, and 80 ng of virus was used for infection of CHO-ACE2 cells. CHO-ACE2 cells were pre-incubated in DMEM with 1% BSA at 4 °C for 1 h prior to infection at 4 °C for 2 h. After infection, the cells were washed 4× using 1× PBS with 1% BSA and harvested in DMEM, freeze–thawed six times and sonicated for 2 min with 20-s intervals. Samples were centrifuged at 13,000 rpm to remove any cell debris and 200 μl of supernatant was used to determine P24 content using the P24 ELISA kit. The concentration of bound virus was then determined using the standard graph.

Western blot and detection of nitrated SARS-CoV S protein

Vero E6 cells grown in 60 mm dishes were infected with rVV-L-S and rVV-L-N and treated with 400 μM SNAP or NAP as described above. After 24 h, the cells were lysed (50 mM Tris [pH 8], 150 mM NaCl, 0.5% NP40, 0.5% deoxycholic acid, 0.005% SDS, 1 mM PMSF) and the concentration of total protein in the cell lysates was determined using Coomassie Plus reagent (Pierce). Appropriate volumes yielding 500 μg of total protein from each sample were added to 20 μl of Nitrotyrosine Affinity Sorbent (Cayman Chemical) after washing the

beads three times in PBS. The samples were left for rotation at 4 °C over night. Next day, the beads were washed 3 times with lysis buffer, resuspended in 20 µl of Laemmli's SDS loading buffer and boiled for 10 min at 100 °C. Samples were separated on a 7.5% SDS-PAGE gel, transferred to a nitrocellulose membrane, and blocked for 1 h in room temperature in 5% non fat dry milk in PBS with 0.1% Tween 20. Membrane was incubated overnight in 5% non-fat dry milk with rabbit anti-SΔ10 antibody (diluted 1:6000) at 4 °C. The next day, the membrane was incubated with HRP-conjugated secondary antibody (goat anti-rabbit antibody diluted 1:2000) for 1 h at room temperature and washed in PBS-Tween. Detection was performed with SuperSignal West Pico Chemiluminescent Substrate (Pierce).

Quantification of viral RNA

Vero E6 cells were grown in 24-well plates and infected with SARS-CoV at an MOI of 1. Cells were treated with SNAP, NAP or mock-treated either 1 h before infection and 1 h, 3 h or 6 h post-infection or only 1 h, 3 h, 6 h post-infection without pretreatment. At 24 h post-infection, cells were harvested in Trizol reagent (Invitrogen) and total RNA was extracted using an RNeasy mini kit (Qiagen). Viral RNA was quantitated using a Nanodrop spectrophotometer and equal amounts of total RNA were added to a reverse transcription reaction using either of the following gene-specific primers: SARSNRTREV-5′ TTATGCCTGAGTTGAATCAGCAGAA 3′; GAPDHRTREV-5′ AGCCTTCTC-CATGCTGGTGAAGAC 3′. Equal amounts of each reverse transcription reaction were then added to a portion of LightCycler Taqman Master reaction mix (Roche) along with either of the following primer pairs: SARSNCCORFP-5′ TGCCTCTGCATTCTTTGGA 3′, SARSNCCORRP-5′-TAAGTCAGCCATGTTCCCG 3′, GAPDHF-5′ GAAGATGGTGATGGGATTTC 3′, GAPDHR-5′ GAAGGTGAAGGTCGGAGT 3′ and the following probes: SARSNCCORP1-5′ FAM (6-carboxy-flourescein)-, TGTGACTTCCATGC-CAATGCGTG-TAMRA (6-carboxy-tetrylrhodamine quencher) 3′ or GAPDHP-5′FAM-,CAAGCTTCCCGTTCTCAGCC-TAMRA 3′. Cycle threshold values obtained for the SARS N gene were normalized against those for GAPDH to obtain relative quotients ($2^{\Delta\Delta Ct}$) which were then plotted for SNAP, NAP and mock treatments.

Acknowledgments

We thank Baxter Vaccine (Orth/Donau, Austria) for sharing their proprietary vaccinia virus expression system, and S. Shen (Institute of Molecular and Cell Biology, Singapore) for technical assistance. The following reagent was obtained through the NIH AIDS Research and Reference Reagent Program, Division of AIDS, NIAID, NIH: pNL4-3.Luc. R-E- from Dr. Nathaniel Landau.

References

Ascenzi, P., Colasanti, M., Persichini, T., Muolo, M., Polticelli, F., Venturini, G., Bordo, D., Bolognesi, M., 2000. Re-evaluation of amino acid sequence and structural consensus rules for cysteine-nitric oxide reactivity. Biol. Chem. 381 (7), 623–627.

Adler, H., Beland, J.L., Del-Pan, N.C., Kobzik, L., Brewer, J.P., Martin, T.R., Rimm, I.J., 1997. Suppression of herpes simplex virus type 1 (HSV-1)-induced pneumonia in mice by inhibition of inducible nitric oxide synthase (iNOS, NOS2). J. Exp. Med. 185, 1533–1540.

Akaike, T., 2001. Role of free radicals in viral pathogenesis and mutation. Rev. Med. Virol. 11, 87–101.

Akaike, T., Maeda, H., 2000. Nitric oxide and virus infection. Immunology 101, 300–308.

Akarid, K., Sinet, M., Desforges, B., Gougerot-Pocidalo, M.A., 1995. Inhibitory effect of nitric oxide on the replication of a murine retrovirus *in vitro* and *in vivo*. J. Virol. 69, 7001–7005.

Akerstrom, S., Mousavi-Jazi, M., Klingstrom, J., Leijon, M., Lundkvist, A., Mirazimi, A., 2005. Nitric oxide inhibits the replication cycle of severe acute respiratory syndrome coronavirus. J. Virol. 79, 1966–1969.

Bizzozero, O.A., Bixler, H., Parkhani, J., Pastuszyn, A., 2001. Nitric oxide reduces the palmitoylation of rat myelin proteolipid protein by an indirect mechanism. Neurochem. Res. 26, 1127–1137.

Boucher, J.L., Moali, C., Tenu, J.P., 1999. Nitric oxide biosynthesis, nitric oxide synthase inhibitors and arginase competition for L-arginine utilization. Cell Mol. Life Sci. 55, 1015–1028.

Cao, W., Baniecki, M.L., McGrath, W.J., Bao, C., Deming, C.B., Rade, J.J., Lowenstein, C.J., Mangel, W.F., 2003. Nitric oxide inhibits the adenovirus proteinase *in vitro* and viral infectivity in vivo. FASEB J. 17 (15), 2345–2346.

Chou, C.-F., Shen, S., Tan, Y.-J., Fielding, B.C., Tan, T.H.P., Fu, J.-L., Xu, X., Lim, S.G., Hong, W., 2005. A novel cell-based binding assay system reconstituting interaction between SARS-CoV S protein and its cellular receptor. J. Virol. Methods 123, 41–48.

Connor, R.I., Chen, B.K., Choe, S., Landau, N.R., 1995. Vpr is required for efficient replication of human immunodeficiency virus type-1 in mononuclear phagocytes. Virology 206, 935–944.

Fan, K., Ma, L., Han, X., Liang, H., Wei, P., Liu, Y., Lai, L., 2005. The substrate specificity of SARS coronavirus 3C-like proteinase. Biochem. Biophys. Res. Commun. 329 (3), 934–940.

Fang, F.C., 2004. Antimicrobial reactive oxygen and nitrogen species: concepts and controversies. Nat. Rev. Microbiol. 2, 820–832.

Greaves, J., Chamberlain, L.H., 2007. Palmitoylation-dependent protein sorting. J. Cell Biol. 176, 249–254.

He, J., Choe, S., Walker, R., Di Marzio, P., Morgan, D.O., Landau, N.R., 1995. Human immunodeficiency virus type 1 viral protein R (Vpr) arrests cells in the G2 phase of the cell cycle by inhibiting p34cdc2 activity. J. Virol. 69, 6705–6711.

Ischiropoulos, H., Zhu, L., Chen, J., Tsai, M., Martin, J.C., Smith, C.D., Beckman, J.S., 1992. Peroxynitrite-mediated tyrosine nitration catalyzed by superoxide dismutase. Arch. Biochem. Biophys. 298 (2), 431–437.

Keng, C.T., Zhang, A., Shen, S., Lip, K.M., Fielding, B.C., Tan, T.H., Chou, C.F., Loh, C.B., Wang, S., Fu, J., Yang, X., Lim, S.G., Hong, W., Tan, Y.J., 2005. Amino acids 1055 to 1192 in the S2 region of severe acute respiratory syndrome coronavirus S protein induce neutralizing antibodies: implications for the development of vaccines and antiviral agents. J. Virol. 79, 3289–3296.

Klingstrom, J., Akerstrom, S., Hardestam, J., Stoltz, M., Simon, M., Falk, K.I., Mirazimi, A., Rottenberg, M., Lundkvist, A., 2006. Nitric oxide and peroxynitrite have different antiviral effects against hantavirus replication and free mature virions. Eur. J. Immunol. 36, 2649–2657.

Kumar, P., Gunalan, V., Liu, B., Chow, V.T., Druce, J., Birch, C., Catton, M., Fielding, B.C., Tan, Y.J., Lal, S.K., 2007. The nonstructural protein 8 (nsp8) of the SARS coronavirus interacts with its ORF6 accessory protein. Virology 366 (2), 293–303.

Li, F., Li, W., Farzan, M., Harrison, S.C., 2005. Structure of SARS coronavirus spike receptor-binding domain complexed with receptor. Science 309, 1864–1868.

Li, F., Berardi, M., Li, W., Farzan, M., Dormitzer, P.R., Harrison, S.C., 2006. Conformational states of the severe acute respiratory syndrome coronavirus spike protein ectodomain. J. Virol. 80, 6794–6800.

Lip, K.M., Shen, S., Yang, X., Keng, C.T., Zhang, A., Oh, H.L., Li, Z.H., Hwang, L.A., Chou, C.F., Fielding, B.C., Tan, T.H., Mayrhofer, J., Falkner, F.G., Fu, J., Lim, S.G., Hong, W., Tan, Y. J., 2006. Monoclonal antibodies targeting the HR2 domain and the region immediately upstream of the HR2 of the S protein neutralize *in vitro* infection of severe acute respiratory syndrome coronavirus. J. Virol. 80, 941–950.

Mannick, J.B., Asano, K., Izumi, K., Kieff, E., Stamler, J.S., 1994. Nitric oxide produced by human B lymphocytes inhibits apoptosis and Epstein-Barr virus reactivation. Cell 79, 1137–1146.

Marra, M.A., Jones, S.J., Astell, C.R., Holt, R.A., Brooks-Wilson, A., Butterfield, Y.S., Khattra, J., Asano, J.K., Barber, S.A., Chan, S.Y., Cloutier, A., Coughlin, S.M., Freeman, D., Girn, N., Griffith, O.L., Leach, S.R., Mayo, M., McDonald, H., Montgomery, S.B., Pandoh, P.K., Petrescu, A.S., Robertson, A.G., Schein, J.E., Siddiqui, A., Smailus, D.E., Stott, J.M., Yang, G.S., Plummer, F., Andonov, A., Artsob, H., Bastien, N., Bernard, K., Booth, T.F., Bowness, D., Czub, M., Drebot, M., Fernando, L., Flick, R., Garbutt, M., Gray, M., Grolla, A., Jones, S., Feldmann, H., Meyers, A., Kabani, A., Li, Y., Normand, S., Stroher, U., Tipples, G.A., Tyler, S., Vogrig, R., Ward, D., Watson, B., Brunham, R.C., Krajden, M., Petric, M., Skowronski, D.M., Upton, C., Roper, R.L., 2003. The Genome sequence of the SARS-associated coronavirus. Science 300, 1399–1404.

Petit, C.M., Chouljenko, V.N., Iyer, A., Colgrove, R., Farzan, M., Knipe, D.M., Kousoulas, K. G., 2007. Palmitoylation of the cysteine-rich endodomain of the SARS-coronavirus spike glycoprotein is important for spike-mediated cell fusion. Virology 360, 264–274.

Pope, M., Marsden, P.A., Cole, E., Sloan, S., Fung, L.S., Ning, Q., Ding, J.W., Leibowitz, J.L., Phillips, M.J., Levy, G.A., 1998. Resistance to murine hepatitis virus strain 3 is dependent on production of nitric oxide. J. Virol. 72, 7084–7090.

Resh, M.D., 2006. Palmitoylation of ligands, receptors, and intracellular signaling molecules. Sci. STKE 2006, re14.

Rota, P.A., Oberste, M.S., Monroe, S.S., Nix, W.A., Campagnoli, R., Icenogle, J.P., Penaranda, S., Bankamp, B., Maher, K., Chen, M.H., Tong, S., Tamin, A., Lowe, L., Frace, M., DeRisi, J.L., Chen, Q., Wang, D., Erdman, D.D., Peret, T.C., Burns, C., Ksiazek, T.G., Rollin, P.E., Sanchez, A., Liffick, S., Holloway, B., Limor, J., McCaustland, K., Olsen-Rasmussen, M., Fouchier, R., Gunther, S., Osterhaus, A.D., Drosten, C., Pallansch, M.A., Anderson, L.J., Bellini, W.J., 2003. Characterization of a novel coronavirus associated with severe acute respiratory syndrome. Science 300, 1394–1399.

Saura, M., Zaragoza, C., McMillan, A., Quick, R.A., Hohenadl, C., Lowenstein, J.M., Lowenstein, C.J., 1999. An antiviral mechanism of nitric oxide: inhibition of a viral protease. Immunity 10, 21–28.

Saxena, S.K., Mathur, A., Srivastava, R.C., 2001. Induction of nitric oxide synthase during Japanese encephalitis virus infection: evidence of protective role. Arch. Biochem. Biophys. 391, 1–7.

Smotrys, J.E., Linder, M.E., 2004. Palmitoylation of intracellular signaling proteins: regulation and function. Annu. Rev. Biochem. 73, 559–587.

Stamler, J.S., Simon, D.I., Osborne, J.A., Mullins, M.E., Jaraki, O., Michel, T., Singel, D.J., Loscalzo, J., 1992. S-nitrosylation of proteins with nitric oxide: synthesis and

characterization of biologically active compounds. Proc. Natl. Acad. Sci. U. S. A. 89 (1), 444–448.
Stamler, J.S., Toone, E.J., Lipton, S.A., Sucher, N.J., 1997. (S)NO signals: translocation, regulation, and a consensus motif. Neuron 18 (5), 691–696.
Tan, Y.J., Teng, E., Shen, S., Tan, T.H.P., Goh, P.Y., Fielding, B.C., Ooi, E.E., Tan, H.C., Lim, S. G., Hong, W., 2004. A novel SARS coronavirus protein, U274, is transported to the cell surface and undergoes endocytosis. J. Virol. 78, 6723–6734.
Tan, Y.J., Lim, S.G., Hong, W., 2006. Understanding the accessory viral proteins unique to the severe acute respiratory syndrome (SARS) coronavirus. Antiviral Res. 72, 78–88.
Thiel, V., Ivanov, K.A., Putics, A., Hertzig, T., Schelle, B., Bayer, S., Weissbrich, B., Snijder, E.J., Rabenau, H., Doerr, H.W., Gorbalenya, A.E., Ziebuhr, J., 2003. Mechanisms and enzymes involved in SARS coronavirus genome expression. J. Gen. Virol. 84 (9), 2305–2315.
Thorp, E.B., Boscarino, J.A., Logan, H.L., Goletz, J.T., Gallagher, T.M., 2006. Palmitoylations on murine coronavirus spike proteins are essential for virion assembly and infectivity. J. Virol. 80, 1280–1289.
Zhang, W., Kuncewicz, T., Yu, Z.Y., Zou, L., Xu, X., Kone, B.C., 2003. Protein–protein interactions involving inducible nitric oxide synthase. Acta Physiol. Scand. 179, 137–142.

III

A putative diacidic motif in the SARS-CoV ORF6 protein influences its subcellular localization and suppression of expression of co-transfected expression constructs

Vithiagaran Gunalan[a,b,c], Ali Mirazimi[a,b], Yee-Joo Tan[d]

[a]*Center for Microbiological Preparedness, Swedish Institute for Infectious Disease Control, SE-171 82 Solna , SWEDEN*

[b]*Department of Microbiology, Tumor and Cell Biology, Karolinska Institutet, Nobels Väg 16, SE-17177 Stockholm, Sweden*

[c]*Institute of Molecular and Cell Biology, Singapore.*

[d]*Department of Microbiology, Yong Loo Lin School of Medicine, National University Health System, National University of Singapore*

Corresponding Author:

Yee-Joo Tan

MD4, 5 Science Drive 2, Singapore 117597

Tel No: (65) 65163692

Fax No: (65) 67775720

Email: Yee_Joo_TAN@NUHS.edu.sg

Other authors:

Vithiagaran Gunalan, Email: oscillatoria@hotmail.com

Ali Mirazimi, Email: ali.mirazimi@smi.se

Abstract

Background

The ORF6 protein is one of the eight accessory proteins of the severe acute respiratory syndrome coronavirus (SARS-CoV). Numerous properties of ORF6 have been documented and this study focuses on two of these, namely, its ability to suppress the expression of co-transfected expression constructs and its subcellular localization to vesicular structures.

Findings

Using a transient transfection system, ORF6's ability to suppress the expression of co-transfected expression constructs was measured in a quantitative manner. While ORF6 does not have a global effect on protein synthesis, quantitative real-time PCR revealed that it down-regulated the mRNA level of the co-transfected myc-nsp8 gene. Furthermore, alanine substitution of a diacidic cluster motif (aa53-56) in the ORF6 gene caused a reduction in the suppression of expression of co-transfected myc-nsp8 gene. Our previous study revealed that ORF6 localized to vesicular structures in SARS-CoV infected Vero E6 cells. Here, ORF6 was observed to be localized to similar vesicular structures in Vero E6 cells which have been transiently transfected with a mammalian expression plasmid encoding for untagged ORF6. ORF6 showed partial colocalization with cellular proteins CD63 and Lamp1, suggesting that the vesicular structures may be a subpopulation of endosomal/lysosomal vesicles. The alanine substitution of the diacidic cluster motif also altered the subcellular localization of the ORF6 protein, indicating a potential relationship between the subcellular localization of the ORF6 protein and its ability to suppress the expression of co-transfected expression constructs.

Conclusion

By combining quantitative real-time PCR and transient transfection system, a simple and safe method is established to measure ORF6's ability to suppress the expression of co-transfected myc-nsp8. In addition, immunofluorescence analysis revealed that the subcellular localization of ORF6 when expressed on its own is similar to that observed in SARS-CoV infected cells. Through the use of these two assays, a putative diacidic motif in the SARS-CoV ORF6 protein was found to influence its subcellular localization and ability to suppress the expression of co-transfected expression constructs.

Background

An outbreak of Severe Acute Respiratory syndrome in 2003 which carried with it a fatality rate of 8% was traced to a novel coronavirus dubbed the SARS Coronavirus (SARS-CoV). This novel coronavirus was eventually classified as a Group IIb coronavirus, a subset of the Group II coronaviruses. The subclassification was, in part, due to the presence of several accessory genes in the coronavirus which have no known homologs within the family *Coronaviridae*. These accessory genes have been the subject of study by many groups (for reviews, see 1 and 2) and have been assigned a plethora of physical characteristics and intracellular functions. Most importantly, almost all of these accessory genes have been shown to be dispensable for viral replication, with the exception of the 3a accessory gene (3). It has been suggested these accessory genes have subtle effects on SARS-CoV replication and may be more important for viral replication or pathogenesis in vivo.

One of these accessory genes, ORF6, encodes for a ~7kDa protein with a hydrophobic N–terminal and that has been suggested to have a N-endo-C-endo conformation (4). Several groups have undertaken to characterize the protein product of the ORF6 gene and found that it interacts with the nsp8 protein from the SARS replicase complex (5), is able to increase infection titer during early infection at low MOI (6), increase the rate of cellular gene synthesis (7), inhibit interferon production (8), and inhibit the nuclear translocation of STAT1 by interacting with karyopherin $\alpha 2$ (9). Most recently, the ORF6 protein has been suggested to induce intracellular membrane rearrangements resulting in a vesicular population in the infected cell which could possibly serve some role in increasing replication (10). Such virus-induced or virus associated vesicles have previously been shown in other viral

infections, such as protein trafficking in Herpes simplex virus (11) and Sendai virus (12). Members of the coronavirus family have been shown by several groups to also utilize vesicular structures within the infected cell; most of these studies suggest that vesicles play a role in viral replication (13-16).

We have previously shown that the ORF6 protein colocalizes with Lamp1-positive vesicles in SARS-CoV infection (5) and also with the nsp8 protein in the same set of infected cells, indicating a possible role for the ORF6 protein in the replicative process of SARS-CoV. However, there has been, to date, little work done to link the subcellular localization of the ORF6 protein to its known functions. Gallagher and co-workers have shown that the ability of ORF6 to impede nuclear translocation resulted in the suppression of expression of transgenes from co-transfected expression constructs if these need transcription in the nucleus (17). Using this knowledge, a simple co-transfection system and alanine substitution mutants in the ORF6 gene is used here to determine regions of the ORF6 protein that modulate its ability to suppress the expression of co-transfected myc-nsp8. The subcellular localization of these mutants is then examined by immunofluorescence experiments and compared to that of wildtype ORF6.

Materials and Methods

Cells, Plasmids and Antibodies

Vero E6 cells were obtained from ATCC, and cultured in DMEM (Invitrogen) supplemented with 10% FBS (Gibco) and penicillin/streptomycin (Sigma). Cells were cultured in a 37˚C incubator with 5% CO2. ORF6 was cloned into the pXJ3'HA vector (T. Leung, Institute of Molecular and Cell Biology, Singapore, personal communication) using the sites *BamHI* and *XhoI* with a stop codon to create pXJ3'-ORF6, expressing an untagged protein. The nsp8 gene from SARS-CoV was cloned using *BamHI* and *XhoI* sites into pXJ40myc to create pXJ40myc-nsp8, with an N-terminal myc tag for detection. GST was cloned into pXJ40flag to create pXJ40flag-GST, which expresses an N-terminal flag tagged GST protein. The ORF6A49-52 and ORF6A53-56 mutants were generated by 2 rounds of PCR: the first round of PCR was used to generate 5' and 3' fragments of ORF6 containing the appropriate alanine substitutions; these were then amplified into full-length ORF6 using end primers for the ORF6 gene and cloned into pXJ3'HA using *BamHI* and *XhoI* sites. The following antibodies were used in this study: rabbit anti-ORF6 was purchased from Abgent, mouse anti-actin from Sigma, mouse anti-Lamp1 from Abcam, mouse anti-myc from Santa Cruz and mouse anti-CD63 was purchased from Biodesign International.

Immunofluorescence

Vero E6 cells were plated in 60mm dishes containing coverslips and subsequently transfected with mammalian expression plasmids relevant to the experiment being performed. Trasfection was performed using Lipofectamine 2000 (Invitrogen) according the manufacturer's instructions. 16 hours after transfection, coverslips were prepared for immunofluorescence as follows: Fixation was carried

out in 100% methanol for 5 minutes and coverslips were left to dry before being blocked with PBS containing 1% BSA for 30 minutes. Primary antibody incubation was carried out in a humidified chamber for 1 hour before coverslips were washed 3 times in blocking solution. Secondary antibody incubation was then carried out for an hour in a humidified chamber before the coverslips were washed 3 times. Coverslips were mounted onto glass slides using a mounting mixture of 70% Fluorsave (Calbiochem) and 30% Vectashield containing DAPI (Vector Laboratories). Slides were imaged using a Zeiss LSM510Meta confocal microscope (Zeiss).

SARS-CoV Infection

Vero E6 cells grown on coverslips were infected with SARS-CoV Frankfurt strain 1. When the cells showed 75 % cytopathic effects, they were subjected to immunofluorescence as described above. All SARS-CoV infection work was carried out at the BSL4 facility at the Swedish Institute for Infectious Disease Control in Solna, Sweden.

Western Blotting

Vero E6 cells were transfected with relevant plasmids for each experiment. 16 hours after transfection, cells were scraped into media before being spun down in a benchtop centrifuge and washed twice with PBS. After washes, the cell pellets were resuspended in RIPA buffer (50 mM Tris (pH 8.0), 150 mM NaCl, 0.5% NP40, 0.5% deoxycholic acid, 0.005% SDS) and freeze-thawed in liquid nitrogen 3 times before being spun down at 13K rpm to remove cellular debris. SDS loading buffer was added to clarified lysates before being boiled at 100˚C and loaded onto an SDS-PAGE gel for separation. Gels containing separated lysates were transferred onto Hybond-C

nitrocellulose membranes (Amersham) before blocking with 5% skimmed milk in PBS-Tween. Antibody incubations were carried out at 4˚C overnight or at room temperature, with constant rotation. After each incubation, membranes were washed 3 times for 10 minutes each with PBS-Tween. Following washes after secondary antibody incubation, membranes were treated with chemiluminescent substrate (Thermo) and exposed to film.

Metabolic labeling

Vero E6 cells were transfected with 1µg or 2ug of either pXJ3'-ORF6 or empty vector. 16 hours post transfection, cells were starved using DMEM without L-glutamine, cysteine and methionine (Invitrogen) before being incubated with 100µCi of ^{35}S-labelled cysteine and methionine (Perkin Elmer) diluted in starvation medium for 30 minutes. At the end of each incubation period, cells were washed in cold PBS and scraped into a centrifuge tube and lysed in RIPA buffer. 20 µg of each lysed sample was boiled with SDS loading buffer and PAGE separated before being fixed and dried in a Model 583 Gel Dryer (Bio-Rad). Dried gels were exposed to film at -80˚C to obtain autoradiograph. Quantification of signals was performed using the gel analysis module in Image J.

Quantitative Realtime PCR

Vero E6 cells were co-transfected with increasing amounts of pXJ3'-ORF6 (0 - 2 µg) and a fixed amount of pXJ40myc-nsp8 (1 µg). For each sample, the total amount of DNA was normalized to 3 µg by addition of the empty vector, pXJ3'HA, when necessary. 16 hours post-transfection, cells were scraped into media and spun down in a benchtop centrifuge. Cells were washed twice with PBS and cell pellets

were resuspended with Trizol reagent (Invitrogen). Trizol samples were mixed with chloroform and spun down in a benchtop centrifuge at 4˚C before being processed with an RNeasy Mini Kit (Qiagen), according to the manufacturer's instructions. RNA samples were quantified with a Nanodrop ND-1000 spectrophotometer (Nanodrop Technologies). Equal amounts of each RNA sample were then reverse transcribed using poly $d(T)_{12-18}$ (Invitrogen) and with Superscript II reverse transcriptase (Invitrogen), following manufacturer instructions. Following reverse transcription, equal amounts of each cDNA sample were added to a portion of reaction mix (Roche) along with either of the following primer pairs: SARS-nsp8-F: 5'-TGAATGCTAAATCTGAGTTTGA-3', SARS-nsp8-R: 5'-CATAGCCTGATCTGCCATCTTTT-3', GAPDH-F: 5'-GAAGGTGAAGGTCGGAGTC-3', GAPDH-R: 5'-GAAGATGGTGATGGGATTTC-3' and one of the following probes: SARS-nsp8-P: 5' 6-FAM-CGTGATGCTGCCATGCAACGC-BHQ 3', GAPDH-P: 5' 6-FAM-CAAGCTTCCCGTTCTCAGCC-BHQ 3'. Reaction mixes were subjected to quantitative real-time PCR in a Roche Lightcycler 2.0. Cycle threshold values obtained for the SARS *nsp8* gene were normalized against those for *GAPDH* to obtain relative quotients which were then plotted for increasing amounts of pXJ3'-ORF6 transfected. Briefly, the Ct for the *GAPDH* control was subtracted from the Ct for the *nsp8* gene (ΔCt). The fold changes were then calculated from the ΔΔCt, which was obtained by subtracting each ΔCt from the ΔCt obtained when 2 μg of pXJ3'HA vector was used. Alternatively, quantitative real-time PCR was carried out using SsoFast EvaGreen SYBR Green Master mix (Bio-Rad) using the same primers for *nsp8* and *GAPDH* as listed above; probes were omitted from these experiments. These reactions were carried out in an ABI 7500Fast Realtime PCR system.

Results

The ORF6 protein exerts an effect on the expression of transgenes from co-transfected expression constructs.

To determine amount of ORF6 required to exert an effect on the expression of transgenes from co-transfected expression constructs, Vero E6 cells were transfected with 1μg of pXJmyc-nsp8 alone or with either 1μg, 2μg or 3μg of pXJ3'-ORF6 plasmid. Western blotting showed a dose-dependent reduction in the expression of nsp8, concomitant with an increase in the expression of ORF6 (Fig. 1A). In order to determine the specificity of this effect, Vero E6 cells were cotransfected with another mammalian expression construct pXJflag-GST and pXJ3'-ORF6 in the same manner as previously done with the construct encoding for nsp8. When titrated against increasing amounts of ORF6 protein, the flag-tagged GST protein was also observed by Western Blotting to show reduced levels of expression in a dose-dependent manner (Fig. 1B). Thus, it seems that ORF6 exerts an effect on the expression of transgenes from co-transfected expression constructs regardless of the nature of the transgenes. However, when increasing amounts of GST were titrated against nsp8 in the same manner, no significant reduction in nsp8 expression was observed, indicating that this effect was specific to the ORF6 protein (Fig. 1C).

ORF6 does not affect total cellular protein synthesis

The ORF6 protein has been observed to cause a reduction in the expression of 2 different proteins, with different epitope tags. In order to examine the possibility that this downregulation could be a global effect, Vero E6 cells were transfected with either empty vector, pXJ3'HA, or pXJ3'-ORF6, and metabolically labeled with ^{35}S for a period of 30 minutes. Quantification of the signals in each lane of the resulting

autoradiograph was performed and the readings were normalized to the reading in the lane from the untransfected cells (Fig. 2). When 1 μg of DNA was used, there is a slight decrease in the total cellular protein synthesis in ORF6 expressing cells when compared to cells which had been transfected with empty vector. However, almost the same degrees of decrease in the total cellular protein synthesis were observed in both pXJ3'HA and pXJ3'-ORF6 transfected cells when 2 μg of DNA was used. Hence, the decrease in total cellular protein synthesis observed seems to be related to the transfection process rather than the expression of ORF6. This suggests that the cellular effect of ORF6 is not global.

ORF6 exerts its effect at a transcriptional level

In order to examine the possibility that ORF6 affects the expression of transgenes from co-transfected expression constructs via a transcriptional mechanism, Vero E6 cells were transfected with 1μg of pXJ40myc-nsp8 and either 1μg, 2μg of pXJ3'-ORF6 or no ORF6 plasmid. 16 hours post-transfection, total RNA was extracted, reverse transcribed and subjected to quantitative real-time PCR. Taqman chemistry was used to assay for *nsp8* and *GAPDH* was used as an endogenous control. The ΔΔCt method was used to calculate the nsp8 mRNA level with respect to the level in the absence of ORF6. As shown in Fig. 3, ORF6 caused a reduction in the level of nsp8 mRNA in a dose-dependent manner, indicating a transcriptional reduction caused by ORF6. These results suggest that ORF6 is able to exert some form of transcriptional inhibition, which is seen in the reduced expression from co-transfected plasmids.

The ORF6 protein localizes to intracellular vesicles positive for Lamp1 and CD63

It has been previously reported that the SARS-CoV ORF6 protein localizes to intracellular membranous compartments, which have been suggested to be induced by ORF6 itself (10). In agreement, it was observed in this study that ORF6 localized to vesicular compartments both in SARS-infected Vero E6 cells and Vero E6 cells transfected with a plasmid encoding for the ORF6 protein (Fig. 4A). Vero E6 cells were infected with SARS-CoV and analyzed by immunofluoresence, using an antibody against the ORF6 protein. ORF6 was observed to localize to a distinct population of intracellular vesicles in these infected cells (Fig 4A). Following this, a mammalian expression plasmid pXJ3'-ORF6 was transfected into Vero E6 cells and analyzed in the same manner with the same antibody. Confocal microscopy showed that the ORF6 protein localized to a similar population of intracellular vesicles.

In our previous work studying the interaction between ORF6 and the nsp8 protein of SARS-CoV (5), we showed a colocalization of ORF6 and Lamp1 in Vero E6 cells infected with the HKU39849 strain of SARS-CoV. Similarly, there was a significant degree of colocalization between the Lamp1 and ORF6 in transiently transfected Vero E6 cells (Fig. 4B), indicating that the ORF6-positive vesicles seen in both infected cells and transiently transfected Vero E6 cells were probably an identical population of vesicles. This allowed us to then use pXJ3'-ORF6-transfected Vero E6 cells to further study the characteristics of this vesicular population. In addition to Lamp1, CD63 (a marker for late endosomes) was used to examine the compartmental characteristics of the vesicles. As shown in Fig. 4B, ORF6-positive vesicles coincide significantly with CD63-positive vesicles in Vero E6 cells. This population of vesicles is therefore a subset of the late endosomal and lysosomal

populations, and shows that the plasmid system employed here yields similar colocalization of ORF6 with cellular markers as seen in previous infection work (5).

Amino Acids 53-56 in ORF6 constitute a putative diacidic motif which affects the suppression of the expression of co-transfected myc-nsp8

Using the CBS Prediction Servers (http://www.cbs.dtu.dk/services/), it was determined that the ORF6 protein had several putative motifs of interest. Of these, aa49-52 (YSEL) was predicted to be a lysosomal targeting motif *YXXL* (18), and aa53-56 (DDEE) bears similarity to a putative diacidic motif *DxE*, which governs ER export and subsequent localization to different membranous compartments (19). These motifs were also predicted by Netland and co-workers (4). In order to determine the contribution of these motifs to the function of the ORF6 protein, alanine substitutions were introduced by two-step PCR to yield ORF6A49-52, which substituted four alanine residues for the YSEL region, and ORF6A53-56, which substituted four alanines for the DDEE region (Fig. 5A).

These alanine substitution mutants were cloned into the same vector as the wildtype ORF6 gene and titrated against the *nsp8* gene, by co-transfection of Vero E6 cells with plasmids encoding for myc-nsp8 and either wildtype ORF6, ORF6A49-52 or ORF6A53-56. It was observed that both mutants showed increased levels of expression compared to wildtype ORF6, and this observation was reproducible (data not shown). The effect of ORF6A49-52 mutant on the expression of the *nsp8* gene was similar to wildtype ORF6 (Fig. 5B). On the other hand, the nsp8 expression in the presence of ORF6A53-56 was higher than that in the presence of wildtype ORF6 (Fig. 5B), which suggest that ORF6A53-56 is less efficient in the suppressing the expression of co-transfected myc-nsp8.

As the difference between wildtype ORF6 and ORF6A53-56 was subtle, a more quantitative approach to assay *nsp8* expression was deemed necessary. Hence, Vero E6 cells were transfected in the same manner and instead RNA was extracted and reverse transcribed and subjected to SYBR Green QPCR using primers for *nsp8*. GAPDH was used as a housekeeping gene in order to normalize the expression levels seen. When pXJmyc-nsp8 was co-transfected with 1µg of pXJ3'-ORF6, ORF6A49-52 or ORF6A53-56, the levels of *nsp8* mRNA were similar (Fig. 5C). However, at 2µg, the levels of *nsp8* mRNA for both ORF6 mutants were slightly higher than wild-type ORF6 (Fig. 5C). In order to determine if these differences are statistically significant, 5 independent experiments were performed, and the results were then used to perform a t-test measuring the significance of the difference between *nsp8* expression levels when either 2µg of wildtype ORF6 or 2µg of each mutant were used. The difference in *nsp8* expression when co-transfected with either wildtype ORF6 and ORF6A49-52 is not statistically significant (a two-tailed p-value of 0.08). On the other hand, the difference in *nsp8* expression when co-transfected with either wildtype ORF6 and ORF6A53-56 is statistically significant (a two-tailed p-value of 0.01). This indicated that the reduction in impedance of nuclear transport by ORF6A53-56 was significant, and therefore that the putative diacidic motif defined by amino acids 53-56 has a role to play in the ability of the ORF6 protein to suppress the expression of co-transfected myc-nsp8. The ORF6A49-52 mutant did not show as high a level of significance.

Alanine substitutions at amino acids 53-56 alter the subcellular localization of ORF6

Next, the subcellular localization of ORF6A49-52 and ORF6A53-56 was compared to wildtype ORF6. Vero E6 cells were transiently transfected with either

pXJ3'-ORF6, pXJ3'-ORF6A49-52 or pXJ3'-ORF6A53-56 and subjected to immunofluoresence analysis. It was observed that the localization of ORF6A49-52 was somewhat similar to wild-type ORF6 with main expression in distinctive vesicles (Fig. 6). However, slightly more ORF6A49-52 than wildtype ORF6 was found to spread diffusely throughout the cytoplasm. The ORF6A53-56 also has some cytoplasmic staining but it was also observed that this mutant protein localized to vesicles that were clustered into groups of 3-5 vesicles to form large aggregates. Careful examination of the localization of the wildtype protein did not yield similar observations of clusters. This indicated that the putative diacidic motif from amino acids 53-56, in addition to being involved in the suppression of the expression of co-transfected myc-nsp8, is also involved in the subcellular localization of the ORF6 protein and therefore these 2 phenomena may be linked.

Discussion

Work done by several groups have shown that the ORF6 protein interacts with the nsp8 primase and localizes to a lysosomal compartment (5), impedes the nuclear translocation of STAT1 and other proteins specifically governed by the importin-ß superfamily (9), is able to enhance replication of both SARS-CoV (6) and MHV-JHM (20), induces membrane rearrangements by means of its C-terminus (10) and induces apoptosis via a JNK-dependent mechanism (21). Through the use of alanine substitutions, many of these functions have been attributed to specific regions of the ORF6 protein.

In this study, we have employed the use of transiently transfected mammalian expression plasmids encoding for ORF6 to study its function. We have shown that ORF6 expressed in our system is functionally similar to that shown by others, by means of 2 assays. Firstly, the ORF6 expressed in our system is able to suppress the expression of a co-transfected CMV promoter-driven plasmid expressing either the nsp8 protein or GST. Secondly, the localization of ORF6 expressed via transient transfection was compared to the localization of virally expressed ORF6, and both display similar subcellular localization as well as colocalization to the Lamp1 marker.

Using a bioinformatics approach to defining regions of interest in the ORF6 gene, we have identified 2 regions of interest, a putative lysosomal targeting motif YSEL between amino acids 49 to 52 and a putative diacidic motif DDEE between amino acids 53 to 56 (Figure 5A). Our results indicate that the putative diacidic motif is involved in both the suppression of expression of co-transfected expression constructs by ORF6 as well as its subcellular localization. While we were not able to completely restore the expression of co-transfected nsp8 in our system, the effect on

nsp8 mRNA level between wildtype ORF6 and ORF6A53-56 was nonetheless found to be significantly different. However, the difference is small and suggests that the diacidic motif is largely dispensable for this function of ORF6. In contrast, the putative lysosomal targeting motif YSEL does not appear to contribute to these properties of ORF6 and this is consistent with a recent report that alanine substitution of the region from amino acids 49 to 53 fails to inhibit the ability of the protein to impede the nuclear translocation of STAT1 (9). Also, others have shown that the ORF6 protein induces membrane rearrangements and that the C-terminus of the protein is important to this function. Our results show that the region from amino acids 53 to 56 is involved in the subcellular localization of the ORF6 protein, since alanine substitution of this region results in a clustered-vesicle phenotype that is not observed with wildtype ORF6. The reason for the difference in the subcellular localization of wild-type ORF6 and ORF6A53-56 mutant is not clear. One possibility is that the substitutions of four acidic residues with alanine residues might have reduced the solubility of ORF6. Alternatively, the substitutions may have disrupted the interaction of ORF6 with certain host proteins.

Conclusions

Taking these results together, the putative diacidic motif in ORF6 seems to be important for two properties of ORF6, namely its ability to suppress the expression of co-transfected expression constructs and its subcellular localization to vesicular structures. The implication of this is that the 2 functions may be inextricably linked. However, a cause-effect relationship has yet to be determined for these functions and in light of our findings, their relationship to the membrane rearrangements induced by the ORF6 protein should be examined in future studies. In addition, while the ability

of ORF6 to suppress the expression of co-transfected expression constructs, was previously linked to the blockage of nuclear translocation (17), further experiments are needed to ascertain if amino acids 53-56 are involved in regulating the nuclear translocation process.

Competing interests

The authors declare that they have no competing interests

Authors' contributions

VG carried out the experiments and drafted the manuscript. AM and YJT participated in the design of the study and coordination and revised the manuscript. All authors read and approved the final manuscript.

References

1. Tan Y-J, Lim SG, Hong W: Understanding the accessory viral proteins unique to the severe acute respiratory syndrome (SARS) coronavirus. *Antiviral Research* 2006, 72(2):78-88.

2. Narayanan K, Huang C, Makino S: SARS coronavirus accessory proteins. *Virus Research* 2008, 133(1):113-21.

3. Yount B, Roberts RS, Sims AC, Deming D, Frieman MB, Sparks J, et al.: Severe Acute Respiratory Syndrome Coronavirus Group-Specific Open Reading Frames Encode Nonessential Functions for Replication in Cell Cultures and Mice. *Journal of Virology* 2005, 79(23):14909-14922.

4. Netland J, Ferraro D, Pewe L, Olivares H, Gallagher T, Perlman S: Enhancement of murine coronavirus replication by severe acute respiratory syndrome coronavirus protein 6 requires the N-terminal hydrophobic region but not C-terminal sorting motifs. *Journal of Virology* 2007, 81(20):11520-5.

5. Kumar P, Gunalan V, Liu B, Chow VTK, Druce J, Birch C, et al.: The nonstructural protein 8 (nsp8) of the SARS coronavirus interacts with its ORF6 accessory protein. *Virology* 2007, 366(2):293-303.

6. Zhao J, Falcón A, Zhou H, Netland J, Enjuanes L, Pérez Breña P, et al.: Severe acute respiratory syndrome coronavirus protein 6 is required for optimal replication. *Journal of Virology* 2009, 83(5):2368-7.

7. Geng H, Liu Y-M, Chan W-S, Lo AW-I, Au DM-Y, Waye MM-Y, et al.: The putative protein 6 of the severe acute respiratory syndrome-associated

coronavirus: expression and functional characterization. *FEBS Letters* 2005, 579(30):6763-8.

8. Kopecky-Bromberg SA, Martínez-Sobrido L, Frieman M, Baric RA, Palese P: Severe acute respiratory syndrome coronavirus open reading frame (ORF) 3b, ORF 6, and nucleocapsid proteins function as interferon antagonists. *Journal of Virology* 2007, 81(2):548-57.

9. Frieman M, Yount B, Heise M, Kopecky-Bromberg SA, Palese P, Baric RS: Severe acute respiratory syndrome coronavirus ORF6 antagonizes STAT1 function by sequestering nuclear import factors on the rough endoplasmic reticulum/Golgi membrane. *Journal of Virology* 2007, 81(18):9812-24.

10. Zhou H, Ferraro D, Zhao J, Hussain S, Shao J, Trujillo J, et al.: The N-terminal region of severe acute respiratory syndrome coronavirus protein 6 induces membrane rearrangement and enhances virus replication. *Journal of Virology* 2010, 84(7):3542-51.

11. Miranda-Saksena M, Boadle RA, Aggarwal A, Tijono B, Rixon FJ, Diefenbach, RJ, et al.: Herpes simplex virus utilizes the large secretory vesicle pathway for anterograde transport of tegument and envelope proteins and for viral exocytosis from growth cones of human fetal axons. *Journal of Virology* 2009, 83(7):3187-99.

12. Chambers R, Takimoto T: Trafficking of Sendai virus nucleocapsids is mediated by intracellular vesicles. *PLoS One* 2010, 5(6):e10994.

13. Sims AC, Ostermann J, Denison MR: Mouse hepatitis virus replicase proteins associate with two distinct populations of intracellular membranes. *Journal of Virology* 2000, 74(12):5647-54.

14. Snijder EJ, van der Meer Y, Zevenhoven-Dobbe J, Onderwater JJM, van der Meulen J, Koerten HK, et al.: Ultrastructure and origin of membrane vesicles associated with the severe acute respiratory syndrome coronavirus replication complex. *Journal of Virology* 2006, 80(12):5927-40.

15. Knoops K, Kikkert M, Worm SHED, Zevenhoven-Dobbe, JC, van der Meer Y, Koster AJ, et al.: SARS-coronavirus replication is supported by a reticulovesicular network of modified endoplasmic reticulum. *PLoS Biology* 2008, 6(9):e226.

16. Reggiori F, Monastyrska I, Verheije MH, Calì T, Ulasli M, Bianchi S, Bernasconi R, de Haan CA, Molinari M: Coronaviruses Hijack the LC3-I-positive EDEMosomes, ER-derived vesicles exporting short-lived ERAD regulators, for replication. Cell Host Microbe 2010, 7(6):500-8.

17. Hussain S, Perlman S, Gallagher TM: Severe acute respiratory syndrome coronavirus protein 6 accelerates murine hepatitis virus infections by more than one mechanism. *Journal of Virology* 2008, 82(14):7212-22.

18. Williams MA, Fukuda, M.: Accumulation of membrane glycoproteins in lysosomes requires a tyrosine residue at a particular position in the cytoplasmic tail. *The Journal of Cell Biology* 1990, 111(3):955-66.

19. Nishimura NA: Di-Acidic Signal Required for Selective Export from the Endoplasmic Reticulum. *Science* 1997, 277(5325):556-8.

20. Pewe L, Zhou H, Netland J, Tangudu C, Olivares H, Shi L, et al.: A Severe Acute Respiratory Syndrome-Associated Coronavirus-Specific Protein Enhances Virulence of an Attenuated Murine Coronavirus. *Journal of Virology* 2005, 79(17):11335-42.

21. Ye Z, Wong CK, Li P, Xie Y: A SARS-CoV protein, ORF-6, induces caspase-3 mediated, ER stress and JNK-dependent apoptosis. *Biochimica et Biophysica Acta* 2008, 1780(12):1383-7.

Figure Legends

Fig. 1 ORF6 specifically impedes expression of co-transfectants. Vero E6 cells were co-transfected with mammalian expression plasmids encoding for ORF6 and nsp8 (A), ORF6 and GST (B) or GST and nsp8 (C). Cells were lysed 16 hours post transfection and subjected to Western Blot analysis using equal amounts of lysate from each transfection. Blots were stripped post-detection and re-probed with an anti-actin antibody as a loading control. Similar results were obtained in three independent experiments, and a representative set of data is presented.

Fig. 2 ORF6 expression in Vero E6 cells does not cause a reduction in total cellular protein. Vero E6 cells were transfected for 16 hours with increasing amounts of pXJ3'-ORF6 or an empty vector, pXJ3'HA. Cells were starved of methionine and cysteine for 1 hour and labeled with a mixture of 35S-labelled methionine and cysteine for 30 minutes, then subjected to PAGE separation and autoradiography (lower panel). Quantification of the signals in each lane of the resulting autoradiograph was performed and the readings, after normalization to the reading in the lane from the untransfected cells, are shown at the bottom of the autoradiography. A fraction of lysate was subjected to Western Blotting using an antibody directed against the ORF6 protein (upper panel). Similar results were obtained in two independent experiments, and a representative set of data is presented.

Fig. 3 The ORF6 protein exerts a transcriptional effect on nsp8 expression. Vero E6 cells were co-transfected with 1μg of pXJ40myc-nsp8 and different amount of pXJ3'-ORF6. For each sample, the total amount of DNA was normalized to 3 μg by addition of the empty vector, pXJ3'HA, when necessary. Total RNA was harvested 16 hours later, reverse transcribed and subjected to quantitative real-time Taqman PCR using

primers and probes specific to nsp8 and cellular protein, GADPH. Relative quotients between the resulting Ct values for each sample were calculated using the ΔΔCt method. Similar results were obtained in three independent experiments, and a representative set of data is presented.

Fig. 4 ORF6 expressed from a plasmid adopts a similar subcellular localization to virally expressed ORF6 and colocalizes partially with CD63 and Lamp1. (A) Vero E6 cells were either transiently transfected with pXJ3'-ORF6 or infected with SARS-CoV. At either 16hrs post-transfection or at 75% CPE, cells were fixed and processed for immunofluorescence using an antibody directed against the ORF6 protein. (B) Vero E6 cells, which have been transiently transfected with ORF6, were fixed and stained for antibodies directed against ORF6 and either Lamp1 or CD63. Similar results were obtained in three independent experiments, and a representative set of data is presented.

Fig. 5 Alanine substitutions in the putative diacidic motif in ORF6 exert an effect on impedance of nsp8 expression. (A) A schematic of the ORF6 amino acid sequence showing the position of two putative motifs, a lysosomal targeting motif and a putative diacidic motif. (B) Vero E6 cells were transfected with 1μg of pXJ40myc-nsp8 and either 0μg, 1μg, 2μg of either pXJ3'-ORF6 (left panel), pXJ3'-ORF6A49-52 (centre panel) or pXJ3'-ORF6A53-56 (right panel). 16 hours post transfection, cells were harvested, lysed and subjected to Western Blotting using an antibody directed against either ORF6 or myc-nsp8. Actin was used as a loading control. Similar results were obtained in three independent experiments, and a representative set of data is presented. (C) Vero E6 cells were similarly transfected as in (A) and total RNA was harvested 16 hours later, reverse transcribed and subjected to SYBR-Green QPCR using specific primers for nsp8, with GAPDH as a housekeeping

control. Relative quotients were calculated and plotted from the Ct values obtained, using the ΔΔCt method. The average values with standard deviations are plotted and the standard deviations are also shown in parentheses in the x-axis labels. Students' T-test was performed on selected results and the *p*-values are indicated. $P < 0.05$ was considered statistically significant. Similar results were obtained in five independent experiments, and a representative set of data is presented.

Fig. 6 Alanine substitution mutant ORF6A53-56 shows altered subcellular localization. Vero E6 cells were transiently transfected with pXJ3'-ORF6, pXJ3'-ORF6A49-5 or pXJ3'-ORF6A53-56 and immunofluorescence analysis performed with an antibody directed against ORF6. Similar results were obtained in three independent experiments, and a representative set of data is presented.

Fig. 1

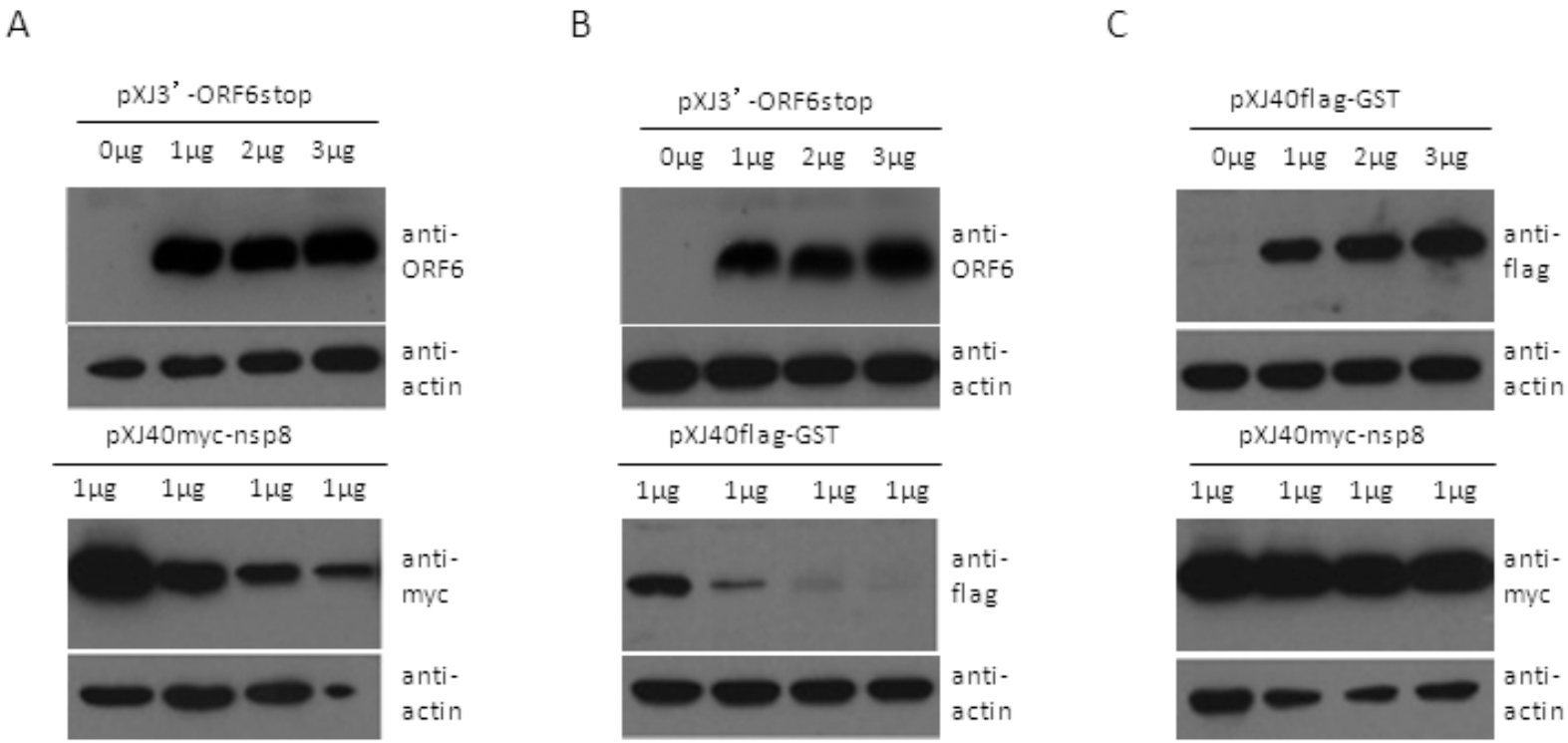
A
pXJ3'-ORF6stop
0μg 1μg 2μg 3μg
anti-ORF6
anti-actin
pXJ40myc-nsp8
1μg 1μg 1μg 1μg
anti-myc
anti-actin
B
pXJ3'-ORF6stop
0μg 1μg 2μg 3μg
anti-ORF6
anti-actin
pXJ40flag-GST
1μg 1μg 1μg 1μg
anti-flag
anti-actin
C
pXJ40flag-GST
0μg 1μg 2μg 3μg
anti-flag
anti-actin
pXJ40myc-nsp8
1μg 1μg 1μg 1μg
anti-myc
anti-actin

Revised Fig. 2

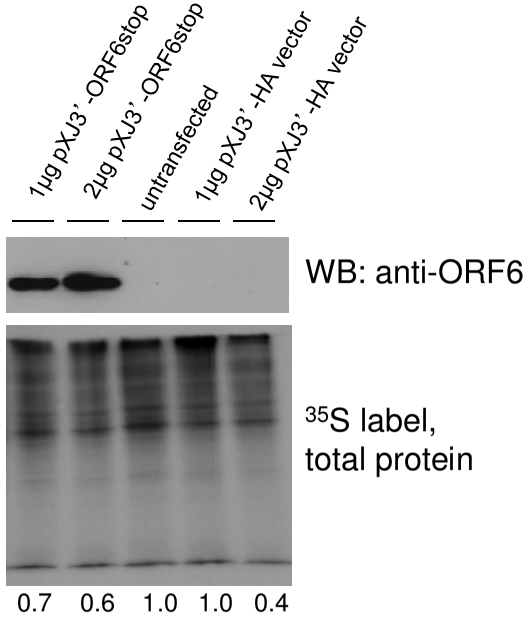

Revised Fig. 3

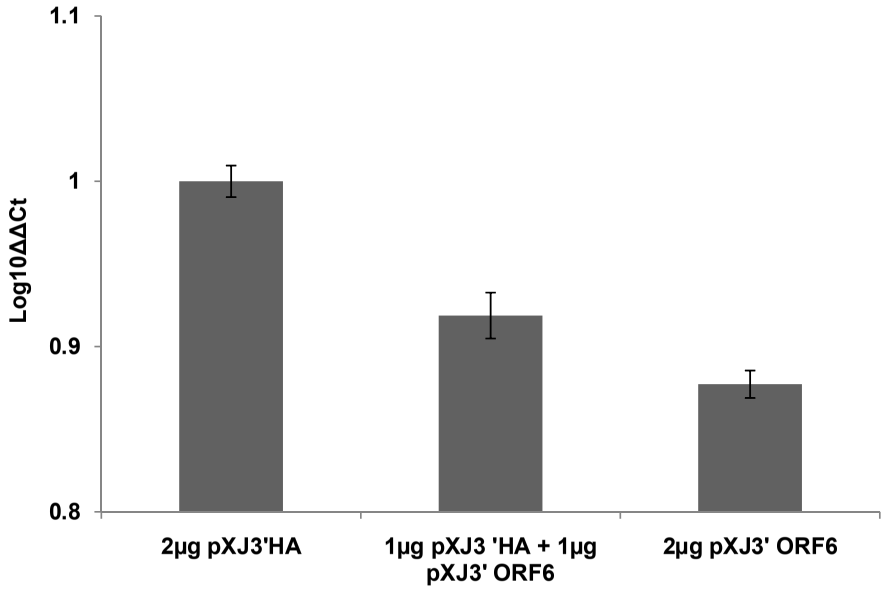

Fig. 4

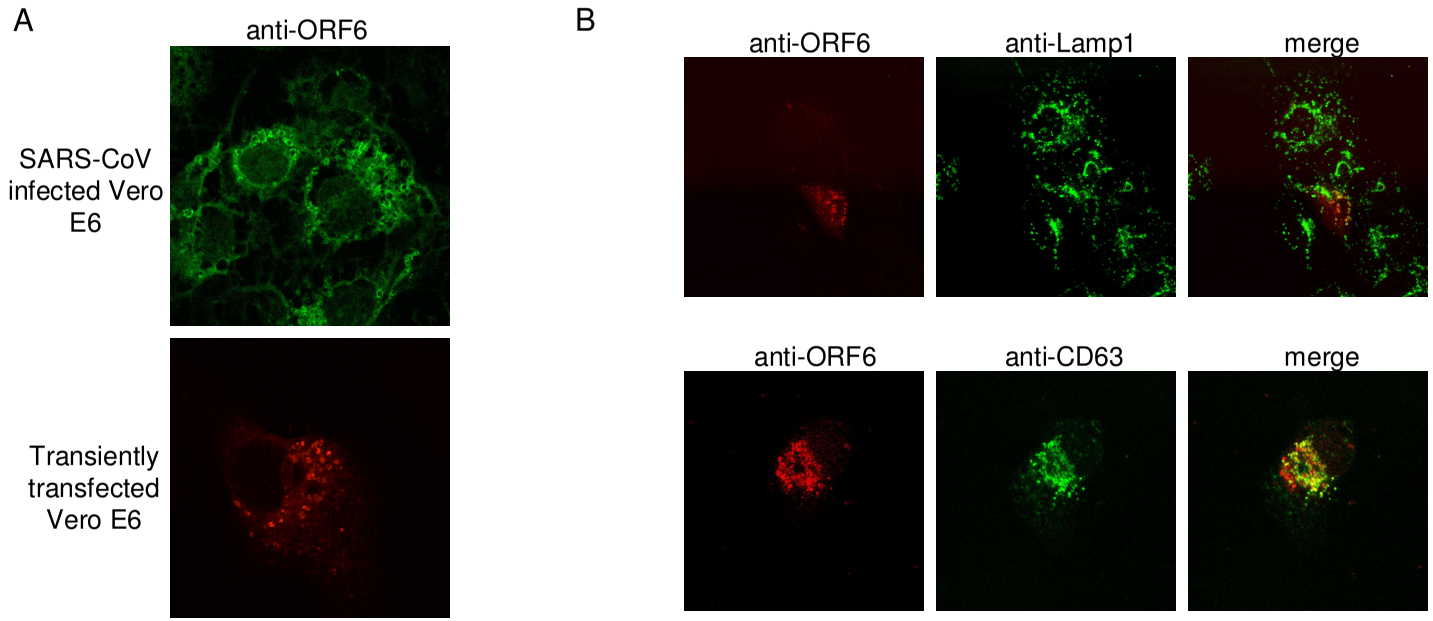
A
anti-ORF6
SARS-CoV infected Vero E6
Transiently transfected Vero E6
B
anti-ORF6
anti-Lamp1
merge
anti-ORF6
anti-CD63
merge

Revised Fig. 5

A

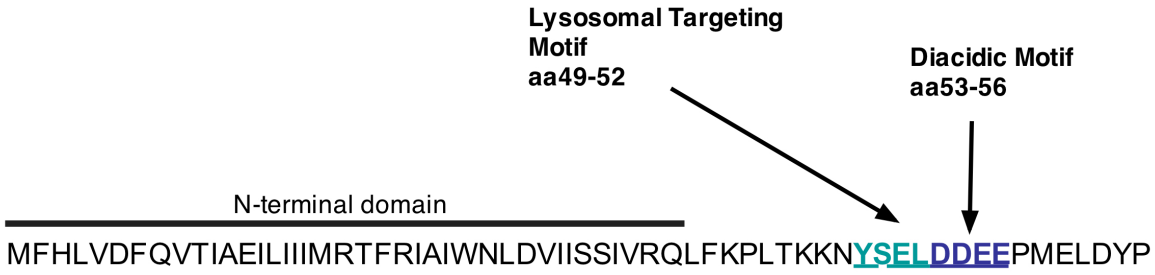

B

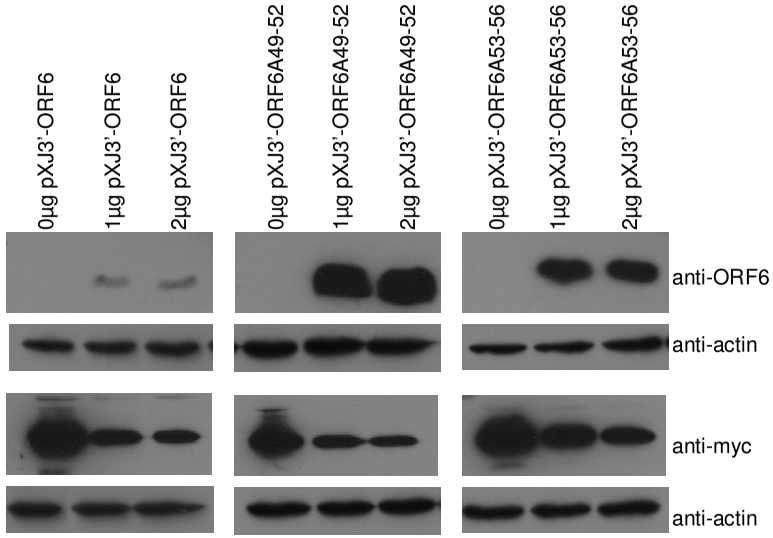

C

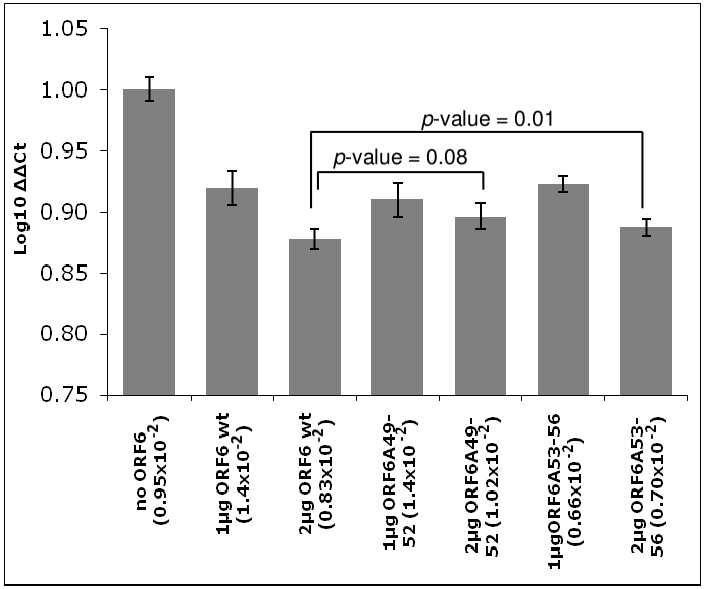

Fig. 6

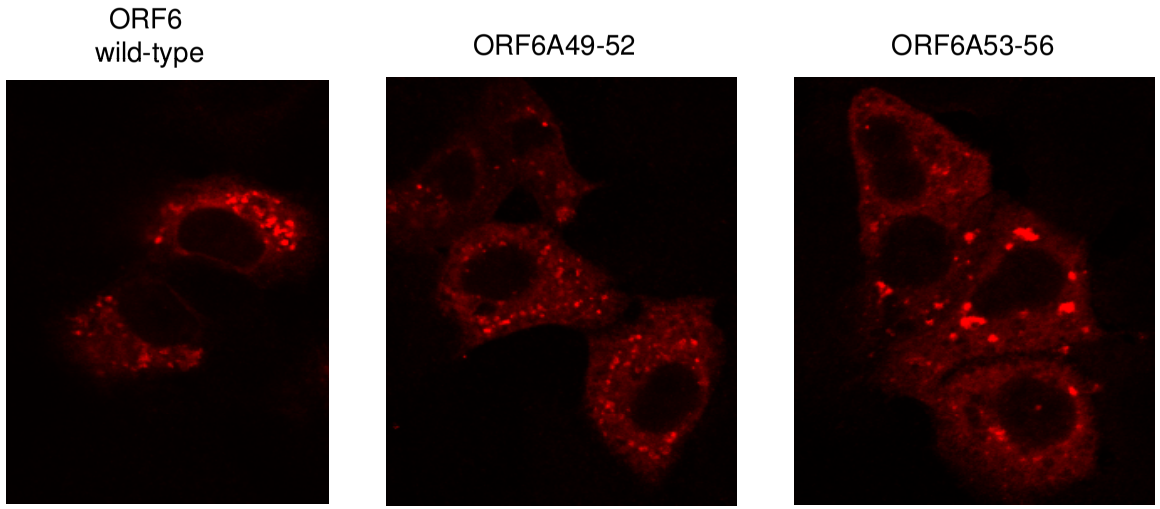

IV

Characterisation of apoptotic induction by the SARS-CoV ORF6 protein expressed via a defective recombinant vaccinia virus system

Vithiagaran Gunalan[a,b], Ali Mirazimi[a,b], Yee-Joo Tan[c]

[a] *Center for Microbiological Preparedness, Swedish Institute for Infectious Disease Control, SE-171 82 Solna , Sweden* [b] *Department of Microbiology, Tumor and Cell Biology, Karolinska Institute, Nobels Väg 16, SE-17177 Stockholm, Sweden* [c] *Department of Microbiology, Yong Loo Lin School of Medicine, National University National University Health System, National University of Singapore*

Abstract

It has been previously shown that the ORF6 protein of the SARS Coronavirus induces ER stress and apoptosis via a JNK-dependent mechanism. In order to further characterize this induction of apoptosis by ORF6, we have generated a replication-defective, recombinant vaccinia virus based on the Lister strain expressing ORF6, and shown that ORF6 expressed using this recombinant system induces apoptosis. Total cDNA from Huh7 cells which were infected with either this recombinant virus or an empty similar virus was analyzed using a SYBR Green-based quantitative realtime PCR (QPCR) array specific to various genes involved in apoptosis. Genes which were observed to be differentially expressed in the array were validated using a different set of primers and probes utilizing Taqman chemistry, and the validated genes pointed to an upregulation of the extrinsic pathway of apoptosis by the ORF6 protein. Further analysis of the validated genes in other human cell lines known to be permissive to SARS-CoV infection showed general agreement in the trend of differential expression, pointing to the possibility that ORF6-indiced apoptosis employed similar mechanisms in different cell lines. Also, microarray analysis was undertaken on the same set of samples, which showed a similar trend of differential expression in the same validated apoptotic genes. Analysis of the microarray data also showed the downregulation of 3 anti-apoptotic genes - *LPRT1*, *MAPK8IP2* and *PTK2B*, and suggested that the induction of apoptosis by ORF6 following ER stress is calcium-dependent.

Introduction

A novel coronavirus was found to have fulfilled Koch's postulates for being the etiological agent for an acute respiratory syndrome originating in southern China in 2002 and was dubbed the Severe Acute Respiratory Syndrome coronavirus (SARS-CoV) (Peiris et al 2003, Ksiazek et al 2003). In its wake it left a fatality rate of 8% and inflicted heavy economic damage on several economies, mostly related to the Chinese diaspora. This virus was subsequently sequenced and found to be rather novel to the coronavirus family, sparking a great deal of research in addition to that already being done to find a means of intervention for its rapid spread. Part of the reason for this was that the SARS-CoV carried in its large 29kb genome, nestled amongst the usual coronavirus structural genes and replicase genes, a few genes dubbed 'accessory genes' which had no known homologs in the coronavirus family. It was hoped that accessory proteins might explain the significantly higher virulence of this novel coronavirus as compared to other circulating coronaviruses (such as HCoV 229E and OC43) which have been observed in the same geographic locations and which mostly caused nothing more than the common cold. If accessory proteins were important to the

pathology of SARS-CoV, they would be attractive targets for intervention. Research into these accessory genes resulted in a flurry of published literature attempting to demonstrate either form or function of these genes (for a review see Tan et al 2007).

One of the most studied accessory genes encoded within the SARS-CoV genome is the ORF6 accessory gene, which encodes for a small protein with a molecular mass of ~7kDa. This protein product of the *ORF6* gene (which has no known homology amongst the coronavirus family) is 63 amino acids long, with a hydrophobic N-terminal and a signal-rich C-terminal, leading to suggestions that the protein may be bifunctional. Biochemical studies have shown that the ORF6 protein localizes to the ER/Golgi and also to intracellular vesicles which stained positive for lysosomal and late endosomal markers (Kumar et al 2007, Gunalan et al 2011). Indeed, a plethora of functions have been assigned to the ORF6 protein – that it functions as an interferon antagonist by impeding the nuclear translocation of STAT1 (Frieman et al 2007), that it is required for optimal SARS-CoV replication especially at low MOIs ((Zhao et al 2009). Also, the ORF6 protein has been shown to cause ER stress and thereby induce apoptosis in a JNK-dependent, caspase-3-dependent manner (Ye et al 2010).

Viral apoptosis is an intriguing aspect of the infection process, as viruses can induce apoptosis towards different, and opposing ends. Viruses may inhibit apoptosis in order to prevent the use of the apoptotic program by infected cells or immune cells to halt the spread of infection, and at the same time, apoptosis may be a useful tool used by viruses either to neutralize cells of the immune system or to aid viral spread by the breakdown of infected cells (Best et al 2008, Galluzzi et al 2008). The pathogenesis observed in several viral infections can be traced to the induction of apoptosis either by the virus or by the immune system. Evidence of SARS-CoV-induced apoptosis has been observed in hepatocytes (Chau et al 2004) as well as thyroid glands from SARS patients (Wei et al 2007), suggesting that the the pathogenesis of SARS might be due to apoptosis in these tissues. SARS-CoV has been observed to induce apoptosis mammalian cell culture (Yan et al 2004, Bordi et al 2004, Ren et al 2005), and several viral proteins from this virus have been shown to possess pro-apoptotic properties (Tan et al 2004, Surjit et al 2004, Yeung et al 2008, Freundt et al 2010). The study and characterization of viral apoptosis also has its utility in having the potential to shed light on cellular processes which are modulated by viral infection or the expression of a particular viral protein. In this study we undertake to characterize the expression of genes in the apoptotic pathway by the ORF6 gene of SARS-CoV, using medium to high throughput methods. We use a defective recombinant vaccinia virus expressing the ORF6 gene in order to create a comprehensive expression background in which the changes in host gene expression can be studied.

Materials and Methods

Cells, plasmids, antibodies

The following cell lines used in this study were purchased from ATCC: CaCo2, Huh7.5, Vero E6 and CV-1. RK-D4R-44.20 cells were a gift from Baxter, and Huh7 cells were a gift from Prof. Hak Hotta (Kobe, Japan). The pDW2 plasmid was a gift from Baxter. Rabbit anti-ORF6 (PUP3) was purchased from Abgent.

Generation of defective recombinant vaccinia virus

The ORF6 gene was cloned into the plasmid pDW2-mh5 using BamHI and NotI sites. CV-1 cells were infected with replicative vaccinia virus (*Lister*) and subsequently transfected with 10µg of pDW2-mh5-ORF6 using Lipofectamine 200 reagent (Invitrogen). 72 hours post-infection, cells were scraped into infection medium and spun down. The pellet was then

resuspended in PBS and freeze-thawed 3 times to yield a recombination crude stock. Crude stock was used to infect the complementing cell line RK-D4R-44.20 and blue plaque selection was performed 3 times under agarose overlays containing *gpt* selection reagents (Falkner and Moss 1988). White plaque selection was then performed under agarose overlays without *gpt* selection in CV-1 cells and selected plaques were picked and amplified in RK44.20 cells and titrated in the same cell line. Titration was performed by infecting RK44.20 cells with serial dilutions of virus stock and 72 hours later, staining with 0.1% crystal violet in 20% ethanol to visualize virus plaques. Plaques were counted and averaged between 2 identically-infected wells at the appropriate dilution of virus stock.

Western Blotting

Huh7 and Vero E6 cells were infected with either dVV-L-ORF6 or dVV-L for the appropriate timepoints, after which cells were scraped into media before being spun down in a benchtop centrifuge and washed twice with PBS. After washes, the cell pellets were resuspended in RIPA buffer (50 mM Tris (pH 8.0), 150 mM NaCl, 0.5% NP40, 0.5% deoxycholic acid, 0.005% SDS) and freeze-thawed in liquid nitrogen 3 times before being spun down at 13k rpm to remove cellular debris. SDS loading buffer was added to clarified lysates before being boiled at 100˚C and loaded onto an SDS-PAGE gel for separation. Gels containing separated lysates were transferred onto Hybond-C nitrocellulose membranes (Amersham) before blocking with 5% skimmed milk in PBS-Tween. Antibody incubations were carried out at 4˚C overnight or at room temperature, with constant rotation. After each incubation, membranes were washed 3 times for 10 minutes each with PBS-Tween. Following washes after secondary antibody incubation, membranes were treated with chemiluminescent substrate (Thermo) and exposed to film.

Immunofluorescence

Huh7 cells were plated in 60mm dishes containing coverslips and subsequently transfected with mammalian expression plasmids relevant to the experiment being performed. Trasfection was performed using Lipofectamine 2000 (Invitrogen) according the manufacturer's instructions. 16 hours after transfection, coverslips were prepared for immunofluorescence as follows: Fixation was carried out in 100% methanol for 5 minutes and coverslips were left to dry before being blocked with PBS containing 1% BSA for 30 minutes. Primary antibody incubation was carried out in a humidified chamber for 1 hour before coverslips were washed 3 times in blocking solution. Secondary antibody incubation was then carried out for an hour in a humidified chamber before the coverslips were washed 3 times. Coverslips were mounted onto glass slides using a mounting mixture of 70% Fluorsave (Calbiochem) and 30% Vectashield containing DAPI (Vector Laboratories). Slides were imaged using a Zeiss LSM510Meta confocal microscope (Zeiss).

Caspase Assay

Huh7 cells were seeded in triplicates in 96-well plates. After being allowed to attach overnight, cells were infected with ether dVV-L-ORF6, dVV-L-7a or dVV-L for either 6, 12 or 24 hours. After each timepoint, WST-1 cell proliferation reagent (Promega) was added to the cells in half the plates and incubated for 1.5hrs, shaken at 500rpm for 1minute and absorbance was measured at 440nm in a spectrophotometer (Tecan), using a reference wavelength of 600nm. Caspase-Glo reagent (Promega) was added to the remaining plates and shaken at 500rpm for 30 seconds to lyse cells in place before incubation at room temperature for 30 mins to 3hrs. Luminescence readings were obtained at 30mins, 1hr, 2hrs and 3hrs and the peaks readings were recorded. These readings were normalized using the WST-1 absorbance readings to yield final caspase activity readings.

Quantitative Realtime PCR

Both Huh7 and Vero E6 cells were infected with either dVV-L or dVV-L-ORF6 at an MOI of 5. At 6 and 12 hours post-infection, cells were scraped into a 15ml Falcon tube and spun down at 1.5k rpm, washed twice with PBS, and resuspended in Trizol Reagent (Invitrogen). Trizol samples were mixed with chloroform and spun down for 15 minutes at 11k rpm, and the upper, aqueous phase was purified using an RNeasy Mini Kit (QIAGEN). RNA concentrations were determined using a spectrophotometer (Tecan). Equal amounts of RNA were then reverse transcribed using poly $d(T)_{12-18}$, and Superscript II reverse transcriptase (Invitrogen). Equal amounts of the resulting cDNA was subjected to realtime PCR using an ABI Fast 7500 Realtime PCR System (Life Technologies) using the following primers: rpo35fwd: 5' - GCCAATGAGGGTTCGAGTTC -3', rpo35rev: 5' – CAACATCCCGTCGTTCATCA - 3', GAPDHQfwd: 5' - GAAGGTGAAGGTCGGAGTC - 3', GAPDHQrev: 5' – GAAGATGGTGATGGGATTTC - 3'. All PCR reactions were performed using SsoFast EvaGreen SYBR Green Master Mix (Bio-Rad). Resulting Ct values for *rpo35* were normalized using GAPDH Ct values and fold changes were calculated using the ΔΔCt method, with *GAPDH* serving as an internal control.

Quantitative Realtime PCR Array

Huh7 cells were infected with either dVV-L or dVV-L-ORF6 at an MOI of 5. At 24 hours post-infection, cells were scraped into a 15ml Falcon tube and spun down at 1.5k rpm, washed twice with PBS, and resuspended in Trizol Reagent (Invitrogen). Trizol samples were mixed with chloroform and spun down for 15 minutes at 11k rpm, and the upper, aqueous phase was purified using an RNeasy Mini Kit (QIAGEN). RNA concentrations were determined using a spectrophotometer (Tecan). Equal amounts of RNA were then reverse transcribed using poly $d(T)_{12-18}$, and Superscript II reverse transcriptase (Invitrogen). Template cDNA was mixed with RT^2 SYBR Green/ROX qPCR master mix (SABiosciences) and 25 µl of this mixture was added to each well of the 96-well PCR array containing specific primer sets. The Human Apoptosis RT^2Profiler PCR Array (SABiosciences) examines 84 genes involved in the apoptotic pathway. These genes include members of the caspase, BCL2, IAP, TRAF, CARD, CIDE, death domain, death effector domain, and TNF receptor and ligand families, as well as genes involved in the p53 and DNA damage pathways. The array also contains primer sets for five housekeeping genes and reverse transcription and PCR positive controls, as well as a control for genomic DNA contamination. The PCR cycling program was performed using an ABI 7500 Fast Real-Time PCR System (Applied Biosystems). The threshold cycle (Ct) values of each gene were used to calculate the fold changes in gene expression using the RT^2 Profiler PCR Array Data Analysis software (http://pcrdataanalysis.sabiosciences.com/pcr/arrayanalysis.php), yielding expression profiles of Huh7 cells infected with either dVV-L-ORF6 or dVV-L for 2 independent experiments

Validation of QPCR Array results

Huh7, Vero E6, CaCo2 and Huh7.5 cells were infected with dVV-L-ORF6 or dVV-L at an MOI of 5. At 24 hours post-infection, cells were scraped into a Falcon tube and spun down at 1.5k rpm, washed twice with PBS, and resuspended in an appropriate amount of Trizol Reagent (Invitrogen). Trizol samples were mixed with chloroform and spun down for 15 minutes at 11k rpm, and the upper, aqueous phase was purified using an RNeasy Mini Kit (Qiagen). RNA concentrations were determined using a spectrophotometer (Tecan). Equal amounts of RNA were then reverse transcribed using poly $d(T)_{12-18}$, and Superscript II reverse transcriptase (Invitrogen). cDNA samples were subjected to quantitative realtime PCR using appropriate TaqMan Gene Expression Assays (Life Technologies) in an ABI Fast 7500 Realtime PCR System (Life Technologies), using *HPRT1* as a housekeeping control. Fold changes were calculated in Microsoft Excel using the ΔΔCt method.

Microarray Analysis

Huh7 cells were infected with either dVV-L-ORF6 or dVV-L. At 12 hours post-infection, cells were scraped into a 15ml Falcon tube and spun down at 1.5k rpm, washed twice with PBS, and resuspended in Trizol Reagent (Invitrogen). Trizol samples were mixed with chloroform and spun down for 15 minutes at 11k rpm, and the upper, aqueous phase was purified using an RNeasy Mini Kit (QIAGEN). RNA concentrations were determined using a spectrophotometer (Tecan). 100ng of each RNA sample was then labelled for microarray hybridization using the GeneChip Whole Transcript Sense Target Labelling Assay (Affymetrix), according to manufacturer's instructions. Briefly, the protocol is as follows: the RNA sample is reverse transcribed twice to yield both positive and negative-strand cDNA. Random hexamers are then used to generate negative-stranded cRNA from the positive-strand cDNA template. cRNA then serves as a template for the production of multiple copies of dUTP-containing positive-stranded cDNA. From here, the cDNA is fragmented with uracil DNA glycosylase (UDG) and fragments are terminally labelled. Labelled fragments are then hybridized overnight to the microarray chip before washing and staining. Washed and stained chips are then scanned to yield signal values for each set of probes corresponding to individual genes in the human genome. Raw signal values were normalized using signal values from control probes in the chip using the Robust Multichip Algorithm and fold changes were calculated in Partek Genomics Suite (Partek Incorporated).

Results

Generation of a defective recombinant vaccinia virus expressing SARS-CoV ORF6

A widely accepted method of introducing a viral gene into a host cell where the use of the virus of origin is not feasible or in order to express individual viral genes in isolation is to use various chemical or electrical transfection methods to transport an expression plasmid encoding the gene of interest across the plasma membrane of the host cell. While this method has enjoyed substantial popularity, there are drawbacks that do not make it ideal for all applications. The efficiency of transfection is typically in the region of 50-70 percent (unpublished observation), making for an incomplete background of expression when examining the effect of the transfected gene on whole cell populations where the isolation of a single transfected cell or the population of positively transfected cells is not feasible, complicating the analysis of results. Also, chemical and mechanical transfection methods are often cytotoxic to various degrees, compromising the viability of the cell or cells in which the effect of the gene of interest is to be studied. An alternative strategy to introduce a gene into a cell *in trans* while achieving a comprehensive expression background is to use a recombinant virus to infect the cells; this virus would express the gene of interest along with its other constituent genes. Several vaccine candidates employ the use of recombinant viruses that are replication-defective in order to introduce a potentially immunogenic gene from a pathogen into individuals in order to elicit a protective immune response. One such virus is the defective vaccinia (*Lister*) which is deficient in uracil DNA glycosylase (Holzer & Faulkner 1997), preventing its replication while allowing for the expression of target genes introduced into the genomic locus previously occupied by this glycosylase, termed D4R. The SARS-CoV ORF6 protein was cloned into the pDW2-mh5 vector to yield pDW2-mh5-ORF6, which contains a recombination cassette in order to facilitate recombination of the ORF6 gene into the vaccina (*Lister*) genome at the D4R locus. This plasmid was then recombined with replicative vaccinia virus by means of infection/transfection in CV-1 cells. By means of *gpt* selection, defective viruses were obtained after 5 rounds of selection and subsequent amplification in RK-D4R-44.20 cells, which stably express the D4R gene to allow for replication and hence amplification of the recombinant virus. In parallel, an empty

recombinant defective vaccinia virus was created and selected in the same manner to serve as a control for experiments involving the recombinant virus expressing ORF6.

After amplification of these viruses, we sought to determine the expression and the prevalence of recombinant ORF6. Huh7 and Vero E6 cells were infected with either dVV-L-ORF6 or dVV-L at an MOI of 5 for 6 and 12 hours and analysed by immunofluorescence using an antibody against the ORF6 protein. The results (Fig.1a) did not show a discernible difference between cells infected with the empty or recombinant viruses. It was suspected that the antibody against ORF6 might be cross-reacting with a vaccinia protein, and therefore a second infection was performed using dVV-L-7a, a defective recombinant vaccinia virus expressing the 7a protein of SARS. Immunofluorescence analysis of this infection compared to infection with dVV-L using a monoclonal antibody against the 7a protein showed a clear difference in signal between the 2 infections. In order to determine if the ORF6 protein was being expressed, Huh7 and E6 cells were infected with dVV-L-ORF6 or dVV-L and subjected to Western Blotting using the same antibody against ORF6. These results (Fig. 1b) showed the expression of the ORF6 protein at a molecular weight of around 7kDa. The Western blot also showed the presence of 2 non-specific bands recognized by the ORF6 antibody at 82kDa and 30kDa, which might explain the lack of a specific ORF6 signal in the immunofluorescence assay. As an assay to determine the relative levels of either dVV-L-ORF6 or dVV-L virus in infected cells, RNA extracted from a parallel set of Huh7 and E6 cells infected with both of these viruses under the same conditions was analysed by quantitative realtime PCR for the *rpo35* gene which encodes the canonical vaccinia DNA polymerase (Amegadzie et al 1991). As seen in Fig. 1c and 1d, the *rpo35* fold change values for each infection are similar, indicating that the levels of defective virus used to infect each cell population are approximately the same. Uninfected cells show no *rpo35* signal, indicating that the QPCR was specific for vaccinia-encoded *rpo35*.

The ORF6 protein expressed by dVV-L-ORF6 is able to induce caspase activity

A previous report has shown that the ORF6 protein from SARS-CoV is able to induce caspase-3-dependent apoptosis (Ye et al 2008) in Vero E6 and COS-7 cells transfected with a GFP-fusion plasmid expressing ORF6. We have also observed caspase-3-dependent apoptosis in Vero E6 cells transfected with a mammalian expression plasmid expressing an untagged form of the ORF6 protein (data not shown), confirming these results. One of the concerns with the use of a recombinant virus expressing a gene of interest is being able to assess whether the use of such a recombinant system compromises the function of the gene of interest; a functional assay is therefore needed to make this assessment. Given previous publication and our own confirmatory data showing the induction of apoptosis by the ORF6 protein, we sought to use this knowledge in order to assess the function of the ORF6 protein expressed by the defective vaccinia system. Vero E6 and Huh7 cells were infected with dVV-L-ORF6 and dVV-L at an MOI of 5. A similar virus, dVV-L-7a, expressing an untagged form of the 7a protein of SARS-CoV, was used as a positive control. At 6, 12 and 24 hours post-infection, cells were subjected to a caspase-3 assay using the Caspase-Glo reagent (Promega). The results, normalized using a cell proliferation assay based on WST-1 (Promega), showed the induction of caspase activity in cells that had been infected with dVV-L-ORF6 and dVV-L-7a in both Huh7 (Fig. 2a) and Vero E6 cells (Fig. 2b), as compared to cells infected with dVV-L. As the data indicates that the relative induction of caspase activity was significantly higher in cells infected with the recombinant dVV-L-ORF6 and dVV-L-7a viruses as compared to the empty virus, it can be concluded that recombinant ORF6 expressed via the defective vaccinia system is functionally intact in that it is able to induce caspase-dependent apoptosis. It is noteworthy, however, that there are differences in the timing of caspase activation between the 2 cell lines. E6 cells show little caspase activation until the 24hr timepoint, while significant caspase activity is observed in the Huh7 cells as early as 12 hours post-infection. It is likely that this difference is dependent on physiological differences between the 2 cell lines.

ORF6 upregulates the extrinsic pathway of apoptosis

Given that we have established a system where defective recombinant viruses are used to introduce virus genes into cell populations where the recombinant proteins are functionally intact, we sought to employ this system to characterize the induction of apoptosis by the ORF6 protein. Because of their ability to undergo caspase dependent apoptosis from a much earlier timepoint (12hrs) as opposed to Vero E6 cells, Huh7 cells were infected with dVV-L-ORF6 or dVV-L at an MOI of 5. Total RNA was extracted from samples taken at 6hrs, 12hrs, and 24hrs post-infection and reverse-transcribed before being subjected to analysis using a Human Apoptosis RT^2Profiler PCR Array (SA Biosciences). The QPCR array plate contained primers for 84 human genes in various apoptotic pathways, along with 5 housekeeping controls as well as other appropriate controls for reverse transcription PCR, as well as genomic DNA contamination. The Ct values obtained for each well was analysed using the RT^2 Profiler PCR Array Data Analysis suite, an online analysis suite provided by the manufacturer (*http://pcrdataanalysis.sabiosciences.com/pcr/arrayanalysis.php*). Using this analysis suite, fold changes for each of the 84 apoptotic genes were obtained for cells infected with dVV-L-ORF6 relative to those infected with dVV-L. This experiment was repeated once to provide a biological replicate. Based on the 2 data sets obtained (Fig. 3), a fold change cut-off was set at 2 and genes which were either upregulated or downregulated by more than 2-fold were identified, yielding a total of 14 genes for validation. Validation of the results was performed by quantitative realtime PCR using pre-fabricated Taqman-based assays specific to each gene (Life Technologies). *HPRT1* was used as a housekeeping control for the validation, given that it was observed to be the most consistent housekeeping gene amongst the 5 housekeeping controls from the QPCR array. Fold changes were calculated for each of the 14 genes identified from the QPCR arrays as being upregulated. Of these, 7 genes were validated (see Fig. 4). The fold change directions of most of these genes were consistent with the literature, such as the observed upregulation of proapoptotic factors such as *BNIP3*, *TNF* and *GADD45A*. One result that stood out from the rest was the observed downregulation of the *TP53* gene, which encodes for the pro-apoptotic p53 protein. Of the rest of the genes that were identified for validation, some showed a fold change in the opposite direction from the arrays, and others failed to amplify altogether.

Given the genes observed to be either upregulated or downregulated in the context of ORF6 expression in Huh7 cells, we sought to determine if there were any cell-specific differences when ORF6 was expressed in other cell lines known to be permissive to SARS-CoV infection. Vero E6, Huh7.5 and CaCo2 cells were infected in the same manner and at 24 hours post-infection, RNA was extracted, reverse transcribed and the resulting cDNA subjected to QPCR using the same Taqman probe-based assays used for validation in Huh7 cells. Using *HPRT1* as a housekeeping gene, fold changes were calculated for each cell line using the $\Delta\Delta$Ct method, and compared to the fold changes for 14 genes obtained for Huh7 cells (Fig. 4). It was observed that most of the genes that were observed to be upregulated in the Huh7 cells, such as *GADD45A*, *LTA*, *TNF* and *BNIP3* were also upregulated in Huh7.5 and CaCo2 cells. Genes which were downregulated consistently in Huh7 cells such as *DAPK1* were also observed to be downregulated in Huh7.5 and CaCo2 cells. Genes which failed to amplify in Huh7 cells such as *CD27* and *TNFSF8* also failed to amplify in these 2 cell lines. However, there were also several differences in the expression of the 14 candidate genes between the 3 cell lines. The *CIDEB* gene, which was consistently observed to be downregulated in Huh7 cells, was also observed to be downregulated in CaCo2 cells, but failed to amplify in Huh7.5 cells. The *FAS* gene was not validated in Huh7 cells but was observed to be upregulated in both Huh7.5 and CaCo2 cells, which indicated further that ORF6 activated the extrinsic pathway of apoptosis independently of cell type. Surprisingly, *TP53* was observed to be upregulated in CaCo2 cells as opposed to the significant downregulation observed in both Huh7 and Huh7.5 cells, albeit below the threshold of 2.

None of the genes selected for validation were amplified in Vero E6 cells, possibly due to sequence differences as the Vero E6 line is of primate origin where the other cell lines were of human origin (data not shown).

Microarray Analysis

In order to further characterize the changes in the expression profile of cells infected with dVV-L-ORF6 beyond an examination of the apoptotic pathway, microarray analysis of the same infected cell populations as used in the QPCR array was carried out. RNA samples from Huh7 cells 12 hours post-infection were processed and eventual cRNA was hybridized to Affymetrix Human Gene 1.0 ST arrays (Affymetrix). Microarray signal values were normalized using RMA (Robust Multichip Average) and log2-transformed across the set of chips to account for differences in hybridization efficiency. Following fold change calculations, we sought to determine if the validated genes from the QPCR array showed the same fold changes or fold change trends in the microarrays. In order to determine if these genes showed the same patterns in the microarray as they did in the QPCR array, average fold changes for each probeset corresponding to these genes (seen in Fig. 4) were plotted (Fig. 5). The resulting graph shows that the fold change trend for the genes from the microarray data concurs with the trend seen from the QPCR array data. The *CIDEB*, *DAPK1* and *TP53* genes are seen to be downregulated and *BNIP3*, *GADD45A*, *LTA* and *TNF* genes are observed to be upregulated as in the QPCR array. The fold change magnitudes, however, are lower than those seen in the QPCR array, possibly due to the fact that the microarray samples were taken from 12hrs post-infection. Following this, a threshold fold change of 5 was selected and the set of genes exhibiting fold changes greater than 5 or lesser than -5 were intersected between 2 biological replicates to yield a list of differentially expressed genes common to both replicates. In order to make a determination of the functional profile of these differentially expressed genes, lists were analyzed using DAVID, an online toolset for functional assignment and grouping of gene lists from microarray data (*http://david.abcc.ncifcrf.gov*). The DAVID toolset uses data from several publicly valuable datasets such as from GO (*www.geneontology.org*), Panther and Interpro in order to assign functional annotations to genes in a given gene list (Huang et al 2009a, Huang et al 2009b). Analysis was performed in DAVID using the GO_xx_FAT datasets (*GO_MF_FAT*, *GO_BP_FAT* and *GO_CC_FAT*), which provide high level functional assignments of molecular function, biological processes and cellular components in order to simplify the data output from these datasets. From the data output, a threshold was set at an enrichment score of 1.0, and these results are represented in Tables 1 & 2, and show the upregulation and downregulation (respectively) of genes in a few pathways. There were many similarities between the pathways affected by genes that were either upregulated or downregulated, indicating that the ORF6 protein was acting on specific pathways in cells infected with dVV-L-ORF6. Interestingly, 3 of the downregulated candidate genes – *LRP1, MAPK8IP2, PTK2B* - were annotated as being related to "positive regulation of anti-apoptosis" (GO:0045768), and these genes were not represented amongst the genes present in the QPCR array.

Discussion

Here we have attempted to characterise the induction of apoptosis by the SARS-CoV ORF6 protein by introducing the ORF6 gene *in trans* using a defective recombinant vaccinia virus based on the *Lister* strain. One of the challenges associated with such studies is the homogeneity of expression in the cell population being studied. Conventional chemical and electrical transfection methods result in a low to medium efficiency of transduction. With the use of a replication-defective recombinant virus expressing ORF6, we were able to achieve a high transduction efficiency for recombinant ORF6, giving us a thorough and largely homogenous expression background in perform the characterisation. The expression,

transduction efficiency and relative amounts of virus were tested for each infection and the result showed that these were adequate for the task of expression profiling of pro- and anti-apoptotic factors in the chosen cell lines. As an assay of the functional viability of the recombinant ORF6 protein, we performed a caspase assay in both Vero E6 and Huh7 cell lines, which showed that in cells infected with dVV-L-ORF6, caspase activation was significantly higher than in cells infected with dVV-L. While this indicated that ORF6 induced caspase-3-dependent apoptosis and was therefore functionally intact, the assay also threw up differences between the 2 cell lines as far as the activation of caspases was concerned. In Vero E6 cells, caspase activation was only seen at 24 hours post-infection, while in Huh7 cells, the induction of caspases was observed to occur much earlier, at the 12-hour timepoint. This can be taken to be indicative of cell-type differences resulting in different responses to the same stimuli, a theme which is seen again in the comparison of the characterisation of apoptotic responses to ORF6 protein in different cell types.

In order to arrive at a profile of the expression of apoptotic pathway genes in cells infected with the recombinant compared to cells which were infected with an empty virus, we employed the use of a commercially-available SYBR Green-based QPCR array, 14 genes from which were subsequently validated by using QPCR, employing a different set of primers and Taqman chemistry. The results of the array and subsequent validation showed that the expression of a total of 7 apoptotic genes were stimulated or repressed by the presence of ORF6 protein, when compared to RNA populations in cells infected with dVV-L, the empty defective virus. These genes were observed to fall into 2 categories – those related to the mitochondrial death pathway and others related to the extrinsic pathway of apoptotic induction. The genes *BNIP3* and *CIDEB* are known to be pro-apoptotic factors in the mitochondrial death pathway, and it is indeed surprising to see a difference in the expression patterns of these pro-apoptotic genes. While *BNIP3* is observed to be upregulated, *CIDEB* undergoes a significant downregulation, which would be at odds with the logic of the upregulation or activation of pro-apoptotic genes during the induction of apoptosis. A resolution to this apparent contradiction will probably require an examination of the protein levels of these 2 proteins – it is recognized that a large majority of the myriad of factors involved in apoptotic induction and execution are regulated at the protein level, and this can differ from patterns observed at the mRNA level.

A few of the 7 genes validated from this study were identified as belonging to the extrinsic pathway of apoptotic activation: *TNF*, *LTA* and *GADD45A*. *TNF* encodes for the TNFα protein that binds to the TNF receptor, one of the major initiators of the extrinsic pathway of apoptosis signaling. The expression of the *TNF* gene here is very interesting, as a previous study on the induction of apoptosis by the ORF6 protein (Ye et al 2008) is indicative of JNK activation. The TNF gene is a known transcriptional target of both JNK and p38 MAPK, which are both mediators of apoptotic signaling in either direction – pro and anti-apoptotic, but in this case, pro-apoptotic. From here, the binding of TNFα to the TNF receptor initiates the activation of caspase-8, which eventually results in the execution of the death program by the activation of executor caspases such as caspase-3 and caspase-9. Further evidence of the involvement of this pathway in the apoptotic activity of the ORF6 protein comes from the results of the microarray studies. The pathway analysis of the most highly upregulated genes in the array point to a myriad of different cellular processes being activated by the ORF6 protein. However, there does exist a commonality to these processes – these are largely calcium-dependent processes. A plausible explanation for the activation of so may calcium-dependent processes in cells infected with dVV-L-ORF6 is that this is indicative of the presence of a large intracellular pool of calcium in these cells. A great deal of published work has implicated elevated calcium levels in the ER as a putative 'trigger' that initiates apoptotic signaling (Demaurex and Distelhorst 2003, Orrenius et al 2003, Timms et al 2009). Such work has also shown that JNK activation in apoptotic cells correlates to sustained elevated ER calcium levels, leading to the transcriptional activation of *TNF*, downstream signaling of the TNF receptor and subsequent caspase recruitment and activation (Brnjic et al 2009). The

elevated levels of intracellular calcium correspond to the activation of the ER stress pathway, a commonality observed in the induction of apoptosis by many viral proteins (Foo et al 2002, Jordan et al 2002, Benali-Furet et al 2005), including the SARS-CoV 3a protein (Law et al 2005, Minakshi et al 2009). In this pathway, ER stress signals initiate large influxes of calcium into cells, sustained levels of which initiate p38 MAPK and JNK signaling, resulting in the transcriptional activation of *TNF* and the eventual caspase signaling cascade leading to caspase-3 activation, as discussed above. To this end, we have observed the differential expression of several genes related to calcium influx and the cellular reponse to elevated intracellular calcium, such as those encoding for subunits for the L-type calcium channels, *CACNA1D*, *CACNA1E*, *CACNA1F*, *CACNA1G*, *CACNA1S* and other genes involved in the transduction of calcium signals such as *CAPN3* (calpain 3) and (calmodulin-binding transactivation factor).

The transduction of pro-apoptotic JNK signaling can occur via either the intrinsic or extrinsic pathways of apoptosis, or a combination of both. While we do observe some degree of activation of the mitochondrial pathway, as evidenced by the observed, reproducible upregulation of *BNIP3*, we also observe a downregulation of a key component of the intrinsic pathway, *TP53*, at the mRNA level in cells infected with dVV-L-ORF6. This could mean that ORF6 apoptosis occurs solely via the extrinsic pathway (downstream of ER stress and JNK activation) or via a p53-independent activation the intrinsic pathway, along with concomitant activation of the extrinsic pathway. The relationship between JNK and p53 is somewhat contentious from the literature, with conflicting reports that JNK either stabilizes and activates p53 transcription (Fuchs et al 1998 PNAS) or that JNK inhibits the activity of p53 (Das et al 2007 PNAS). Given the pleiotropic nature of JNK itself, this relationship may be dependent on physiological context and therefore one could surmise, in this instance, that JNK might be inhibiting p53 and therefore apoptotic activation by the ORF6 gene, is independent of p53. It is however, necessary to examine the protein levels of p53 as the downregulation of *TP53* expression need not necessarily indicate the lack of p53 activity, as the proapoptotic activity of p53 could only require the stabilization and nuclear accumulation of p53 already present in the cell. As such, the involvement of p53 in the induction of apoptosis by the ORF6 protein cannot be ruled out until such studies are performed.

Indeed, it would be prudent to examine the protein products of the genes discussed here, as it is widely recognized that a large part of apoptotic regulation in eukaryotic cells occurs at the protein level. However, studies like this help to isolate targets for such further study at the protein level. An example of this would be factors upstream and downstream of JNK, such as *TNF* and *GADD45A*, and the protein products of downregulated anti-apoptotic genes such as *LRP1, MAPK8IP2* and *PTK2B*. Further analysis of the microarray data may also shed light on the host expression changes induced by the ORF6 protein, which lead to its cellular effects.

References

Amegadzie, B. Y., Ahn, B Y, & Moss, B. (1991). Identification, sequence, and expression of the gene encoding a Mr 35,000 subunit of the vaccinia virus DNA-dependent RNA polymerase. *The Journal of Biological Chemistry*, *266*(21), 13712-8.

Benali-Furet, N. L., Chami, M., Houel, L., De Giorgi, F., Vernejoul, F., Lagorce, D., Buscail, L., et al. (2005). Hepatitis C virus core triggers apoptosis in liver cells by inducing ER stress and ER calcium depletion. *Oncogene*, *24*(31), 4921-33.

Best, S. M. (2008). Viral subversion of apoptotic enzymes: escape from death row. *Annual Review of Microbiology*, *62*, 171-92.

Brnjic, S., Olofsson, M. H., Havelka, A. M., & Linder, S. (2010). Chemical biology suggests a role for calcium signaling in mediating sustained JNK activation during apoptosis. *Molecular bioSystems*, *6*(5), 767-74.

Chau, T.-N., Lee, K.-C., Yao, H., Tsang, T.-Y., Chow, T.-C., Yeung, Y.-C., Choi, K.-W., et al. (2004). SARS-associated viral hepatitis caused by a novel coronavirus: report of three cases. *Hepatology, 39*(2), 302-10.

Coulibaly, S., Brühl, P., Mayrhofer, J., Schmid, K., Gerencer, M., & Falkner, F. (2005). The nonreplicating smallpox candidate vaccines defective vaccinia Lister (dVV-L) and modified vaccinia Ankara (MVA) elicit robust long-term protection. *Virology*, *341*(1), 91-101.

Demaurex, N., & Distelhorst, C. (2003). Cell biology. Apoptosis--the calcium connection. *Science*, *300*(5616), 65-7.

Falkner, F. G., & Moss, B. (1988). Escherichia coli *gpt* gene provides dominant selection for vaccinia virus open reading frame expression vectors. *Journal of Virology*, *62*(6), 1849-54.

Foo, N. C., Ahn, B.Y., Ma, X., Hyun, W., & Benedict Yen, T. (2002). Cellular Vacuolization and Apoptosis Induced by Hepatitis B Large Surface Protein. *Hepatology*, *36*(6), 1400–1407.

Freundt, E. C., Yu, L., Goldsmith, Cynthia S, Welsh, S., Cheng, A., Yount, B., Liu, W., et al. (2010). The open reading frame 3a protein of severe acute respiratory syndrome-associated coronavirus promotes membrane rearrangement and cell death. *Journal of Virology*, *84*(2), 1097-109.

Frieman, M., Yount, B., Heise, M., Kopecky-Bromberg, S. a, Palese, P., & Baric, R. S. (2007). Severe acute respiratory syndrome coronavirus ORF6 antagonizes STAT1 function by sequestering nuclear import factors on the rough endoplasmic reticulum/Golgi membrane. *Journal of Virology*, *81*(18), 9812-24.

Galluzzi, L., Brenner, C., Morselli, E., Touat, Z., & Kroemer, G. (2008). Viral control of mitochondrial apoptosis. *PLoS Pathogens*, *4*(5), e1000018.

Holzer, G. W., & Falkner, F. G. (1997). Construction of a vaccinia virus deficient in the essential DNA repair enzyme uracil DNA glycosylase by a complementing cell line. *Journal of Virology*, *71*(7), 4997-5002.

Huang, D. W., Sherman, B. T., & Lempicki, R. a. (2009). Bioinformatics enrichment tools: paths toward the comprehensive functional analysis of large gene lists. *Nucleic Acids Research*, *37*(1), 1-13.

Huang, D. W., Sherman, B. T., & Lempicki, R. a. (2009). Systematic and integrative analysis of large gene lists using DAVID bioinformatics resources. *Nature Protocols*, *4*(1), 44-57.

Jordan, R., Wang, L., Graczyk, T. M., Block, T. M., & Romano, P. R. (2002). Replication of a cytopathic strain of bovine viral diarrhea virus activates PERK and induces endoplasmic reticulum stress-mediated apoptosis of MDBK cells. *Journal of Virology*, *76*(19), 9588.

Kruse, J.-P., & Gu, W. (2009). Modes of p53 regulation. *Cell*, *137*(4), 609-22.

Ksiazek, T. G., Erdman, D., Goldsmith, C.S., Zaki, S.R., Peret, T., Emery, S., Tong, S., et al. (2003). A novel coronavirus associated with severe acute respiratory syndrome. *New England Journal of Medicine*, *348*(20), 1953–1966.

Kumar, P., Gunalan, V., Liu, B., Chow, V. T. K., Druce, J., Birch, C., Catton, M., et al. (2007). The nonstructural protein 8 (nsp8) of the SARS coronavirus interacts with its ORF6 accessory protein. *Virology*, *366*(2), 293-303.

Law, P. T. W., Wong, C.-H., Au, T. C. C., Chuck, C.-P., Kong, S.-K., Chan, P. K. S., To, K.-F., et al. (2005). The 3a protein of severe acute respiratory syndrome-associated coronavirus induces apoptosis in Vero E6 cells. *The Journal of General Virology*, *86*(7), 1921-30.

Minakshi, R., Padhan, K., Rani, M., Khan, N., Ahmad, F., & Jameel, S. (2009). The SARS Coronavirus 3a protein causes endoplasmic reticulum stress and induces ligand-independent downregulation of the type 1 interferon receptor. *PloS ONE*, *4*(12), e8342.

Ober, B., Brühl, P., Schmidt, M., Wieser, V., Gritschenberger, W., Coulibaly, S., Savidis-Dacho, H., et al. (2002). Immunogenicity and safety of defective vaccinia virus lister: comparison with modified vaccinia virus Ankara. *Journal of Virology*, *76*(15), 7713. Am Soc Microbiol.

Orrenius, S., Zhivotovsky, B., & Nicotera, P. (2003). Regulation of cell death: the calcium-apoptosis link. *Nature reviews. Molecular Cell Biology*, *4*(7), 552-65.

Peiris, J. S. M., Lai, S. T., Poon, L. L. M., Guan, Y., Yam, L. Y. C., Lim, W, Nicholls, J., et al. (2003). Coronavirus as a possible cause of severe acute respiratory syndrome. *Lancet*, *361*(9366), 1319-25.

Surjit, M., Liu, B., Jameel, S., Chow, V. T. K., & Lal, S. K. (2004). The SARS coronavirus nucleocapsid protein induces actin reorganization and apoptosis in COS-1 cells in the absence of growth factors. *The Biochemical Journal*, *383*(Pt 1), 13-8.

Tan, Y.-J., Lim, S. G., & Hong, W. (2006). Understanding the accessory viral proteins unique to the severe acute respiratory syndrome (SARS) coronavirus. *Antiviral Research*, *72*(2), 78-88.

Tan, Y.-J., Lim, S. G., & Hong, W. (2007). Regulation of cell death during infection by the severe acute respiratory syndrome coronavirus and other coronaviruses. *Cellular Microbiology*, *9*(11), 2552-61.

Timmins, J. M., Ozcan, L., Seimon, T. A., Li, G., Malagelada, C., Backs, J., Backs, T., et al. (2009). Calcium/calmodulin-dependent protein kinase II links ER stress with Fas and mitochondrial apoptosis pathways. *The Journal of Clinical Investigation*, *119*(10), 2925.

Wei, L., Sun, S., Xu, C.-H., Zhang, J., Xu, Y., Zhu, H., Peh, S.-C., et al. (2007). Pathology of the thyroid in severe acute respiratory syndrome. *Human Pathology*, *38*(1), 95-102.

Ye, Z., Wong, C. K., Li, P., & Xie, Y. (2008). A SARS-CoV protein, ORF-6, induces caspase-3 mediated, ER stress and JNK-dependent apoptosis. *Biochimica et Biophysica Acta*, *1780*(12), 1383-7.

Yeung, Y.-S., Yip, C.-W., Hon, C.-C., Chow, K. Y. C., Ma, I. C. M., Zeng, F., & Leung, F. C. C. (2008). Transcriptional profiling of Vero E6 cells over-expressing SARS-CoV S2 subunit: insights on viral regulation of apoptosis and proliferation. *Virology*, *371*(1), 32-43.

Figure Legends

1. Expression of recombinant ORF6 from a defective vaccinia virus. (**a**) Huh7 cells plated on glass coverslips were infected with dVV-L and dVV-L-ORF6 or dVV-L and dVV-L7a at an MOI of 5 for either 6 or 12 hours. At the appropriate timepoints, coverslips were fixed in methanol and subjected to immunofluorescence analysis using antibodies against the ORF6 and 7a proteins, and FITC-conjugated secondary antibodies, before being mounted on glass slides and imaged with a Zeiss LSM510Meta confocal microscope. (**b**) Western blot for expression analysis of ORF6 expressed from recombinant vaccinia virus. Huh7 and E6 cells were infected with dVV-L or dVV-L-ORF6 at an MOI of 5 for 6 or 12 hours. Cells were lysed at the appropriate timepoints and subjected to SDS-PAGE separation and Western blotting using an antibody against ORF6 (indicated by arrow). Comparison of virus levels used in each infection. **(c)** Huh7 cells and **(d)** Vero E6 cells were infected with dVV-L-ORF6 or dVV-L at an MOI of 5 for 6 or 12 hours, after which cells were lysed and total RNA extracted and subjected to SYBR-Green QPCR using primers against the *rpo35* gene of vaccinia. Relative quotients for each QPCR were calculated using the ΔΔCt method, with GAPDH as a housekeeping gene.

2. Induction of caspase activity by ORF6 expressed from a defective recombinant vaccinia virus. Huh7 cells **(a)** or Vero E6 cells **(b)** were infected with either dVV-L-ORF6 or dVV-L or dVV-L-7a (as a positive control for caspase induction) at an MOI of 5 for either 6, 12 or 24 hours and were subjected to a luminescent assay for caspase-3 activity. A WST-1 assay for cell proliferation was used to normalize the readings from the caspase assay and the resulting values were plotted for each virus at each timepoint.

3. The ORF protein induces differential expression of genes in the apoptotic pathway. Huh 7 cells were infected at an MOI of 5 for 24 hrs in 2 independent experiments and resulting total cDNA was subjected to a commercially available SYBR-Green QPCR array for selected pro- and anti-apoptotic genes. Using the *HPRT1* gene as a housekeeping control, fold changes were calculated by the ΔΔCt method, using the manufacturer's data analysis suite (*http://pcrdataanalysis.sabiosciences.com/pcr/arrayanalysis.php*). Genes exhibiting fold changes either greater than 2 or lower than -2 were plotted for 2 biological replicates, along with validation fold changes for these genes (see next figure).

4. Validation of differentially expressed apoptotic genes in multiple cell lines. Huh7, Huh7.5, CaCo2 and Vero E6 cells were infected with either dVV-L-ORF6 or dVV-L for 24 hours and resulting total cDNA was subjected to QPCR analysis using alternative primer and probe sets for candidate genes based on Taqman chemistry, with *HPRT1* as a housekeeping gene. Fold changes were calculated using the ΔΔCt method and plotted for each cell line. E6 samples showed no amplification (not shown).

5. Fold change comparison of validated genes from QPCR array with microarray results. Huh7 cells were infected with either dVV-L-ORF6 or dVV-L at an MOI of 5 for 12 hours and total RNA was subjected to microarray analysis using the HuGene 1.0 ST Gene array (Affymetrix). Fold changes were calculated in Partek Genomic Suite and these fold changes were plotted for genes found in the microarray data which were validated from the QPCR array results. Data is collated from 2 independent experiments.

Table 1. Functional analysis of upregulated genes from microarray study. Genes from the microarray study which showed fold changes lower than -5 were selected and input into the DAVID functional annotation database to yield functional information on highly downregulated genes. A total of 161 genes were analysed in this manner and the results were filtered by setting a threshold enrichment score of 1.0 and collated into a table showing the genes clustered by functional annotation using the *GO_xx_FAT* databases.

Table 2. Functional analysis of downregulated genes from microarray study. Genes from the microarray study which showed fold changes lower than -5 were selected and input into the DAVID functional annotation database to yield functional information on highly downregulated genes. A total of 175 genes were analysed in this manner and the results were filtered by setting a threshold enrichment score of 1.0 and collated into a table showing the genes clustered by functional annotation using the *GO_xx_FAT* databases.

Figures

1a

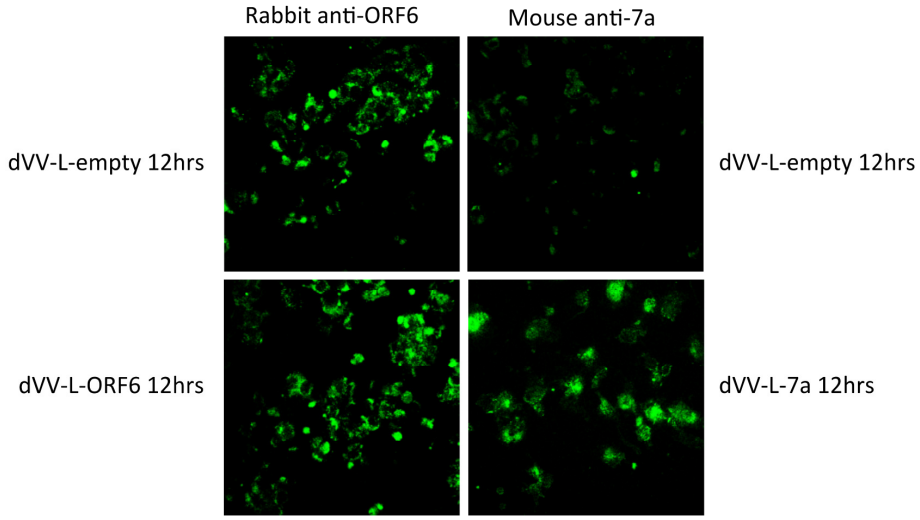

1b

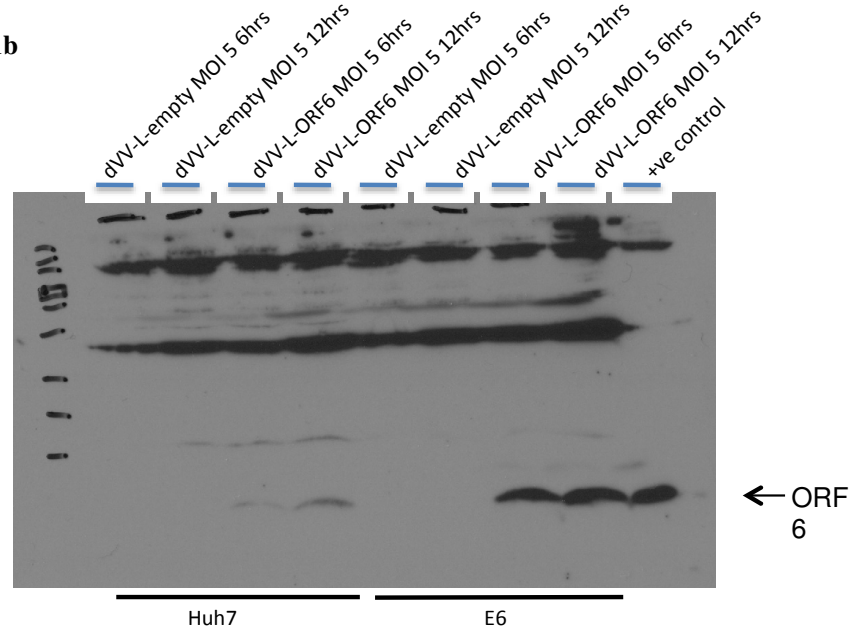

1c

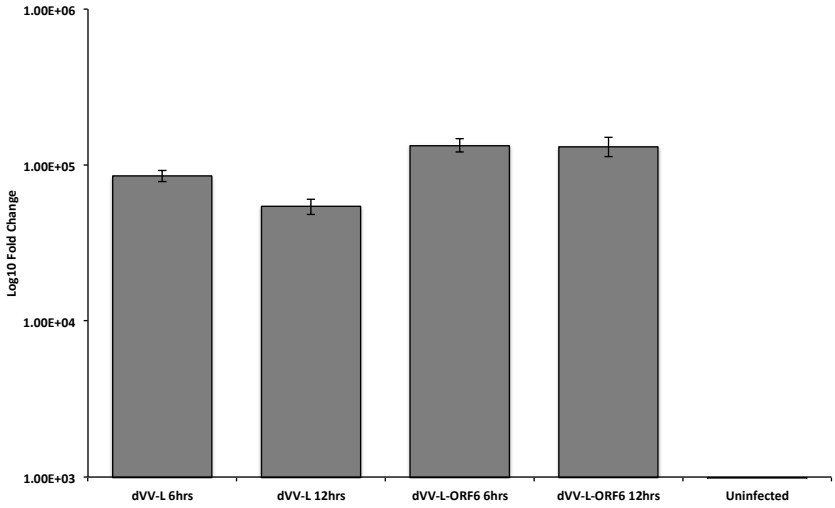
1.00E+06
1.00E+05
1.00E+04
1.00E+03
Log10 Fold Change
dVV-L 6hrs
dVV-L 12hrs
dVV-L-ORF6 6hrs
dVV-L-ORF6 12hrs
Uninfected

1d

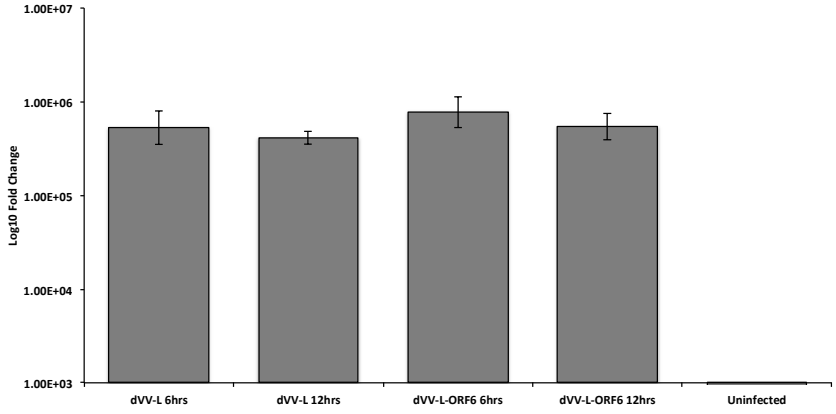
1.00E+07
1.00E+06
1.00E+05
1.00E+04
1.00E+03
Log10 Fold Change
dVV-L 6hrs
dVV-L 12hrs
dVV-L-ORF6 6hrs
dVV-L-ORF6 12hrs
Uninfected

2a

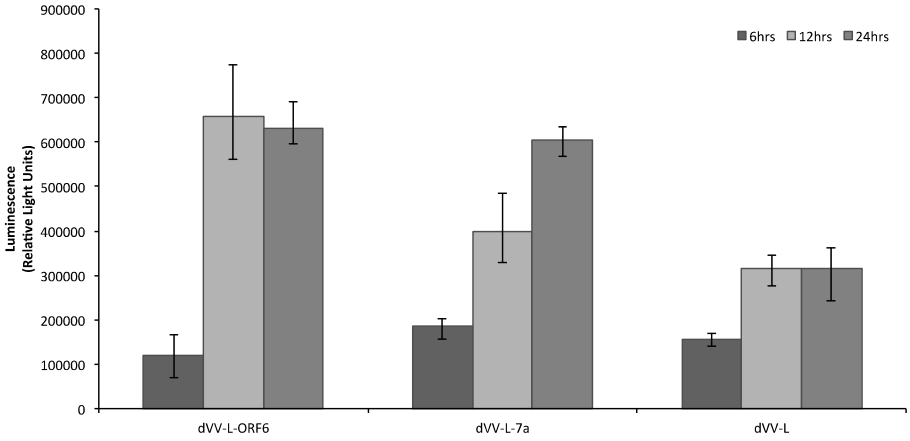
900000
800000
700000
600000
500000
400000
300000
200000
100000
0
Luminescence (Relative Light Units)
6hrs
12hrs
24hrs
dVV-L-ORF6
dVV-L-7a
dVV-L

2b

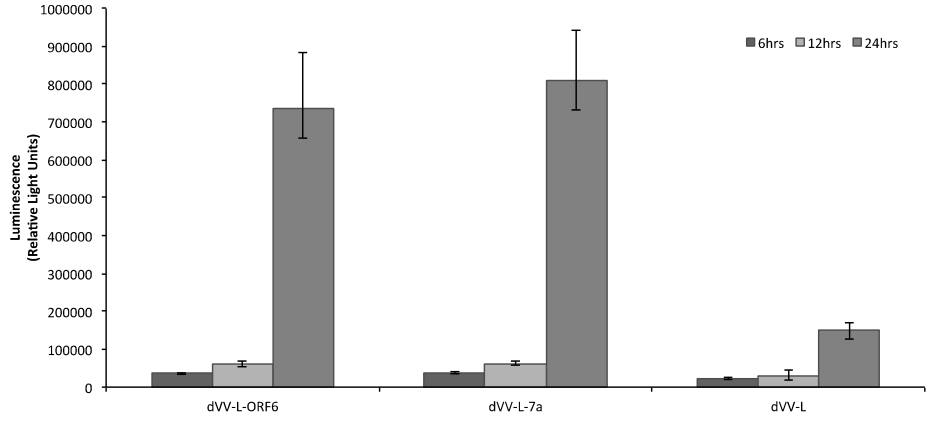
1000000
900000
800000
700000
600000
500000
400000
300000
200000
100000
0
Luminescence (Relative Light Units)
6hrs
12hrs
24hrs
dVV-L-ORF6
dVV-L-7a
dVV-L

3

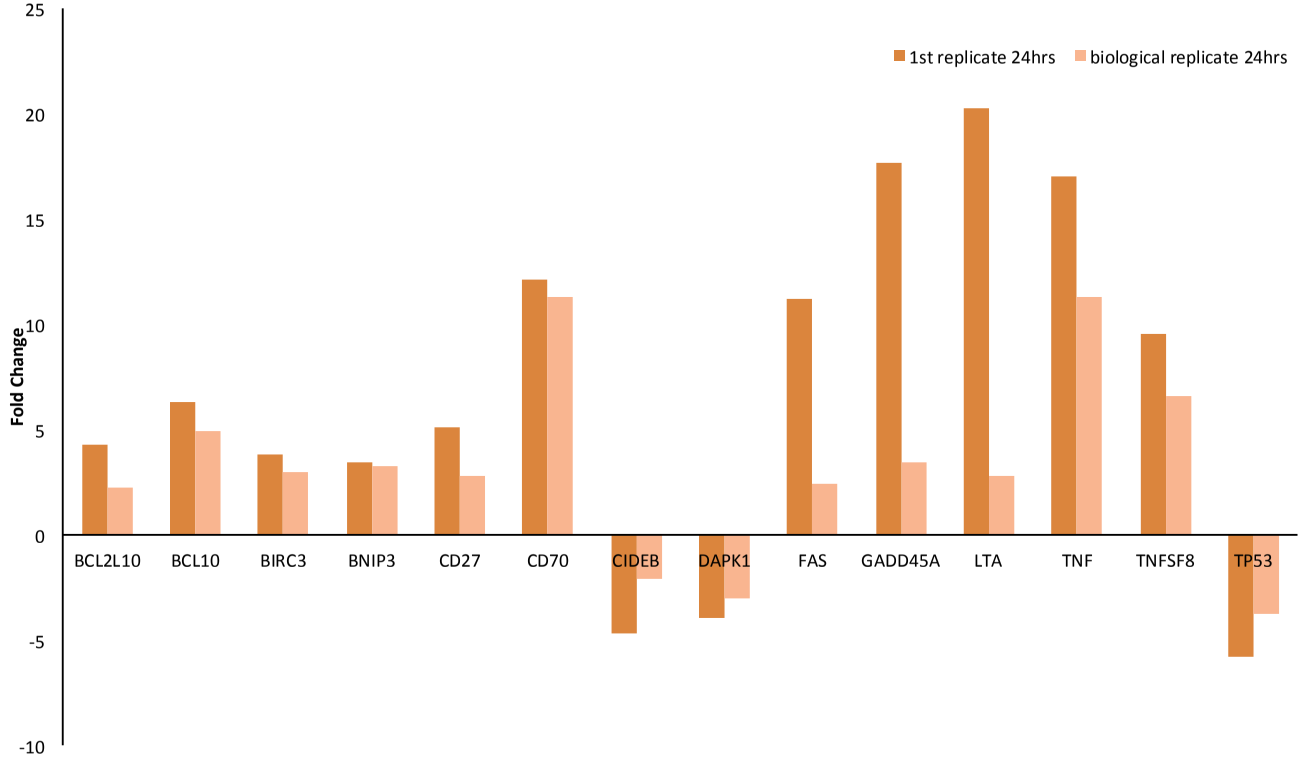
25
20
15
10
5
0
-5
-10
Fold Change
1st replicate 24hrs
biological replicate 24hrs
BCL2L10
BCL10
BIRC3
BNIP3
CD27
CD70
CIDEB
DAPK1
FAS
GADD45A
LTA
TNF
TNFSF8
TP53

4

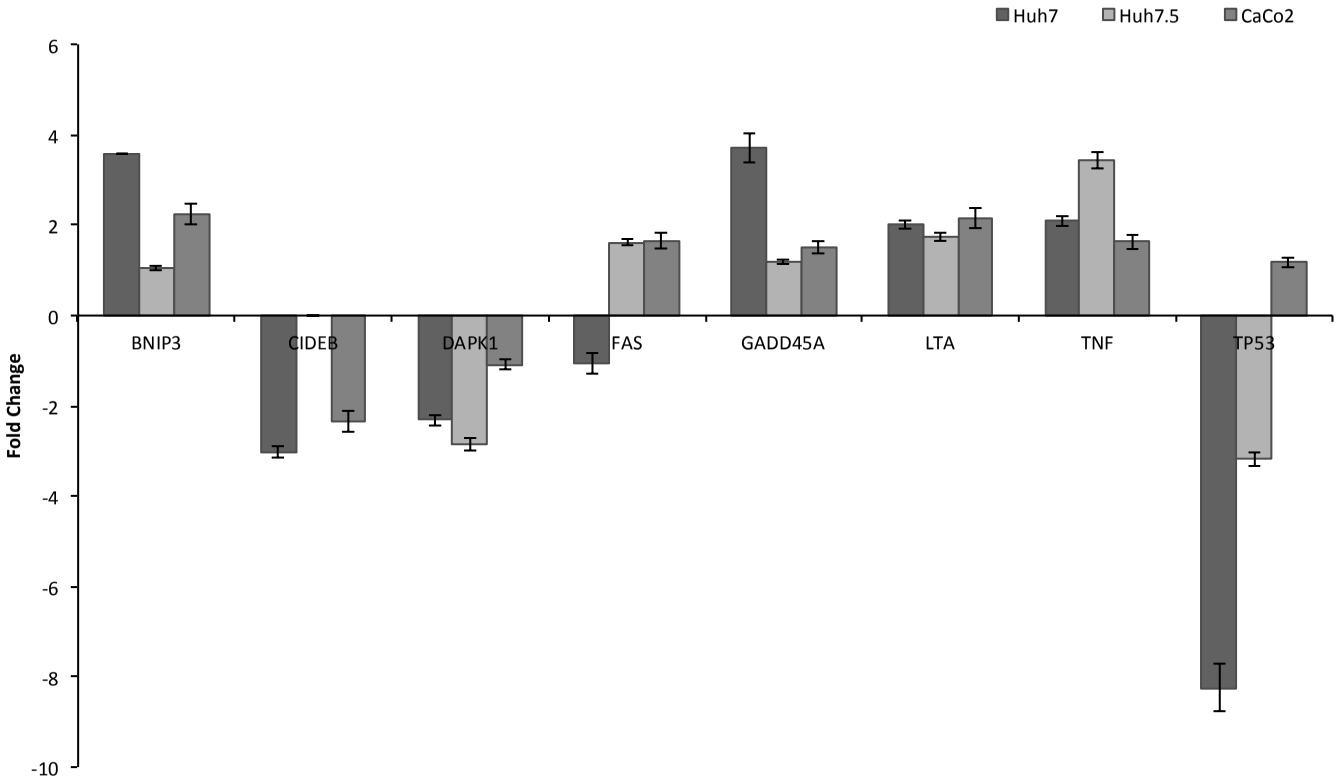
Huh7
Huh7.5
CaCo2
Fold Change
6
4
2
0
-2
-4
-6
-8
-10
BNIP3
CIDEB
DAPK1
FAS
GADD45A
LTA
TNF
TP53

5

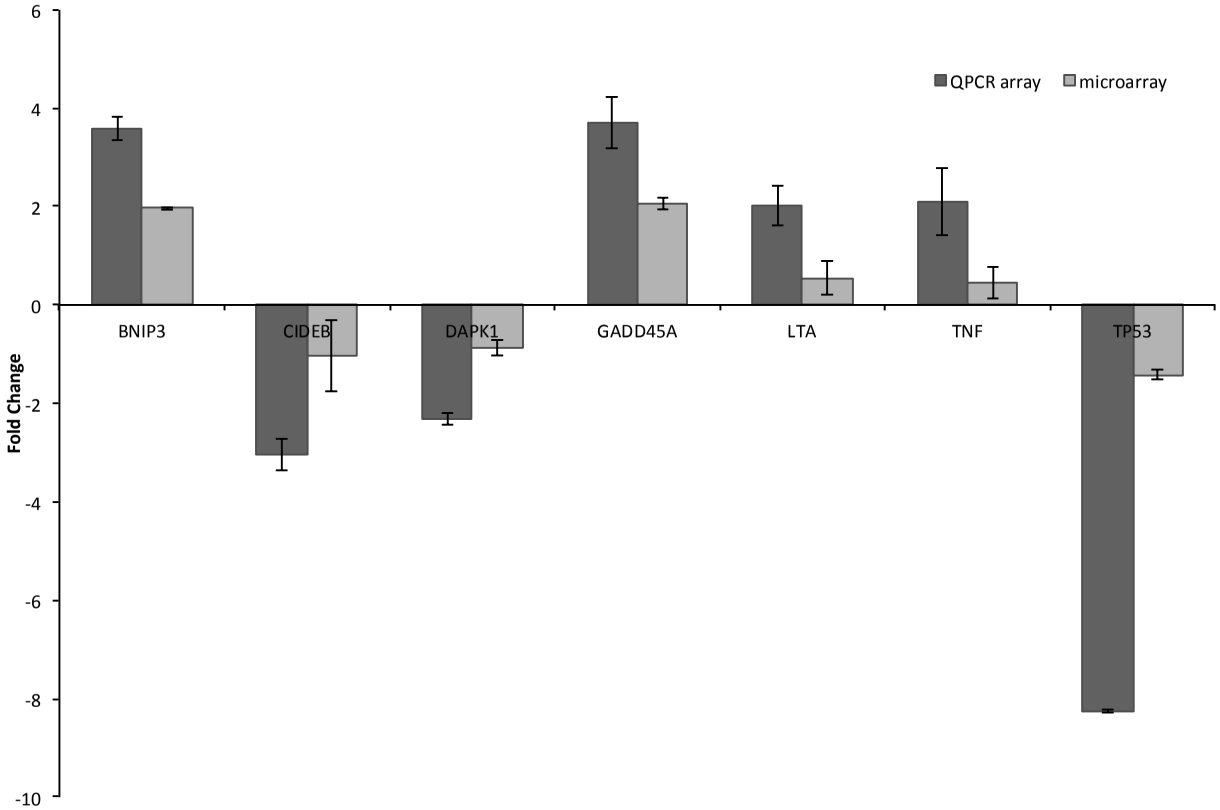
6
4
2
0
-2
-4
-6
-8
-10
Fold Change
QPCR array
microarray
BNIP3
CIDEB
DAPK1
GADD45A
LTA
TNF
TP53

Table 1

Annotation	No. of Genes	Genes
ATP-Binding and ATPase activity	37	ABCA12, ABCA7, ABCB11, ABCC12, ACSM1, ADCY1, ALK, ATP8B2, DGKA, DHX30, DNAH1, DNAH11, DNAH6, DNAH8, GUCY2F, IFIH1, KDR, KIT, KSR1, LIMK2, LRGUK, MAST2, MCM7, MOV10L1, MSH4, MYH6, OBSCN, OXSR1, PAN3, PASK, PRKCG, RET, RUNX1, SLC22A4, STK32A, TTN, WNK2
Ion Channel Activity	13	CACNA1G, CACNA1S, CACNA2D1, FXYD4, GRIK5, KCNK16, NALCN, RYR1, SCN3A, SCN4A, SCN7A, SCN10A, TRPM3,
Plasma Membrane	62	ABCA7, ABCB11, ACTN2, ADCY1, ALK, ATP6V1G3, CACNA1G, CACNA1S, CACNA2D1, CALCR, CD163L1, CD44, CLTCL1, CSMD2, DGKA, DIAPH1, DYSF, EFNA5, EPB41, FAP, GRIK5, GUCY2F, HLA-F, IL1RL1, ITGA11, ITGAL, JAG2, KDR, KIT, LGR4, LILRB3, MAST2, MGAM, MRC1, MUC16, MYH6, NBEA, OBSCN, PCDH15, PDE6C, PDZD11, PDZD2, PKHD1, PLB1, PLXNA3, PLXND1, PTPRD, RASGRF1, RYR1, SCN10A, SCN3A, SCN4A, SCN7A, SECTM1, SHROOM3, SLC22A4, SPTB, TMEM67, TPO, VAMP1, ZAN
Cation Binding	66	ACAP1, ACSM1, ACTN2, ADAM32, ADAMTS20, ADCY1, AMY2B, ATP8B2, BMP1, C20ORF12, CACNA1G, CACNA1S, CACNA2D1, CAPN3, COL9A1, DCHS2, DGKA, DNASE1, DZIP3, FBN2, FGD5, FOXP2, HMCN1, IFIH1, ITGA11, ITGAL, JAG2, KCNK16, KSR1, LIMK2, LMBRD1, LRP4, MAST2, MCTP2, MLL4, MOV10L1, MRC1, NALCN, NEBL, OBSCN, OXSR1, PCDH15, PHF8, POMGNT1, PRDM15, PRKCG, RABGGTB, RET, RNF160, RORB, RUNX1, RYR1, SCN10A, SCN3A, SCN4A, SCN7A, SFXN2, SLC22A4, STK32A, TP63, TPO, TRPM3, TTN, USP20, ZFYVE26, ZNF323,
Cytoskeletal Protein Binding	16	ACTN2, DAAM2, DIAPH1, DNASE1, EPB41, FHOD3, IPP, MYBPC1, MYH6, MYPN, NEBL, OBSCN, RET, SHROOM3, SPTB, TTN
Structural Molecule Activity	14	ACTN2, COL15A1, COL16A1, COL4A4, COL5A2, COL9A1, CYLD, EPB41, FBN2KRT31, IMPG2, MYBPC1,NEBL, OBSCN

Table 2

Annotation	No. of Genes	Genes
ATP-Binding and ATPase activity	41	ABCA12, ABCA2, ABCC12, ACSM1, ADCY1, ALK, ATP10A, ATP8B2, ATR, DGKA, DGKD, DHX29, DHX30, DNAH1, DNAH6, KDR, KIF11, KIF15, KIF1A, KIF4A, KIF6, KIT, LIG3, MCM7, MKI67, MOV10L1, MYH14, MYH6, OBSCN, OPLAH, ORC1L, OXSR1, PASK, PTK2B, RECQL5, RET, STK32A, TEK, TEP1, TTN, UBE2J2, ULK2
Ion Channel Activity	11	ANO7, CACNA1D, CACNA1G, CACNA1S, FXYD4, GRIK5, KCNK16, KCNQ1, NALCN, RASA3, SCN7A
Microtubule/Cytoskeleton	23	ABCA2, CENPF, CEP152, DNAH1, DNAH6, DNASE1, HDAC6, IPP, KIF11, KIF15, KIF1A, KIF4A, KIF6, MED12, MYH14, MYH6, PKHD1, RAB3IP, SHROOM3, SPTB, TACC2, TTLL9, TTN
Calcium Ion Binding	26	ACTN2, AMY2B, ANO7, BMP1, CACNA1D, CACNA1G, CACNA1S, CAPN3, DCHS2, DGKA, DNASE1, FBN2, HMCN1, ITGA2B, ITGAL, JAG2, LRP1, LRP4, LTBP2, MAN1B1, NELL2, PCDH15, PLCG2, RET, RYR1, TTN
Muscle System Process	7	CACNA1G, KCNQ1, MYH6, RYR1, SCN4A, SCN7A, TTN
Positive Regulation of Anti-Apoptosis	3	LRP1, MAPK8IP2, PTK2B

US-AB universitetsservice digitaltryck
Printed in Sweden 2011, www.us-ab.com